Technische Universität München
TUM School of Medicine and Health

Enhancement of radiosensitivity by TPP-coupled gold nanoparticles in triple-negative breast cancer cells

Alicia Hernández Schnelzer

Vollständiger Abdruck der von der TUM School of Medicine and Health der Technischen Universität München zur Erlangung einer Doktorin der Medizin (Dr. med.) genehmigten Dissertation.

Vorsitz: Prof. Kathrin Schumann, Ph.D.

Prüfende der Dissertation:

1. Prof. Dr. Gabriele Multhoff
2. Prof. Dr. Susanne Kossatz

Die Dissertation wurde am 09.04.2024 bei der Technischen Universität München eingereicht und durch die TUM School of Medicine and Health am 09.10.2024 angenommen.

Table of Contents

List of Abbreviations

ABC	Accelerated blood clearance
ADP	Adenosine diphosphate
AIF	Apoptosis-inducing factor
AP	Apurinic or apyrimidinic
Apaf-1	Apoptotic protease activating factor 1
APC	Allophycocyanin
APCs	Antigen-presenting cells
ATP	Adenosine triphosphate
AuNPs	Gold-(coated) nanoparticles
AuNRs	Gold nanorods
BBB	Blood-brain barrier
BCS	Breast-conserving surgery
BRCA-1 & 2	“BReast CAncer”-1 and 2
BSA	Bovine serum albumin
CA-125	Cancer antigen 125
CA-15-3	Cancer antigen 15-3
CEA	Carcinoembryonic antigen
CF	Carboxy-fluorescein
CFA	Colony forming assay
CIS	Carcinoma in situ
CPP	Cell-penetrating peptides
CT	Computed tomography
DCIS	Ductal carcinoma in situ
DEF	Dose enhancement factor
DMSO	Dimethyl sulfoxide
DNA	Deoxyribonucleic Acid
DSB	Double-strand breaks
E	Photon energy
EDTA	Ethylenediaminetetraacetic acid
EGFR	Epidermal growth factor receptor
EPR	Enhanced permeability and retention effect
ER	Endoplasmic reticulum

ER	Oestrogen receptor
eV	Electronvolt
FACS	Fluorescence-activated cell sorting
FBS	Foetal bovine serum
FITC	Fluorescein isothiocyanate
FSC	Forward scatter
Gb3	Globoyltriaosylceramide
GnRH	Gonadotropin-releasing hormone
GNRT	Gold nanoparticle-assisted radiation therapy
GrP	Glucose-related proteins
Gy	Gray
HDFs	Human dermal fibroblasts
HER2	Human epidermal growth receptor
HLA	Human leucocyte antigen
HR	Hormone receptors
Hsc70	Heat shock cognate protein 70
HSFs	Heat shock factors
Hsp70	Heat shock protein 70
Hsp70-1	Heat shock protein 70 (Hsp70-1a and Hsp70-1b and HSPA1A)
Hsp70-8	Heat shock cognate protein 70
Hsp90	Heat shock protein 90
HSPs	Heat shock proteins
HSR	Heat shock response
IgG	Immunoglobulin G
IGRT	Image-guided radiation therapy
IMRT	Intensity-modulated radiotherapy
IOERT	Intraoperative electron radiation therapy
kDa	Kilodalton
keV	Kilo electronvolt
kVp	Peak kilovoltage
LA-HNSCC	Locally advanced head and neck squamous cell carcinoma
LAMP1	Lysosomal-associated membrane protein-1
LCIS	Lobular carcinoma in situ
LET	Linear energy transfer

LEM	Local effect model
LHRH	Luteinising hormone receptor
LSPR	Local surface plasmon resonance
mAB	Mouse monoclonal antibody
MC	Monte Carlo
mHsp70	Membrane heat shock protein 70
MeV	Mega electronvolt
MFI	Mean fluorescent intensity
MHC-I	Major histocompatibility complex class I
MPS	Mononuclear phagocyte system
MRI	Magnetic resonance imaging
NAC	N-acetyl-L-cysteine
NanoEL	Nanomaterial-induced endothelial leakiness
NHEJ	Non-homologous end joining
NIR	Near infrared
NIRF	Near-infrared fluorescence
NK	Natural killer cells
NLS	Nuclear localisation signals
NOS- type	Not otherwise specified type
PBL	Peripheral blood lymphocytes
PBS	Dulbecco's phosphate-buffered saline
PDT	Photodynamic therapy
PE	Phycoerythrin
PE	Plating efficiency
PEG	Polyethylene glycol
PEI	Polyethylenimine
PET	Positron emission tomography
PI	Propidium Iodide
PLD	Potentially lethal radiation damage
PR	Progesterone receptor
PSS	Poly-styrene sulfonate
PTT	Photothermal therapy
PVP	Polyvinylpyrrolidone
RBE	Relative biological effectiveness

RES	Reticuloendothelial system
RGD	Arginine-glycine-aspartic acid
rhTNF	Human recombinant TNF
RME	Receptor-mediated endocytosis
ROS	Reactive oxygen species
RPMI	Roswell Park Memorial Institute
SERM	Selective oestrogen receptor modulators
SF	Survival fraction
siRNA	Small interfering RNA
SLD	Sublethal radiation damage
SSB	Single strand breaks
SSC	Side scatter
TDDS	Targeted drug delivery systems
TDLUs	Terminal duct lobular units
TNBC	Triple-negative breast cancer
TNF-α	Tumour necrosis factor-alpha
TNM	Tumour, node, metastasis
TPP	Tumour cell-penetrating peptide
UV	Ultraviolet radiation
Z	Atomic number

List of Figures

List of Tables

Summary

Breast cancer is the most prevalent malignancy among women, constituting 30% of cancer diagnoses and nearly 18% of cancer-related mortality in the female population in Germany. Breast carcinomas are classified according to their hormone receptor expression, with triple-negative breast cancers (TNBC), expressing neither oestrogen, progesterone, nor human epidermal growth factor receptor 2 (HER2), comprising over 12% of cases. Radiotherapy is an established treatment for malignancies such as breast cancer, utilising ionising radiation to administer both lethal and sub-lethal doses to tumour cells, impeding proliferation, and inducing cell death. One of the major limitations of radiotherapy lies in the non-specific deposition of energy along the photon pathway, causing inadvertent damage and limiting the dose application. Addressing this limitation, a novel approach emerges through the application of 'radiosensitisers'—substances capable of increasing the susceptibility of tumour cells towards radiation-induced killing without affecting healthy tissue. Due to its high atomic number and, therefore, strong photoelectric effect and X-ray absorption properties, gold is an ideal radiosensitiser. To achieve high intratumoural concentrations, the membrane protein Hsp70, selectively expressed on malignant cells but not on corresponding healthy cells, was used as a target.

In this study, human TNBC cells, MDA-MB-231, were incubated with hybrid gold (Au)-iron oxide (Fe_3O_4)-nanoparticles coupled to either tumour cell-penetrating peptide (TPP-PEG4-FeAuNPs), which specifically binds membrane-bound Hsp70, or NGL (NGL-PEG4-FeAuNPs), a scavenger peptide with unspecific binding. MDA-MB-231 cells are highly positive for membrane Hsp70, which served as the target protein for the TPP-PEG4-FeAuNPs. Upon binding to Hsp70, gold nanoparticles (AuNPs) are internalised and accumulate in the perinuclear area. Toxicity assays and colony-forming assays were performed using MDA-MB-231 cells incubated with 0.5 µg/ml and 1.0 µg/ml of TPP-PEG4-FeAuNPs or NGL-PEG4-FeAuNPs and irradiated 24 hours later. The results showed a strong trend towards increased cell killing following irradiation with TPP-PEG4-FeAuNPs compared to standard irradiation without nanoparticles, as well as an increased cell killing compared to NGL-PEG4-FeAuNPs. Moreover, toxicity assays showed no significant decrease in cell viability when applying AuNPs at concentrations up to 5 µg/ml. This work demonstrates the safety and efficacy of TPP-coupled AuNPs as diagnostic and therapeutic agents for targeting mHsp70-positive tumour cells.

Zusammenfassung (Summary in German)

Brustkrebs ist die häufigste Krebserkrankung bei Frauen und macht 30 % der Krebsdiagnosen und rund 18 % der krebsbedingten Sterblichkeit in der weiblichen Bevölkerung in Deutschland aus. Brustkarzinome werden nach ihrer Hormonrezeptorexpression klassifiziert, wobei Triple-negative Mammakarzinome (TNBC), die weder Östrogen, Progesteron noch den humanen epidermalen Wachstumsrezeptor (HER2) exprimieren, über 12% der Fälle ausmachen. Die Strahlentherapie ist eine bewährte Behandlung für bösartige Erkrankungen wie Brustkrebs. Mittels ionisierender Strahlung werden tödliche und subletale Energiedosen an die Tumorzellen abgegeben, die die Proliferation hemmen und den Zelltod verursachen. Eine der größten Einschränkungen der Strahlentherapie ist die unspezifische Deposition von Energie entlang des Photonenpfads, die zu ungewollten Schäden führt und die Dosisanwendung begrenzt. Ein neuer Lösungsansatz ist die Anwendung von ‚strahlensensibilisierenden Substanzen', d. h. Substanzen, die die Empfindlichkeit von Tumorzellen gegenüber der strahleninduzierten Abtötung erhöhen, ohne gesundes Gewebe zu beeinträchtigen. Aufgrund der hohen Ordnungszahl und der damit verbundenen photoelektrischen Wirkung sowie Röntgenabsorptionseigenschaften ist Gold ideal zur Radiosensibilisierung. Um hohe intratumorale Konzentrationen zu erreichen, wurde das Oberflächenprotein Hsp70 genutzt, welches auf malignen Zellen aber nicht korrespondierenden gesunden Zellen expliziert wird.

In dieser Arbeit wurden TNBC-Zellen, MDA-MB-231, mit Gold (Au)-Eisenoxid (Fe_3O_4)-Nanopartikeln inkubiert, die mit einem Tumorzell-penetrierenden Peptid (TPP-PEG4-FeAuNPs) das spezifisch membrangebundenes Hsp70 bindet, oder mit NGL (NGL-PEG4-FeAuNPs) das unspezifisch bindet, gekoppelt waren. MDA-MB-231-Zellen sind stark positiv für Membran-Hsp70. Nach der Bindung an Hsp70 werden die Goldnanopartikel (AuNPs) internalisiert und reichern sich im perinukleären Bereich an. Toxizitätstests und Koloniebildungstests wurden durchgeführt bei Konzentrationen von 0,5 µg/ml und 1,0 µg/ml TPP-PEG4-FeAuNPs oder NGL-PEG4-FeAuNPs mit anschließender Bestrahlung 24 Stunden später. Die Ergebnisse zeigten eine verstärkte Zelltötung nach Bestrahlung mit TPP-PEG4-FeAuNPs im Vergleich zu einer Standardbestrahlung ohne Nanopartikel, sowie eine erhöhte Zelltötung im Vergleich zu NGL-PEG4-FeAuNPs. Darüber hinaus zeigten Toxizitätstests keine signifikante Abnahme der Zell-Viabilität bei der Anwendung von AuNPs bei Konzentrationen bis zu 5 µg/ml. Diese Arbeit zeigt, dass TPP-gekoppelte AuNPs ein sicheres und wirksames diagnostisches und therapeutisches Mittel zur Bekämpfung von mHsp70-positiven Tumorzellen sein können.

1 Introduction

1.1 Breast cancer

1.1.1 Epidemiology and aetiology

Breast cancer is the most frequent cancer among women, accounting for 30.0% of cancer diagnoses and responsible for 17.7% of female cancer mortality in Germany (Erdmann et al., 2021). Current numbers suggest one in eight women will suffer from breast cancer (Erdmann et al., 2021), amounting to a lifetime risk of around 12.8% (Leitlinienprogramm Onkologie, 2020). Only 0.1% of breast cancer cases are found in men (Leitlinienprogramm Onkologie, 2020). Since the 1980s, the number of cases has continuously increased, reaching 69,900 cases in 2018 (Erdmann et al., 2021), while the number of breast cancer-related deaths has remained nearly constant with around 18,000 women per year (Bertz et al., 2010; Erdmann et al., 2021). The average age of onset is about 65 years (Erdmann et al., 2021), with the majority of cases between the ages of 50 and 69 (Sauer, 2010a). One out of six women are younger than 50 when first diagnosed (Erdmann et al., 2021).

Several risk factors involved in the development of breast cancer are known. Hormones, for instance, play an important role: An early first and late last menstruation, childlessness, older age during the first pregnancy, hormone replacement therapies, for instance, after menopause, or hormone-containing ovulation inhibitors for contraception are considered to increase the risk of disease (Erdmann et al., 2021; Harbeck & Heywang-Köbrunner, 2011). Other risk factors include dense breast tissue, a previous breast cancer disease, benign transformations, as well as lifestyle factors such as smoking, alcohol consumption, and obesity (Erdmann et al., 2021; Sauer, 2010a). Additionally, 5–10% arise due to modifications in the tumour-suppressor gene BRCA-1 and BRCA-2 (Böcker et al., 2008; Harbeck & Heywang-Köbrunner, 2011; Sauer, 2010a). These carriers benefit from intensified early detection programmes or prophylactic bilateral mastectomy and/or a prophylactic bilateral salpingo-oophorectomy around the age of 40 – additionally reducing the risk of ovarian cancer (Leitlinienprogramm Onkologie, 2020).

1.1.2 Diagnostics

The first diagnostic step consists of taking a medical history and a clinical examination with inspection and palpation of the breast. Possible symptoms include nodes in the breast, skin alterations, nipple secretion, size or shape change, and lymph node swelling (Harbeck &

Heywang-Köbrunner, 2011). In the case of abnormal findings, the diagnosis is completed by an imaging modality and a histological examination (Harbeck & Heywang-Köbrunner, 2011; Leitlinienprogramm Onkologie, 2020; Sauer, 2010a). In breast cancer screening, mammography plays the most crucial role as it is the only method enabling a proven reduction in breast cancer mortality (Harbeck & Heywang-Köbrunner, 2011; Leitlinienprogramm Onkologie, 2020). Since 1971, annual breast cancer screening has been a statutory health insurance benefit in Germany from the age of 30. Since 2004, an additional mammography screening programme has been granted every two years for women aged 50 to 69 and even yearly in cases with increased risk (Bertz et al., 2010; Erdmann et al., 2021; Harbeck & Heywang-Köbrunner, 2011; Leitlinienprogramm Onkologie, 2020). The mammography screening can be complemented by an ultrasound examination and a contrast-enhanced magnetic resonance imaging (MRI) (Sauer, 2010a). Particularly in young women with dense mammary glands and an increased familial risk of disease, for instance, carriers of a BRCA-1 or BRCA-2 mutation, as well as in the case of suspected recurrence, contrast-enhanced-MRI is used (Leitlinienprogramm Onkologie, 2020; Sauer, 2010a). The use of gold in mammography could be beneficial due to the enhanced contrast achieved (Lee et al., 2014).

The diagnosis is confirmed by histological examination of an image-guided biopsy specimen (Harbeck & Heywang-Köbrunner, 2011; Leitlinienprogramm Onkologie, 2020). If an invasive carcinoma is diagnosed, clinical staging is performed consisting of an X-ray of the thorax, an ultrasound examination of the abdomen, scintigraphy of the skeleton, and, if necessary, further diagnostics using computerised tomography (CT) scans (Harbeck & Heywang-Köbrunner, 2011; Leitlinienprogramm Onkologie, 2020; Sauer, 2010a). The tumour markers cancer antigens (CA) CA-125, CA-15-3, and carcinoembryonic antigen (CEA) play a role in the monitoring progress (Sauer, 2010a).

1.1.3 Histology

Near to all breast carcinomas are adenocarcinomas (Böcker et al., 2008). A distinction is made between invasive and non-invasive forms, as well as ductal (milk ducts) and lobular (glandular lobules) carcinomas (Böcker et al., 2008; Sauer, 2010a). The non-invasive adenocarcinomas, also called carcinoma in situ (CIS), of the ductal (DCIS) and lobular systems (LCIS) account for 5–30% of all breast carcinomas (Böcker et al., 2008). A characteristic feature is a non-penetrated basal membrane. DCIS is precancerous, and with 95% of CIS cases, it is much more frequent than LCIS (Böcker et al., 2008). In contrast to DCIS, LCIS carries an increased risk of carcinoma but is not considered precancerous (Harbeck & Heywang-

Köbrunner, 2011). DCIS usually presents with a continuous, segmental spread (Harbeck & Heywang-Köbrunner, 2011). They arise from malignant neoplasms of the epithelia of terminal duct lobular units (TDLUs) and account for around 20% of newly detected breast carcinomas (Harbeck & Heywang-Köbrunner, 2011). The risk of progression to an invasive carcinoma is approximately 30–50% in 10 years (Sauer, 2010a). In contrast, LCIS tend to show a multifocal and diffuse spread (Böcker et al., 2008). They also arise from neoplasms of the TDLUs and account for 1% of all breast cancer diagnoses (Harbeck & Heywang-Köbrunner, 2011). These adenocarcinomas are most frequently localised in the outer upper quadrant (Harbeck & Heywang-Köbrunner, 2011).

Invasive breast carcinomas arise from non-invasive CIS (Böcker et al., 2008). Invasive ductal carcinoma of the not otherwise specified (NOS) type accounts for 40–75% of cancers, making it the most common subtype (Böcker et al., 2008). Invasive lobular carcinoma accounts for around 10% (Sauer, 2010a). Other less common subtypes include medullary, tubular, mucinous, papillary, and intradermal adenocarcinoma, also called Paget's disease of the breast (Sauer, 2010a). The route of metastasis for invasive carcinomas is most commonly lymphogenic to axillary and infra- or supraclavicular lymph nodes (Harbeck & Heywang-Köbrunner, 2011). Hematogenous spread occurs mainly to the skeleton (70%), lungs (60%), liver (50%), and brain (Harbeck & Heywang-Köbrunner, 2011). In about 7% of patients, metastases can already be found at first diagnosis (Erdmann et al., 2021).

The classification of carcinomas is based on the TNM stages (Böcker et al., 2008; Harbeck & Heywang-Köbrunner, 2011), where tumour size (T), infestation of lymph nodes (N), and the occurrence of distant metastases (M) are taken into account (Sauer, 2010a). Tumour grading is classified according to Elston and Ellis (1991), also known as the ‘Nottingham Grading System’, where histologic malignancy criteria such as nuclear atypia, mitotic rate, altered glandular architecture, tubule formation, etc. are taken into account (Leitlinienprogramm Onkologie, 2020). As illustrated in Figure 1, low-grade tumours (grade 1) are well-differentiated and homologous with a normal TDLU, low nuclear polymorphism, and low mitotic rate. In contrast, grade 2 tumours are moderately differentiated, and high-grade (grade 3) tumours are poorly differentiated with increased mitotic activity, nuclear atypia, and strongly altered glandular architecture (Rakha et al., 2010).

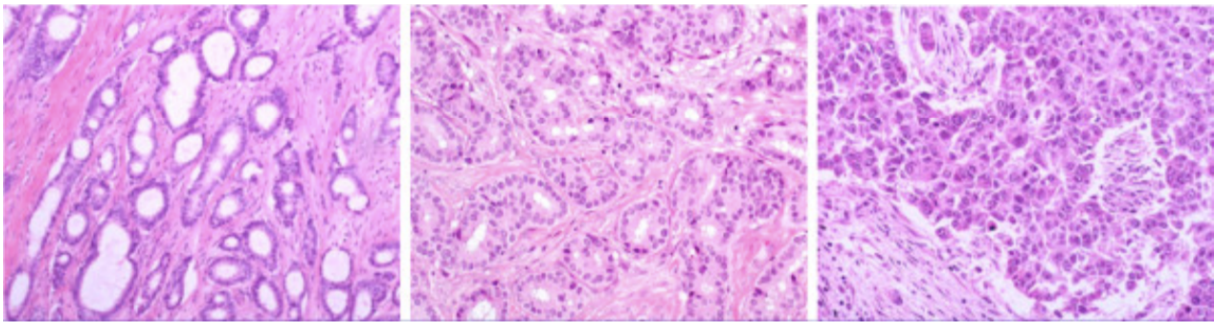

Grade 1 Grade 2 Grade 3

Figure 1 – Histological grading of breast carcinomas using the 'Nottingham Grading System'

Image source *"Breast cancer prognostic classification in the molecular era: The role of histological grade"* by Rakha et al. (2010).

Immunohistochemical staining is used to determine the proliferation rate using Ki-67 and the receptor status, testing for progesterone receptor (PR), oestrogen receptor (ER), and human epidermal growth receptor (HER2) (Leitlinienprogramm Onkologie, 2020). If more than 1% of the tumour cell nuclei express a given receptor, the tumour is considered receptor-positive (Leitlinienprogramm Onkologie, 2020). In the USA, 83.0% of patients were positive for hormone receptors (HR), 14.9% positive for HER2, whereas 12.2% were triple-negative breast cancers (TNBC), expressing neither ER, PR, nor HER2. The receptor status is essential, especially in later targeted therapeutical options (Böcker et al., 2008).

Prognostic factors include tumour size, histological subtype, grading according to Elston and Ellis (1991), HR status, HER2 status, proliferation activity, as well as lymph node status, metastases, recurrences, and patient age (Leitlinienprogramm Onkologie, 2020; Sauer, 2010a). Overall, survival after ten years varies from as low as 22% to as high as 90% of patients (Sauer, 2010a).

1.1.4 Therapy

1.1.4.1 Operation

The therapeutic options for the treatment of breast cancer are diverse and include a range of interdisciplinary approaches. The primary therapeutic goal for DCIS is the complete removal, i.e., an R0 resection (Harbeck & Heywang-Köbrunner, 2011) with a safety margin of 2 mm (Leitlinienprogramm Onkologie, 2020). Subsequently, the affected breast is irradiated, reducing the local recurrence risk by 50% (Leitlinienprogramm Onkologie, 2020). The recommendation of excision of LCIS, seeing it is not precancerous, is still inconsistent and depends on various pathologic criteria (Harbeck & Heywang-Köbrunner, 2011). Complete surgical excision is also crucial for invasive breast carcinomas (Harbeck & Heywang-Köbrunner, 2011). The radicality of resection is decisive for the further prognosis (Harbeck & Heywang-Köbrunner, 2011). Depending on tumour size, breast constitution, etc., a breast-conserving surgery (BCS) or mastectomy is performed (Leitlinienprogramm Onkologie, 2020; Sauer, 2010a). BCS, followed by radiation, equates to a mastectomy alone (Leitlinienprogramm Onkologie, 2020). Indications for a radical mastectomy include inflammatory carcinomas, contraindications against subsequent radiation, incomplete tumour removal after re-resection, and, of course, the patient's preference (Leitlinienprogramm Onkologie, 2020). In addition to surgical removal, axillary staging is performed for invasive carcinomas (Harbeck & Heywang-Köbrunner, 2011). For this purpose, a ‘sentinel lymph node’ biopsy is performed, where a dye or radioactive tracer is injected into the area of the tumour, and the draining lymph nodes are examined (Böcker et al., 2008; Harbeck & Heywang-Köbrunner, 2011). If the sentinel node is histopathologically tumour-free, no additional surgery is necessary (Leitlinienprogramm Onkologie, 2020). However, if it is infested, an axillary dissection with removal of 8–10 lymph nodes is performed (Sauer, 2010a).

1.1.4.2 Radiotherapy

In recent years, radiotherapy has dramatically reduced the previously difficult-to-treat and frequent recurrences of breast cancer down to only 5–10%. On average, it prolongs survival for roughly 8% of affected women (Sauer, 2010a). The decision for adjuvant radiotherapy or system therapy is based on the risk of recurrence: In the case of BCS, a mandatory postoperative, whole-breast radiotherapy must be performed – regardless of tumour size (Harbeck & Heywang-Köbrunner, 2011; Sauer, 2010a). For locally advanced tumours or tumours with positive lymph nodes after mastectomy, postoperative radiotherapy of the chest wall and lymphatic drainage area is recommended, seeing it additionally lowers the risk of

locoregional recurrence and improves overall survival (Leitlinienprogramm Onkologie, 2020; Sauer, 2010a). Radiation therapy options include hypofractionation and conventional fractionation, with 40 Gy or 50–60 Gy, respectively (Leitlinienprogramm Onkologie, 2020). These are administered in single sessions with a dose of 1.8–2.0 Gy each (Leitlinienprogramm Onkologie, 2020; Tudda et al., 2022). Boost irradiation of the tumour bed with local dose saturation reduces the risk of recurrence (Leitlinienprogramm Onkologie, 2020). For dose saturation, intraoperative electron radiation therapy (IOERT), percutaneous electron irradiation, or brachytherapy are suitable (Sauer, 2010a).

1.1.4.3 Systemic therapy

Systemic therapies include chemotherapy, endocrine, and antibody therapy (Leitlinienprogramm Onkologie, 2020). These can be administered individually, in combination, or sequentially (Leitlinienprogramm Onkologie, 2020). Postoperative chemotherapy usually starts 1–2 weeks after surgery, typically using anthracyclines and taxanes (Leitlinienprogramm Onkologie, 2020). Patients with high-risk tumours, lymph node involvement, or TNBC benefit from chemotherapy (Leitlinienprogramm Onkologie, 2020). Neoadjuvant and adjuvant systemic chemotherapy are treated equally in the interdisciplinary S3 guideline (Leitlinienprogramm Onkologie, 2020). Neoadjuvant therapies shrink the tumour size pre-operatively to achieve a BCS (Sauer, 2010a).

If the HR status is positive for OR and/or PR, accounting for 83.0% of tumours (Howlader et al., 2014), endocrine therapy, also known as hormone therapy, can additionally be administered following surgery for five years (Harbeck & Heywang-Köbrunner, 2011; Leitlinienprogramm Onkologie, 2020). In pre-menopausal women, selective OR modulators (SERM), such as tamoxifen, and gonadotropin-releasing hormone (GnRH) analogues, such as goserelin, are used to suppress the ovarian function (Harbeck & Heywang-Köbrunner, 2011; Leitlinienprogramm Onkologie, 2020). Post-menopausal women are given aromatase inhibitors, such as formestane, anastrozole, or letrozole, which prevent the conversion of androgen precursors to oestrogen (Harbeck & Heywang-Köbrunner, 2011; Leitlinienprogramm Onkologie, 2020). For HER2 receptor positivity, a therapy with trastuzumab, a specific monoclonal antibody directed against the epidermal growth factor receptor (EGFR), is recommended (Harbeck & Heywang-Köbrunner, 2011; Leitlinienprogramm Onkologie, 2020). Trastuzumab lowers the recurrence rate by 50% within the first two years (Harbeck & Heywang-Köbrunner, 2011). In addition, supportive therapies for existing metastases are

available, such as irradiation of skeletal and brain metastases (Harbeck & Heywang-Köbrunner, 2011; Sauer, 2010a).

1.1.5 Recurrence

Most locoregional recurrences occur within the first two years after primary therapy (Harbeck & Heywang-Köbrunner, 2011). These recurrences are still potentially curable; however, 50% of patients develop distant metastases within one year and up to 70–80% within two years (Sauer, 2010a). The treatment of choice is a secondary mastectomy or, rather, a complete removal of the tumour tissue with additional radiotherapy and systemic therapy in a curable or palliative approach (Leitlinienprogramm Onkologie, 2020). 20–25% of patients with a cancer recurrence are still alive after five years (Sauer, 2010a). The ten-year recurrence-free rate is around 18–19% of patients (Sauer, 2010a).

1.2 Radiotherapy

Radiotherapy is an established therapeutic approach that utilises ionising radiation to treat malignant cells. It plays a significant role in modern cancer treatments and distinguishes three primary endpoints: First, tumour control with the goal of curative radiotherapy where no further tumour growth can be detected; second, tumour growth delay in incurable but radiosensitive tumours to prolong survival and improve the quality of life; and lastly, tumour progression or non-response to radiotherapy with continued tumour growth (Schulz-Ertner et al., 2006).

1.2.1 Types of radiation

Radiation can be subdivided into ionising and non-ionising radiation. During ionising radiation, the energy transferred excites and ionises atoms or molecules (Herrmann et al., 2006). If a bound electron is transferred to an outer shell, i.e., into a higher energy state, it is called an 'excitation' (Herrmann et al., 2006). One speaks of 'ionisation' if a valence electron is expelled from the atom after the energy absorption (Herrmann et al., 2006). Examples of ionising radiation are ultraviolet radiation (UV), X-rays, gamma-rays, and particle radiation (Münter & Weber, 2006; Sauer, 2010b). Non-ionising radiation includes visible light and thermal radiation (Münter & Weber, 2006).

1.2.2 Ionising radiation

Ionising radiation can be further subdivided into particle and wave radiation, as well as directly or indirectly ionising radiation (Sauer, 2010b). Particle radiation, also called corpuscular radiation, refers to energy carriers with mass, for instance, ion- or proton-radiation (Sauer, 2010b). Wave radiation, also called electromagnetic wave radiation, includes X-rays or Gamma-rays (Münter & Weber, 2006; Sauer, 2010b). Following the irradiation of an organism, a series of stages take place, which can be subdivided into a primary physical, followed by a secondary chemical and biological stage (Her et al., 2017; Münter & Weber, 2006). The primary physical stage describes the direct interaction of photons (or ion beams) with the medium a few nanoseconds after exposure (Münter & Weber, 2006). Energy is deposited, causing either direct damage or inducing secondary electrons and free radicals, which may cause further damage (Haume et al., 2016). The secondary stage describes the chemical and biological aftermath in the cell triggered by irradiation (Münter & Weber, 2006). During the chemical stage, reactive species interacting with their surroundings are produced (Haume et al., 2016). Reactive species are atoms or molecules with an unpaired spin electron on the outer

electron orbit, which are chemically highly reactive and cause oxidative stress (Sauer, 2010b), such as hydroxyl radicals, superoxide radicals, hydrogen peroxide, free radicals, and products of the radiolysis of water (Her et al., 2017). Oxidative stress is the main pathway in which radiation mediates cell killing (Her et al., 2017; Herrmann et al., 2006). Studies have shown that DNA is primarily damaged by these radicals instead of direct DNA fragmentation in a 70:30 proportion, respectively (Haume et al., 2016; Kavanagh et al., 2013). The biological stage further defines how the cell copes with the induced damages from minor disturbances, including cell cycle disruption, to major complications, such as cell death (Münter & Weber, 2006).

1.2.3 Interaction of direct ionising radiation

During directly ionising radiation, the energy absorption and biological effect occur in the same molecule (Herrmann et al., 2006; Sauer, 2010b). When particle radiation penetrates matter, the surrounding electric field can knock electrons out of their atomic shell, leaving ions behind (Münter & Weber, 2006). Upon entry, the radiation is decelerated and thus has a finite range, as opposed to indirectly ionising radiation (Herrmann et al., 2006; Münter & Weber, 2006). During indirect ionising radiation, the energy absorption and biological effect occur in different atoms, where the damage of target molecules occurs via the intermediate reactive radicals (Herrmann et al., 2006; Münter & Weber, 2006). The probability of an ionising effect in the tissue rises with the particle's increasing charge and decreasing velocity (Herrmann et al., 2006).

1.2.4 Interaction of indirect ionising radiation

Suppose photons, i.e., wave radiation, collide with atoms, energy can be absorbed or scattered, enabling the following physical interactions: The photoelectric effect describes a phenomenon whereby an incoming photon is taken up by an electron of an atom's inner shell, causing the electron to be expelled (Jäkel & Karger, 2006). This ionisation process is followed by the de-excitation process, where a high-energy outer electron fills the vacancy (Jäkel & Karger, 2006). The difference in energy between the shells is emitted as low-energy photons (fluorescence) or secondary electrons, so-called Auger electrons (Hainfeld et al., 2008; Haume et al., 2016; Her et al., 2017; Jäkel & Karger, 2006; Kobayashi et al., 2010; Sauer, 2010b). In this work, an irradiation energy of 200 keV was used, utilising Auger electrons as a method of radioenhancement. The Compton effect is an example of inelastic scattering. When an incoming photon collides with a weakly bound electron, energy is transferred to the electron with consecutive ejection from its orbit and scattering of the incoming photon (Her et al., 2017;

Jäkel & Karger, 2006; Kobayashi et al., 2010). The Compton scattering process becomes especially relevant at energies higher than 500 keV (Kuncic & Lacombe, 2018). In turn, the emission of Compton electrons leads to a successive photoelectric effect (Mesbahi, 2010; Sauer, 2010b). At very high energies (>1022 MeV), pair formation may occur, where a photon and an atomic nucleus are transformed into an electron-positron pair (Jäkel & Karger, 2006; Sauer, 2010b). Other phenomena, such as Rayleigh-scattering, where photons collide with an entire atom, are nearly negligible since virtually no energy is deposited in the surrounding tissue (Hainfeld et al., 2008).

1.2.5 Linear energy transfer

The linear energy transfer (LET) (defined as keV/µm) is a unit of measurement to objectify the effect of radiation (Münter & Weber, 2006). It determines the ionisation density, i.e., the number of ionisation events along the radiation path in the tissue (Münter & Weber, 2006). However, since it is challenging to determine the ionisation density, the average energy loss per distance is used instead (Herrmann et al., 2006; Münter & Weber, 2006; Sauer, 2010b). A distinction is made between radiation with high LET, that is, densely ionising radiation such as alpha rays, protons, and neutrons, and radiation with low LET (<3.5 keV/µm), that is, loosely ionising radiation such as X- and gamma-rays (Münter & Weber, 2006). Radiation with low LET predominantly causes indirect damage (Münter & Weber, 2006). As the LET increases, the proportion of direct damage also increases (Herrmann et al., 2006; Münter & Weber, 2006).

1.2.6 Relative biological effectiveness

The relative biological effectiveness (RBE) is a distinguishing factor for different types of radiation with respect to their biological results (Herrmann et al., 2006; Sauer, 2010b). It depends, among other things, on the LET, the fractionation mode, the irradiated tissue, and the effect under consideration (Herrmann et al., 2006). The RBE is defined by the following equation, where the dose of any radiation under investigation is compared to the dose of the reference radiation, X-rays of 250 keV (Herrmann et al., 2006; Münter & Weber, 2006; Sauer, 2010b):

$$\mathrm{RBE} = \frac{\text{Energy (Gy) of the reference radiation}}{\text{Energy (Gy) of the radiation to be examined}}.$$

1.2.7 Effect of ionising radiation on cells

As seen before, the secondary stage summarises the effect of ionising radiation on cells. It involves the chemical and biological aftermath following irradiation (Herrmann et al., 2006; Münter & Weber, 2006). The biological stage includes DNA damage, metabolism disturbances, gene mutation, inhibition of proliferation, and cell death (Münter & Weber, 2006). However, the most important effects on cells are mutations and clonogenic cell death (Herrmann et al., 2006). Clonogenic cell death describes the loss of the unlimited ability to divide, meaning cells are no longer able to form colonies of 50 cells or more (Herrmann et al., 2006).

1.2.8 Effect of radiation on the cell cycle

The extent of the radiation effect on the cells depends on the cell cycle phase and the time point of the irradiation (Münter & Weber, 2006). The cell cycle can be divided into two main stages: Mitosis, where the cell replicates, and interphase (Münter & Weber, 2006). Interphase can be further subdivided into the G_1-Phase, the first phase following mitosis characterised by the synthesis of the cytoplasm and cell organelles, as well as enzymes and DNA in preparation for DNA-replication (Münter & Weber, 2006). It is also known as the growing phase (Münter & Weber, 2006). During the S-Phase, DNA replication takes place. Chromosomes now comprise two sister chromatids (Münter & Weber, 2006). During the G_2-Phase, protein synthesis and cell growth occur in preparation for mitosis (Münter & Weber, 2006). The G_0-Phase is a resting phase where cells leave the cell cycle indefinitely (Münter & Weber, 2006). They may return to the G_1 phase or differentiate and eventually die (Münter & Weber, 2006; Sauer, 2010b).

Different phases of the cell cycle show varying radiosensitivity: In the late G_2-Phase and mitosis, the radiosensitivity is highest, whereas during the S-Phase, cells are most radioresistant (Herrmann et al., 2006; Münter & Weber, 2006; Pawlik & Keyomarsi, 2004; Sauer, 2010b). Under physiological conditions, the cell cycles of various cells in an organism are asynchronous (Münter & Weber, 2006; Sauer, 2010b). Radiation also influences the movement through various phases by activating checkpoint inhibitors (Kastan & Bartek, 2004). Checkpoint inhibitors mediate the progression into the next phase, allowing for damages to the genome to be repaired or for apoptosis to be activated if the damage is irreparable (Cui, Her, Borst, et al., 2017; Her et al., 2017; Kastan & Bartek, 2004).

1.2.9 Effect of radiation on the DNA

DNA is considered the principal target of radiotherapy (Cui, Her, Borst, et al., 2017). As a result of irradiation, a series of DNA damages may occur: Base damage, with modification or loss of a base or base pair; single-strand breaks (SSB), showing an interruption of a DNA strand due to a split in the phosphodiester bonds; double strand breaks (DSB), where both DNA strands are interrupted; DNA-crosslinking, where a link between both DNA strands forms as a result of high radiation dose; DNA-protein-crosslinking, where DNA strands bind to surrounding proteins; or bulky lesions, representing locally multiply damaged lesions where several of the damages above occur near one another (Herrmann et al., 2006; Münter & Weber, 2006). Bulky lesions are usually irreparable (Münter & Weber, 2006). Which form of DNA damage occurs depends on the dose and type of irradiation administered, where high LET predominantly causes severe and irreparable damage, and low LET generally causes milder impairments (Herrmann et al., 2006). In addition to the DNA, damage to proteins or cell organelles may occur (Herrmann et al., 2006; Münter & Weber, 2006; Sauer, 2010b).

1.2.10 DNA repair mechanism

As a consequence of irradiation, around 4,000–5,000 DNA damages occur per cell, of which around 30–40 are DSB (Herrmann et al., 2006). Minor damages, such as base loss or modification, are usually corrected effectively by base excision repair (Haume et al., 2016; Herrmann et al., 2006). The DNA-glycosylase removes the modified base, leaving behind an apurinic or apyrimidinic (AP) site (Netzker, 2012). The AP-endonuclease hydrolyses the DNA backbone's phosphodiester bond, creating a SSB (Netzker, 2012). The DNA-polymerase removes the damaged region and inserts the correct nucleotide using the complementary strand as a template (Netzker, 2012). Finally, the DNA-ligase fuses the strands (Netzker, 2012).

The nucleotide excision repair is necessary when large, bulky damages occur. The enzyme helicase unwinds around 25 base pairs, and endonucleases remove the damaged region (Netzker, 2012). The DNA-polymerase adds the correct nucleotides and the DNA-ligase fuses the strands (Netzker, 2012). For simple SSB, joining the sugar-phosphate backbone with the help of a ligase is often sufficient (Netzker, 2012; Sauer, 2010b). A mismatch-repair system recognises and corrects mispaired base pairs (Netzker, 2012; Sauer, 2010b).

DSB, where both double helix strands are detached, are more fatal to the cell (Netzker, 2012). Chromosomal translocations or gaps may occur (Netzker, 2012). The lost information

cannot be recovered by the complementary strand since neither strand serves as a template (Netzker, 2012). Primarily, two mechanisms for the repair of DSBs exist (Netzker, 2012; Sauer, 2010b): Homologous recombination can only take place at the end of the S-Phase or the G_2-Phase, where two identical copies of the double helix are present (Netzker, 2012). The sister chromatid serves as a template to repair the damage (Netzker, 2012). Non-homologous end joining (NHEJ) may take place at any point during the cell cycle; however it often contains errors (Netzker, 2012). In NHEJ, ligation of the severed ends of the strand occurs, whereby small deletions may arise (Netzker, 2012; Sauer, 2010b).

1.2.11 Cell death

If these damages are only partially or incorrectly repaired, mutations may occur (Münter & Weber, 2006). If the cell is unable to eliminate the existing errors, cell death is initiated to contain irreparable damages. Three forms of cell death may arise following irradiation, as illustrated in Figure 2: First, apoptosis (Figure 2B) is a form of programmed cell death where the cell decomposes in an organised manner and is phagocytised without an inflammatory reaction (Herrmann et al., 2006; Münter & Weber, 2006). Second, necrosis (Figure 2C) describes the non-directed cell death with an accompanying inflammatory response (Herrmann et al., 2006). It is rapid and non-physiological as a result of major damage (Herrmann et al., 2006; Münter & Weber, 2006). Third, clonogenic cell death (Figure 2D) arises from the inability to form a colony from a cell clone (Herrmann et al., 2006; Münter & Weber, 2006). Cells are initially intact after irradiation; however, after a few replications, cells lose their ability to divide and perish (Herrmann et al., 2006; Münter & Weber, 2006). This is the most common form of cell death following irradiation (Münter & Weber, 2006). This phenomenon of clonogenic cell death can be represented in a dose-effect curve (Münter & Weber, 2006; Sauer, 2010b). At low irradiation doses, cells can effectively eliminate damages incurred, and the curve shows a shallow stretch (Münter & Weber, 2006; Sauer, 2010b). At higher doses, there is an exponential decrease in cell survival as damages become more lethal (Münter & Weber, 2006; Sauer, 2010b).

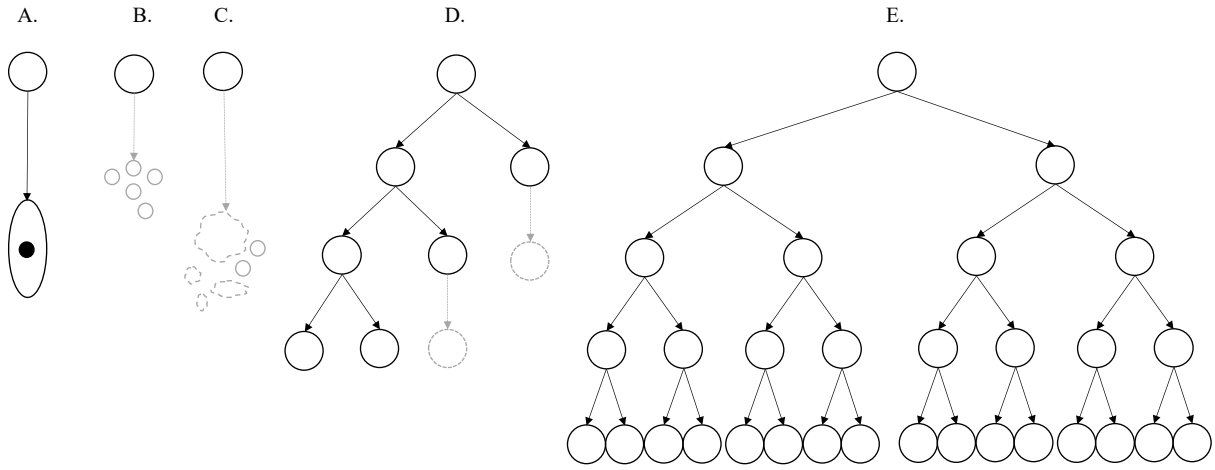

Figure 2 – Fate of irradiated cells

The fate of irradiated cells: A: The cell differentiates and stops dividing; B: The cell perishes from apoptosis; C: The cell perishes from necrosis with an accompanying inflammatory response; D: Clonogenic cell death, a cell is incapable of forming colonies; E: A cell survives and forms a colony. Diagram adapted from Herrmann et al. (2006).

1.2.12 Fractionated irradiation and radiosensitivity

In fractionated irradiation, the total dose is divided into several smaller doses (Herrmann et al., 2006; Sauer, 2010b). In conventional fractionation, this corresponds to a single dose of 1.8–2.0 Gy per unit of irradiation (Sauer, 2010b). These are administered five times per week for 5–7 weeks, which amounts to a cumulative dose of 45–60 Gy (Sauer, 2010b). The Bergonié-Ribondeau law states, that cells with a higher proliferation rate and lower degree of differentiation are generally more susceptible to irradiation (Münter & Weber, 2006). It is based on the theory, that healthy cells have a more remarkable ability to eliminate sublethal radiation damage (SLD), which does not kill the cell directly, than rapidly proliferating tumour cells (Münter & Weber, 2006). This finding can be described by the Elkind-recovery, where recuperation of SLDs occurs during radiation pauses (Herrmann et al., 2006; Sauer, 2010b; Schulz-Ertner et al., 2006).

The radiosensitivity of a tumour depends on many factors: The intrinsic and genetic radiosensitivity, tumour size, oxygenation (Cui et al., 2014), duration of irradiation, and individual lifestyle factors of the patient (Münter & Weber, 2006). Larger tumours and those with hypoxic areas tend to be more radioresistant (Cui et al., 2014; Münter & Weber, 2006). A long irradiation period may also increase radioresistance (Chen et al., 2020; Herrmann et al., 2006; Münter & Weber, 2006; Sauer, 2010b). In addition, the 5 Rs of radiotherapy are of great

importance: Repopulation, where cell proliferation may occur between irradiation sessions, meaning higher doses are needed to kill the larger number of cells (Münter & Weber, 2006; Sauer, 2010b); repair, where increased survival of tumour cells occurs due to the repair of SLDs and potentially lethal radiation damage (PLD) (Münter & Weber, 2006; Sauer, 2010b); reoxygenation, where radiation has a greater effect on oxygenated cells than on hypoxic cells, meaning as the radiation therapy progresses, the number of tumour cells decreases and the oxygen supply to the remaining cells improves increasing the radiation effect with the course of treatment (Münter & Weber, 2006; Sauer, 2010b); redistribution, meaning cells located in radioresistant cell cycle phases at one point of irradiation will be in a radiosensitive phase at another timepoint of irradiation (Münter & Weber, 2006; Sauer, 2010b); and radiosensitivity, describing the intrinsic radiosensitivity of the tumour. In summary, reoxygenation and redistribution increase radiosensitivity, whereas repair and repopulation increase radioresistance (Münter & Weber, 2006).

1.2.13 Side effects of radiotherapy

Radiation therapy is generally very well tolerated. Side effects are undesirable associated symptoms that may limit the dose application. A distinction is made between acute and chronic side effects depending on the time of occurrence, as well as between local and systemic side effects according to their extent (Münter & Weber, 2006). Acute damage occurs within 90 days, and the extent typically depends on the duration of exposure (Münter & Weber, 2006). Tissues with high cell turnover are particularly affected (Münter & Weber, 2006). Chronic damage, which occurs 90 days or more after irradiation, is more likely to affect tissues with low cell turnover, connective tissue, and the vascular system (Münter & Weber, 2006). Regarding breast irradiation, the damage is predominantly to the lungs, heart, skin, carotid vessels, and brachial plexus (Münter & Weber, 2006; Sauer, 2010b; Tudda et al., 2022). This study aims to help develop and improve existing methods using radiosensitisers to enhance the energy deposited in the tumour while preserving surrounding tissue and minimising side effects.

1.3 Gold nanoparticles

The involuntary damage caused by the non-specific deposition of energy in healthy tissue along the photon pathway still poses a major issue for modern radiotherapy, limiting the radiation dose one can administer (Greish, 2007; Hainfeld et al., 2008; Haume et al., 2016; van de Looij et al., 2022). In recent years, many improvements have been made to tackle this issue, such as intensity-modulated radiotherapy (IMRT), image-guided radiation therapy (IGRT), stereotactic radiotherapy, or multimodal cancer therapies (Chen et al., 2020; Cui, Her, Borst, et al., 2017; Haume et al., 2016; Tudda et al., 2022; Wang et al., 2018). Nonetheless, there is a need to further reduce the radiation delivered to surrounding tissue to decrease the risk of toxic side effects while maintaining the therapeutic dose delivered to malignant cells (Kobayashi et al., 2010; Li et al., 2020).

A novel technique under investigation is the use of so-called 'radiosensitisers'. Radiosensitisers are defined as substances that increase the susceptibility of tumour cells towards radiation-induced killing without affecting healthy tissue (Chen et al., 2020; Li et al., 2020; Wang et al., 2018). Radiosensitisers include chemotherapeutics such as Docetaxel, Cisplatin (Alhussan et al., 2021), or nanotechnology. Nanotechnology is a burgeoning field in medicine and pharmaceutics that uses nanometre dimensions to improve and establish diagnosis and treatment methods (Aminabad et al., 2019; Gerosa et al., 2020). These radiosensitisers can be classified into five subgroups, namely suppressors of thiols and endogenous protective substances against irradiation damage, generators of radicals through the radiolysis of water, inhibitors of repair mechanisms, thymine analogues with the ability to integrate into the DNA, and substances that mimic oxygen and its electrophilic properties (Adams, 1973; Fowler et al., 1976; Wang et al., 2018). When using radiosensitisers, the radiation effect can be enhanced by up to 100 times (Chen et al., 2020; van de Looij et al., 2022; Wu et al., 2023).

This work will focus on gold and gold-coated nanoparticles (AuNPs) and their effect on increasing the radiosensitivity of tumour cells. This is known as 'gold nanoparticle-assisted radiation therapy (GNRT)' (Cooper et al., 2014; Li et al., 2020; Zygmanski & Sajo, 2016).

1.3.1 Physicochemical properties of nanoparticles

1.3.1.1 Synthesis

There are two main ways in which AuNPs can be produced: First, the top-down method, where structures are removed from bulk materials until nanosized structures are reached, and second, the bottom-up method, where atoms or molecules are assembled to form nanoparticles (Aminabad et al., 2019; Sibuyi et al., 2021; Yu et al., 2020). By changing the ratio of reactants, adding ligands (Fan et al., 2020), UV radiation, changing the pH, reaction time, etc., the shape and size of the nanoparticles can be modified (Aminabad et al., 2019; Mieszawska et al., 2013; Tao, 2018; Yu et al., 2020). The most common and simplest synthesis method is reducing gold salts to metallic gold using reducing agents (Mieszawska et al., 2013).

1.3.1.2 Size

Nanoparticle size is vital in determining biodistribution properties and their interaction with radiation. To avoid accumulation and toxicity of the liver, heart, and other organs, nanoparticle elimination from an organism should occur within a few days (Haume et al., 2016). Nanoparticles smaller than 6–10 nm are typically cleared rapidly by the kidneys, whereas larger particles are more likely to accumulate in the liver (Alexis et al., 2008; Almeida et al., 2011; Bertrand & Leroux, 2012; Haume et al., 2016; Longmire et al., 2008).

Size also affects the cellular uptake of nanoparticles. To date, the maximum uptake is achieved for particles ranging from 20–60 nm in size (Chithrani et al., 2006; Perrault et al., 2009; S. Zhang et al., 2009). Smaller particles, however, are able to penetrate further into the tumours and accumulate in tumour cells due to the enhanced permeability and retention effect (EPR) (Chen et al., 2020; de Lazaro & Mooney, 2020; Haume et al., 2016; Lee et al., 2014; van de Looij et al., 2022). This enables a more even distribution in large tumours. Some studies suggest nanoparticles less than 10 nm in size may even enter the nucleus (Cui, Her, Borst, et al., 2017; Fan et al., 2020; Huang et al., 2012; Lee et al., 2014).

Smaller nanoparticles interact more with the radiation (Carter et al., 2007; Lin et al., 2015). This might be explained as follows: As AuNPs become larger, more ionising events and interactions of secondary electrons occur within the particle structure, meaning less dose is deposited around the nanoparticle (Haume et al., 2016; McMahon et al., 2011). In addition, the highly curved surface of smaller particles causes structural defects and disruption in the electron configuration, leading to the enhanced formation of reactive sites (Cui, Her, Borst, et al., 2017).

In conclusion, the optimal nanoparticle size is believed to be around 5 nm in size (Cui, Her, Borst, et al., 2017).

Interestingly, shape also influences cellular uptake and toxicity, where spherical AuNPs show superior uptake and toxicity compared to nanorods or nanospikes (Aminabad et al., 2019; Gerosa et al., 2020; Ma et al., 2017). Concerning toxicity and nanoparticle size, no definite statement has been made (Haume et al., 2016); however, most studies suggest little toxicity for the currently used AuNP sizes (Lee et al., 2014). Considering the aforementioned factors, a spherical AuNP sized 4 nm was chosen for this study.

1.3.1.3 Surface charge

AuNPs with a positive surface charge are believed to be taken up by cells more readily due to interactions with the lipid membrane bearing a negative charge (Albanese et al., 2012; Beddoes et al., 2015; Tao, 2018). Simulations performed by Da Rocha et al. (2013) suggested that the charge on the particles influences the uptake pathway, where neutral or slightly positively charged AuNPs may exert a passive translocation across the membrane. In contrast, highly cationic AuNPs were predominately taken up via endocytosis. Positively charged AuNPs, however, are more likely to be opsonised by negatively charged proteins in the bloodstream and thus eliminated faster (Alexis et al., 2008; Alric et al., 2013; Haume et al., 2016; Owens & Peppas, 2006). Alterations to the surface charge can be made by adding peptides or other molecules as surface coating (Haume et al., 2016).

1.3.1.4 Concentration

The concentration of any agent is a critical factor in the effectiveness of a treatment. In early studies completed by Hainfeld et al. (2004), the effect of radiosensitisation was strongly dependent on the concentration of nanoparticles inside the cell. Since then, studies have suggested that in addition, the location of AuNPs within the cell is essential in determining the dose enhancement factor (DEF) (Babaei & Ganjalikhani, 2014; Chithrani et al., 2010; Kong et al., 2008; Mesbahi et al., 2013).

1.3.1.5 Coating and conjugating

The coating and conjugation of nanoparticles enable targeted delivery and selective uptake into cancer cells (Haume et al., 2016), addressing the desire for high intratumoural concentrations. Coating of nanoparticles is performed for several reasons: First, it helps to modify the interactions with other molecules and proteins in the blood (Krpetic et al., 2014;

Monopoli et al., 2012; Monopoli et al., 2011). Second, the surface charge can be controlled via nanoparticle coating, altering the opsonising and aggregation (Alexis et al., 2008; Alkilany & Murphy, 2010; Haume et al., 2016; Owens & Peppas, 2006). Third, the lifetime of nanoparticles in the organism and cellular uptake can be mediated (Chithrani et al., 2009; Saptarshi et al., 2013). Finally, it allows for passive and active targeting of tumour cells (Akhter et al., 2012; Chen et al., 2020; Gehrmann et al., 2015).

1.3.1.6 Passive targeting

Abnormal vessels as a result of rapid angiogenesis and poor lymphatic drainage (de Lazaro & Mooney, 2020; Gao et al., 2021; van de Looij et al., 2022), combined with high endocytic uptake and altered metabolic activity of tumour cells result in an EPR effect of molecules (Chen et al., 2020; de Lazaro & Mooney, 2020; Gao et al., 2021; Haume et al., 2016; Lee et al., 2014; Liu et al., 2010; van de Looij et al., 2022). By coating AuNPs with polyethylene glycol (PEG), for instance, which is a hydrophilic linker of low molecular weight, the opsonising and uptake by the reticuloendothelial system (RES) in vivo can be avoided (Chen et al., 2020; Gao et al., 2021; Gerosa et al., 2020). The nanoparticles thus feature a higher blood circulation time, allowing for an increased passive uptake into cancer cells (Alexis et al., 2008; Aminabad et al., 2019; Chen et al., 2020; Gao et al., 2021; Gerosa et al., 2020; Haume et al., 2016; Liu et al., 2010; Mieszawska et al., 2013; Owens & Peppas, 2006). This concept is known as the 'PEGylation' (Gerosa et al., 2020). Alternative coating polymers include polystyrene sulfonate (PSS), polyvinylpyrrolidone (PVP) (Yu et al., 2020), and bovine serum albumin (BSA), demonstrating colloidal biocompatibility with the absence of haematological response (Gao et al., 2021). Furthermore, not only do nanoparticles influence cellular junctions, morphology, and motility but also induce gaps between adjacent cells (Wang et al., 2018). This is known as nanomaterial-induced endothelial leakiness (NanoEL) and aids nanoparticle accumulation in tumour tissue (Wang et al., 2018). However, the stance of the EPR effect has been challenged in recent years, with studies suggesting that transcytosis plays the predominant role in the extravasation of nanoparticles (de Lazaro & Mooney, 2020; Sindhwani et al., 2020).

1.3.1.7 Active targeting

During active targeting, nanoparticles are functionalised with, among others, specialised antibodies (Chen et al., 2020; Gehrmann et al., 2015; Singh et al., 2018), peptides (Kumar et al., 2012), or hormones (Dreaden et al., 2012; Dreaden et al., 2009) to selectively target tumour cell receptors, antigens, or surface molecules (Chen et al., 2020). This enables an increase in

uptake from 2–5% in passive targeting to 6–13% in active targeting (Yu et al., 2020). Such targets include the EGFR (Liu et al., 2015; Shevtsov et al., 2014), the luteinising hormone receptor (LHRH) in prostate cancer (Wolfe et al., 2015), HER2-targetting with trastuzumab (Chattopadhyay et al., 2013; Chattopadhyay et al., 2010; Hainfeld et al., 2011), and membrane heat shock protein 70 (Hsp70) (Gehrmann et al., 2015; Shevtsov et al., 2015; Stangl, Gehrmann, Dressel, et al., 2011; Wu et al., 2023). The SH end of PEG-linkers binds the surface of the AuNP, while molecules for specific tumour targeting can be attached at the other end (Aminabad et al., 2019).

1.3.2 Use in diagnostics and therapy

As previously stated, AuNPs have several advantageous properties that make them effective radiosensitisers: They express good biocompatibility (Lee et al., 2014; Singh et al., 2018), their synthesis is easy and versatile (Aminabad et al., 2019; Mieszawska et al., 2013; Singh et al., 2018), and they possess unique behaviour for diagnostic imaging and therapeutic purposes (Hainfeld et al., 2008; Haume et al., 2016; Lee et al., 2014).

1.3.2.1 Photothermal therapy

The local surface plasmon resonance (LSPR), which enables the absorption of light, is a unique property of gold (Aminabad et al., 2019; Gao et al., 2021; Singh et al., 2018). LSPR describes a phenomenon, where electrons oscillate and resonate collectively at the metal interface when interacting with an electric field, causing absorption and scattering of light (Aminabad et al., 2019; Gao et al., 2021; Her et al., 2017; Singh et al., 2018; Yu et al., 2020). The wavelength of the LSPR depends on the size and shape of the AuNP, ranging from UV to near infrared (NIR) (Gao et al., 2021; Gerosa et al., 2020; Her et al., 2017; Lee et al., 2014). In photothermal therapy (PTT), this conversion of electromagnetic energy to thermal energy is used against tumours (Her et al., 2017; Kaur et al., 2011; Singh et al., 2018; van de Looij et al., 2022; Yu et al., 2020). Mild hyperthermia sensitises cells to both radio- and chemotherapy (Her et al., 2017; Kaur et al., 2011) by enhancing the blood flow and consecutively reducing the number of hypoxic, radioresistant cells (Diagaradjane et al., 2008; Her et al., 2017), increasing vascular permeability following localised necrosis (Diagaradjane et al., 2008; Her et al., 2017), altering DNA damage response (Her et al., 2017; Kaur et al., 2011), and activating immunological pathways (Kaur et al., 2011).

1.3.2.2 Chemotherapy

AuNPs can be conjugated with anti-cancer drugs and used as targeted drug delivery systems (TDDS) to increase drug concentration at the desired site, while allowing lower therapeutic dosage (Aminabad et al., 2019; Singh et al., 2018). The application of Cisplatin, a common radio-enhancing drug used in chemotherapy, is limited due to hematologic and renal toxicities (Begg, 1990; Yang et al., 1995). Such dose limitations could be addressed by conjugation to AuNPs and consequently improved tumour delivery (Cui, Her, Dunne, et al., 2017; Her et al., 2017). Cui et al. (2017) showed, that combining Cisplatin and AuNPs significantly enhanced the radiation effect in TNBC cells, rendering superior effects compared to individual treatments. The combination of AuNPs with Paclitaxel and Docetaxel has also been tested (Lee et al., 2014).

1.3.2.3 Photodynamic therapy

Photodynamic therapy (PDT) is a non-invasive method of cancer treatment, where photosensitisers such as porphyrin are used to generate reactive oxygen species (ROS) and damage cancerous cells (Gao et al., 2021; Garcia Calavia et al., 2018; Singh et al., 2018). The photosensitising agent is administered intravenously and excited by light at various wavelengths, causing an energy transfer and the generation of ROS, fluorescent light, or heat (Gao et al., 2021). AuNPs pose a drug delivery system for radiosensitisers, enhancing their uptake into tumour cells. Additionally, AuNPs provide stability, enhance ROS formation, and enable the combination of PTT and PDT (Gao et al., 2021; Garcia Calavia et al., 2018; Singh et al., 2018).

1.3.2.4 Radiotherapy

Nanoparticles used in radiotherapy have improved dose localisation (Hainfeld et al., 2008; Liu et al., 2010; Polf et al., 2011). Hainfeld et al. (2004) published a pioneering study, showing a significant increase in the survival of mice from 20% to 86% with xenograph mammary carcinomas after being treated with 1.9 nm-sized AuNPs and undergoing radiation therapy with 250 kVp (Hainfeld et al., 2004). The mechanism by which AuNPs enhance radiation can be divided into three major stages: Physical, chemical, and biological (Her et al., 2017).

As seen before, the physical stage describes the immediate interaction of irradiation with the tissue. The relevant interactions of photons with gold are photoelectric absorption,

Compton scattering, Rayleigh scattering, and electron-positron pairing (Chen et al., 2020; Kuncic & Lacombe, 2018; Li et al., 2020). Which emission takes place depends on the energy of the irradiation beam and the binding energy of the affected electrons (Cui, Her, Borst, et al., 2017; Her et al., 2017). Gold can enhance the radiation energy deposited in the surrounding tissue due to its strong photoelectric effect and X-ray absorption properties (Her et al., 2017). In the keV range, photons primarily interact with matter through the Compton and photoelectric effect (Her et al., 2017; Kuncic & Lacombe, 2018). During the photoelectric effect, Auger electrons may be given off, contributing most to the enhancement of radiation (Hainfeld et al., 2008; Kuncic & Lacombe, 2018; Li et al., 2020). Auger electrons are low-energy electrons of a few hundred eV emitted from an outer shell after irradiation (Li et al., 2020). If provided with sufficient energy, they will travel and collide with further atoms and AuNPs, causing subsequent ionisation of surrounding molecules or DNA and a cascade of further Auger electrons (Chen et al., 2020; Her et al., 2017; Kobayashi et al., 2010; Porcel et al., 2010). Auger electrons, however, only have a short travelling range of around 10 nm (Chen et al., 2020; Hainfeld et al., 2008; Kuncic & Lacombe, 2018; Li et al., 2020). Porcel et al. (2010) further suggested that after the emission of Auger electrons, the remaining positively charged gold ion may cause surrounding water molecules to dissociate, additionally increasing the formation of radicals. The high atomic number of gold ($Z_{Au} = 79$) in comparison to that of organic material ($Z_C = 6$, $Z_N = 7$) means more radiation is attenuated, and Auger electron emission is more likely to occur, described by $(Z/E)^3$, with Z being the atomic number and E the photon energy (Chen et al., 2020; Coulter et al., 2013; Her et al., 2017; Kobayashi et al., 2010; Porcel et al., 2010; Tudda et al., 2022; van de Looij et al., 2022).

During the chemical stage, reactive species interact with the matter. AuNPs can enhance this effect depending on their localisation inside the cell: Direct chemical sensitisation of DNA requires nuclear localisation and binding of AuNPs to the DNA (Her et al., 2017). The formation of radicals via activation of the AuNP surface is possible elsewhere in the cell (Her et al., 2017). Very low energy electrons (<10 eV), emitted from AuNPs in the presence of DNA, induce the production of transient-negative ions, weakening DNA bonds despite their non-ionising properties (Her et al., 2017; Yao et al., 2015). Most studies to date, however, show an endo-lysosomal pathway of AuNPs upon uptake, hindering a nuclear entry (Her et al., 2017).

During the biological stage, the cell deals with the consequences of radiation exposure. The key pathways affected are the cell cycle disruption, oxidative stress, and the inhibition of DNA damage repair (Cui, Her, Borst, et al., 2017). Oxidative stress caused by the formation of

ROS plays a vital role in determining the cell's fate (Cui, Her, Borst, et al., 2017). For instance, Pan et al. (2009) correlated increased ROS production after AuNP treatment with a loss of mitochondrial membrane potential and apoptosis. The additional treatment with thiol group antioxidants, such as glutathione, neutralised and counteracted the oxidative effects of AuNPs (Pan et al., 2009). Wu et al. (2023) showed increased ROS formation after treatment with TPP-PEG4-FeAuNPs and subsequent irradiation compared to irradiation alone. This effect could be counteracted by N-acetyl-L-cysteine (NAC), an effective ROS scavenger (Wu et al., 2023). These findings suggest, that AuNPs promote ROS formation as well as bind thiol groups of antioxidants, depriving the cell of its endogenous reducing agents (Her et al., 2017). Furthermore, metallic nanoparticles have been shown to mediate the 'bystander effect', whereby tumour cells release cytokines, ROS, and other signalling molecules to interact with their surroundings (Wang et al., 2018). This mechanism has been predicted to play an additional important role in radiosensitisation (Wang et al., 2018).

1.3.2.5 Cell cycle effects

Different studies on the cell cycle disruption caused by AuNPs have been completed. Some suggest cell cycle alterations with enhanced radiation effect (Wang et al., 2018), while others reported no impact (Cui et al., 2014; Pan et al., 2009). For instance, in human oral squamous cell carcinoma, AuNP treatment showed an increase in the S-phase population (Mackey & El-Sayed, 2014). In ovarian (SKOV-3), breast (MDA-MB-231 and 4T1), lung (A549), and prostate (DU-145) cancer cells, AuNPs caused an accumulation of cells in the G2/M phase leading to increased radiosensitivity (Geng et al., 2011; Wang et al., 2015; Wang et al., 2013; Wu et al., 2023).

To summarise, the use of AuNPs to enhance radiosensitivity in conventional radiotherapy is a growing branch of research. Gold can enhance the radiation energy deposited in the tissue due to its strong photoelectric effect and X-ray absorption properties, enabling the production of Auger electrons and reactive species (Her et al., 2017). Nanoparticle production is simple and versatile, with countless conjugation options. This allows for the specific targeting of malignant cells, optimising uptake and tumour control (Haume et al., 2016). This study used hybrid AuNPs with an iron oxide core coupled to PEG4 and TPP, a peptide specifically targeting mHsp70 on the cell surface of malignantly transformed cells, to enhance radiosensitisation in TNBC.

1.4 Heat shock protein 70

The heat shock response (HSR) was first described in the early 1960s by Ferruccio Ritossa, who discovered an upregulation in the expression of heat shock proteins (HSPs) after exposure to elevated temperatures in the salivary glands of *Drosophila melanogaster* (Ritossa, 1962). Since then, HSPs have been intensely studied. In addition to heat, a variety of other extrinsic stressors, such as anoxia, ethanol, irradiation, pH alteration, and oxidative stress (Lindquist & Craig, 1988), as well as intrinsic stressors, including replicative or oncogenic stress (Lindquist & Craig, 1988; Murphy, 2013), nutrient deprivation, inflammation, infection, and tissue injury (Jindal, 1996) have been found to upregulate HSPs for cytoprotection.

HSPs are highly conserved proteins in evolution that are ubiquitously expressed in all organisms, from archaebacteria to plants and animals (Daugaard, Rohde, et al., 2007; Kiang & Tsokos, 1998; Lindquist & Craig, 1988). They are distinguished and named according to their molecular weight, ranging from 8 kDa to 110 kDa (Moseley, 2000), as well as their location or function (Li & Srivastava, 2004). The term 'heat shock protein' includes the HSPs, glucose-related proteins (GrP), and ubiquitin (Moseley, 2000). In the following section, the structure, function, and role in oncology of Hsp70 will be discussed.

1.4.1 Structure and occurrence

The human Hsp70 family of molecular chaperones consists of 13 known gene products that are highly homologous, varying in size between 66 kDa and 78 kDa (Tavaria et al., 1996), differing in their sub-cellular location, tissue-specific occurrence, and expression level (Daugaard, Rohde, et al., 2007; Murphy, 2013; Radons, 2016). The Hsp70s are made up of an approximately 44 kDa amino-terminal fragment, which contains the ATPase domain responsible for the hydrolysis of adenosine triphosphate (ATP) to adenosine diphosphate (ADP), and an approximately 28 kDa carboxy-terminal substrate binding domain (Flaherty et al., 1990; Hartl, 1996; Kiang & Tsokos, 1998; Murphy, 2013; Radons, 2016). HSPs which are not specific to the endoplasmic reticulum (ER) or the mitochondrion, have a C-terminal EEDV motif domain, involved in the regulation of Hsp70 activity and the interaction with other molecular chaperones (Freeman et al., 1995; Hartl, 1996; Murphy, 2013; Radons, 2016). Figure 3 provides a visual illustration of the Hsp70 structure.

Figure 3 – Hsp70 structure

Common domain structure of Hsp70 chaperones. Own representation adapted from Radons (2016)

Hsp70 is constitutively expressed and can predominantly be found intracellularly (Tavaria et al., 1996) in the nucleus, cytosol, mitochondria (Daugaard, Rohde, et al., 2007; Radons, 2016), ER (Daugaard, Rohde, et al., 2007; Haas, 1994; Kiang & Tsokos, 1998), and in lysosomes (Mambula & Calderwood, 2006; Terlecky, 1994). Additionally, Hsp70 has been found in the extracellular space (Pockley et al., 2014; Radons, 2016; Vega et al., 2008) and on the plasma membrane of virally infected cells or cells which are malignantly transformed (Gehrmann et al., 2005; Hantschel et al., 2000; Moseley, 2000; Multhoff, Botzler, Wiesnet, Muller, et al., 1995; Multhoff & Hightower, 1996).

The two major representatives of the Hsp70 family, which exert 86% identity (Radons, 2016), are the constitutively expressed heat shock cognate protein 70 (Hsc70 or Hsp70-8) with a molecular weight of 73 kDa (De Maio, 1999) and the major stress-inducible heat shock protein 70 (Hsp70 or Hsp70-1) with a molecular weight of 72 kDa (Kiang & Tsokos, 1998). Hsp70-1 is a collective name for Hsp70-1a and Hsp70-1b and can be upregulated in response to different stressors (Lindquist & Craig, 1988). In newer literature, it is also called HSPA1A (Kampinga et al., 2009). In this work, I will focus on the major stress-inducible heat shock protein 70, henceforth referred to as Hsp70.

1.4.2 Function

1.4.2.1 Protein homeostasis

Molecular chaperones have been defined as proteins that bind and preserve unstable polypeptide chains and, through controlled binding and releasing, help achieve their correct outcome, be it folding, proper assembly of subunits, transport across membranes, or appropriate disposal (Hartl, 1996). As molecular chaperones, HSPs are involved in a variety of cellular processes. Under physiological conditions, they play an essential role in protein synthesis by mediating the correct folding of nascent proteins, preventing protein aggregation, refolding misfolded proteins, and dissolving aggregated proteins (Hartl, 1996; Hartl & Hayer-Hartl, 2002; Kiang & Tsokos, 1998; Mayer & Bukau, 2005; Radons, 2016). Under stress, be it exogenous or endogenous, polypeptides tend to unfold, denature, and degrade (Hartl, 1996).

This increases the need for protein repair and cytoprotection, demanding an upregulation of HSPs (Morimoto, 1998).

1.4.2.2 Apoptosis

The two most common forms of cell death are apoptosis and necrosis. Necrosis follows irreversible damage from the outside, causing the uncontrolled release of cell organelles into the extracellular space accompanied by an inflammatory response. In contrast, apoptosis is an active and programmed cell death triggered by extrinsic or intrinsic stimuli. During the latter, the cell shrinks, chromatin condenses, the DNA is disassembled, and the cell's content is released in vesicles in a controlled manner to be phagocyted by macrophages. This mechanism is essential for cell differentiation, cell count homeostasis, elimination of damaged and infected cells, or development of immunotolerance. (Netzker, 2012)

During the intrinsic apoptosis pathway, stress signals activate the translation of pro-apoptotic proteins, causing an imbalance. This imbalance of anti- and pro-apoptotic proteins causes a release of mitochondrial apoptosis mediators such as Cytochrome C. Cytochrome C activates the apoptotic protease activating factor 1 (Apaf-1) and triggers its oligomerisation as well as the formation of the ‘apoptosome’, which in turn activates caspase-9. Caspase-9 activates the effector caspases, which break down vital cell proteins such as protein kinases, transcription factors, and the cytoskeleton, leading to cell death. (Beere et al., 2000; Netzker, 2012)

Hsp70 inhibits this process by binding to Apaf-1 and stopping the recruitment of pro-caspase-9 to the apoptosome (Beere et al., 2000; Ravagnan et al., 2001). Apaf-1 is one of many targets of Hsp70. Apoptosis-inducing factor (AIF) is a flavoprotein of the mitochondrial intermembrane and caspase-independent cell death effector (Joza et al., 2009; Ravagnan et al., 2001), which is translocated into the nucleus after permeabilization of the mitochondrial outer membrane (Joza et al., 2009; Ravagnan et al., 2001). AIF mediates nuclear apoptosis through chromatin condensation and DNA fragmentation (Joza et al., 2009). Hsp70 was found to bind and neutralise AIF, antagonising its pro-apoptotic function (Ravagnan et al., 2001).

1.4.2.3 Other functions

Besides protein synthesis and anti-apoptotic function, Hsp70 has been shown to assist in the transportation of newly synthesised products into the corresponding cell organelle (Hartl, 1996; Hartl & Hayer-Hartl, 2002; Kiang & Tsokos, 1998; Mayer & Bukau, 2005; Radons,

2016), control the activity of regulatory proteins and steroid HR (Mayer & Bukau, 2005; Zylicz et al., 2001), disassemble clathrin-coated vesicles after endocytosis (Daugaard, Rohde, et al., 2007; Hartl, 1996; Sousa et al., 2016), influence DNA replication (Helmbrecht et al., 2000), protect cells during mitosis against division abnormalities (Daugaard, Rohde, et al., 2007), and regulate cell growth by interacting with cell cycle control molecules (Zylicz et al., 2001). This involvement in regulating the cell cycle, signal transduction, and cell death, stresses the importance of Hsp70 in pathological processes, such as oncogenesis, autoimmune, and degenerative diseases (Mayer & Bukau, 2005).

1.4.3 Regulation and heat shock factors

The HSR is a defence mechanism of cells against endogenous and exogenous stress, whereby HSPs are upregulated (primarily Hsp70-1, the major stress-inducible HSP) (Lindquist & Craig, 1988), mediated mainly on a transcriptional level by heat shock factors (HSFs) (Mathew et al., 2001; Radons, 2016). In vertebrates, HSF-1 to HSF-4 are known to regulate the heat shock genes (Mathew et al., 2001). HSF-1 is considered the key transcription factor (Morimoto, 1998; Radons, 2016), which is activated rapidly in response to stress (Mathew et al., 2001). HSF-2, in contrast, is less of a transcriptional regulator but instead binds DNA, protecting it from damage (Mathew et al., 2001). Its activation is more selective, for instance, during differentiation (Mathew et al., 2001). Under physiological conditions, the HSFs are expressed in the cytosol in an inert, monomeric state, bound to Hsp70 and Hsp90 (Mathew et al., 2001; Radons, 2016). When cellular stress arises, the HSFs dissociate, enter the nucleus, and initiate the transcription and translation of HSPs (Kiang & Tsokos, 1998; Mathew et al., 2001; Morimoto, 1998; Radons, 2016; Shu & Huang, 2008; Wu, 1995).

1.4.4 Hsp70 in oncology

Malignant cells also make use of the manifold of functions exerted by Hsp70. Hsp70 performs various functions within cells, on the surface membrane, and in the extracellular space. Similar to physiological functions as a molecular chaperone, the upregulation of Hsp70 inside the cell might allow tumour cells to adapt to harsh microenvironments (Shu & Huang, 2008). Why Hsp70 is upregulated in tumour cells has yet to be fully understood. One hypothesis states, that the harsh intracellular environment, characterised by, for instance, low glucose, hypoxia, and proteotoxic stress in association with rapid proliferation, induces Hsp70 (Ciocca & Calderwood, 2005; Murphy, 2013; Radons, 2016). Another theory stipulates that the

increased existence of oncoproteins in the cell, both mutated and altered proteins, elicit Hsp70 upregulation (Ciocca & Calderwood, 2005; Murphy, 2013; Radons, 2016).

Multhoff et al. (1995) discovered the presence of Hsp70 on the membrane of tumour cells but not on corresponding healthy cells (Ferrarini et al., 1992; Hantschel et al., 2000; Multhoff, Botzler, Wiesnet, Muller, et al., 1995). Since then, a series of different tumour entities have been shown to express Hsp70 on their surface membranes, such as Ewing sarcoma, osteosarcoma (Multhoff, Botzler, Wiesnet, Muller, et al., 1995), pancreas carcinoma (Gastpar et al., 2005), acute myeloid leukaemia (Gehrmann et al., 2003), head and neck (Kleinjung et al., 2003), colorectal, lung, gastric, and breast cancer (Botzler, Schmidt, et al., 1998; Hantschel et al., 2000; Pfister et al., 2007). The density of mHsp70 expressed on tumour cells can be upregulated, similarly to the cytosolic Hsp70, after a series of stressors, such as irradiation (Gehrmann et al., 2005), hypoxia (Schilling et al., 2009), and treatment with tubulin-interacting chemotherapeutics, such as Vincristine and Paclitaxel (Gehrmann et al., 2002).

The association of Hsp70 with the surface membrane has been thoroughly studied. Hsp70 does not possess a transmembrane domain (Multhoff & Hightower, 1996). It is likely to interact directly with the lipid bilayer, as opposed to other membrane proteins as first described in 1989 by Hightower and Guidon (Hightower & Guidon, 1989). Further research revealed, that under physiological conditions, Hsp70 interacts with globotriaosylceramide (Gb3), a component of cholesterol-rich microdomains (lipid rafts) in the membrane of tumour cells, but not normal cells (Gehrmann, Liebisch, et al., 2008). Tumour cells, which were Gb3 positive, could bind soluble, extracellular Hsp70 with Gb3 acting as an anchor in the plasma membrane of the tumours (Gehrmann, Liebisch, et al., 2008).

Tumour cells can release Hsp70 into the extracellular space in lipid vesicles called exosomes (Gastpar et al., 2005) as an indicator of stress and to activate signalling pathways (De Maio, 2011). The method by which Hsp70 is released is still unknown, yet two major mechanisms are being discussed. Hsp70 might be released from the cytosol of necrotic cells (Gastpar et al., 2005). However, never evidence suggests that intact, viable cells actively release the larger part of extracellular Hsp70 via vesicular transport (Gastpar et al., 2005). This leads to elevated Hsp70 levels in the serum of cancer patients (De Maio, 2011).

1.4.4.1 Autophagy

As previously described, Hsp70 plays a vital role in preventing apoptosis. An upregulation of Hsp70 levels can provide selective survival advantages to tumour cells (Murphy, 2013) and increase anti-apoptotic pathways (Gabai et al., 1998; Jaattela, 1999; Wei et al., 1995). Autophagy is an intracellular process involved in both tumour suppression and promotion (Dokladny et al., 2015; Yun & Lee, 2018). It allows a controlled degradation and recycling of intracellular components following damage to organelles, the presence of abnormal or dysfunctional proteins, nutrient deprivation, and other cellular stressors (Dokladny et al., 2015; Yun & Lee, 2018). These defective components are engulfed by autophagosomes which later fuse with lysosomes initiating recycling (Dokladny et al., 2015; Yun & Lee, 2018). Autophagy-associated cell death promotes tumour suppression in the early stages of tumour growth and coincidentally increases the survival of tumour cells subject to cell stress during tumour progression (Bhutia et al., 2013). The lysosome-stabilising function of Hsp70, inhibiting the permeabilization of the lysosomal membrane, promotes cell survival (Daugaard, Kirkegaard-Sorensen, et al., 2007; Nylandsted et al., 2004).

1.4.4.2 Senescence

The state of permanent cell cycle arrest, which limits the proliferative life span of cells, is known as senescence (Calcinotto et al., 2019). Over time, DNA damages accumulate in any cell. To prevent genomic instability, the cell cycle is arrested (Calcinotto et al., 2019). The activation of oncogenes and the resulting proliferative stress can induce senescence, thus limiting tumour growth (Calcinotto et al., 2019). Therefore, the anti-proliferative function of senescence appears to be a physiological tumour-suppressor mechanism (Calcinotto et al., 2019; Sherman & Multhoff, 2007). The upregulation of Hsp70 in cancer cells suppresses senescence, consequently promoting cell proliferation (Sherman & Multhoff, 2007; Yaglom et al., 2007).

1.4.4.3 Immune response

In contrast to the intracellular protective functions, Hsp70 exerts a series of immune modulatory actions in the extracellular matrix and in its membrane-bound form (De Maio, 2011; Shu & Huang, 2008), acting as ‘danger signals’ to the adaptive and innate immune system (Moseley, 2000; Todryk et al., 2003). Some of these functions are listed below: First, the membrane expression of Hsp70 on tumour cells (Multhoff, Botzler, Wiesnet, Muller, et al., 1995) and virally infected cells (Moseley, 2000) affects natural killer cells (NK cells) (Botzler

et al., 1996; Multhoff et al., 1997; Multhoff, Botzler, Wiesnet, Eissner, et al., 1995; Multhoff, Botzler, Wiesnet, Muller, et al., 1995; Multhoff et al., 2000). Multhoff et al. (1995) showed that the membrane expression of Hsp70 correlates positively with susceptibility to NK-cell-mediated lysis (Botzler et al., 1996; Multhoff et al., 1997; Multhoff, Botzler, Wiesnet, Eissner, et al., 1995; Multhoff et al., 2000). Second, HSPs can promote specific cytotoxic T-lymphocyte responses (Singh-Jasuja et al., 2000). Upon lysis of tumour or virus-infected cells, Hsp70-antigen complexes are released into the extracellular space, acting as carrier molecules (Srivastava, 1994; Srivastava et al., 1994). These complexes can be recognised by antigen-presenting cells (APCs), such as macrophages or dendritic cells, and taken up in a receptor-mediated way. The tumour cell-derived antigens are processed intracellularly and presented on membrane-bound major histocompatibility complex class I (MHC-I) molecules (Arnold-Schild et al., 1999; Basu & Srivastava, 2000; Blachere et al., 1997; Srivastava et al., 1994). These, in turn, cause an antigen-specific immune response from CD8+ cytotoxic T-cells (Arnold-Schild et al., 1999; Basu & Srivastava, 2000; Blachere et al., 1997; Schild et al., 1999; Singh-Jasuja et al., 2000).

In summary, Hsp70 exerts various vital cellular functions, differing according to its location. Intracellularly, it is involved in protein synthesis, transportation, and protection of cells against stress-induced damage (Radons, 2016). On the surface membrane or in the extracellular space, Hsp70 plays a vital role in the immune response (Botzler et al., 1996; Multhoff et al., 1997; Multhoff, Botzler, Wiesnet, Eissner, et al., 1995; Multhoff et al., 2000). In oncogenesis and malignantly transformed cells, Hsp70 has a series of functions, both protecting (Calcinotto et al., 2019; Murphy, 2013) and harming tumour cells (Multhoff, 2007; Multhoff, Botzler, Wiesnet, Eissner, et al., 1995). The exclusive localisation of Hsp70 on the membrane of tumour cells but not healthy cells, and its high turn-over rate make it a potential and promising target for cancer therapies (Wu et al., 2023).

2 Aim

Cancer is one of the primary causes of death worldwide, with increasing incidence rates. Among women, breast cancer is the leading malignancy responsible for 17.7% of cancer-related mortality (Erdmann et al., 2021). Despite constant treatment advances in addition to the optimisation of established treatments such as radiotherapy, chemotherapy, hormone treatments, or antibody therapies, many malignancies are still untreatable. This emphasises the need to further expand treatment horizons. Nanomedicine is a novel and increasing branch in medicine utilising nanosized molecules for therapeutic and diagnostic purposes. Among many others, AuNPs are being used to increase the radiosensitivity of tumour cells towards irradiation. Hsp70 is a ubiquitous molecular chaperone with manifold intracellular and extracellular functions. On the surface of tumour cells, Hsp70 has been shown to operate as a biomarker for highly aggressive tumours, where high surface expression correlates with a more aggressive phenotype and poor prognosis. Corresponding healthy cells do not express Hsp70 on their surface membrane, making Hsp70 a suitable target for diagnostic and therapeutic purposes. The TNBC cell line MDA-MB-231 is a very aggressive and treatment-resistant form of breast cancer, exerting a high Hsp70 expression on its membrane.

In this in vitro experimental setup, MDA-MB-231 cells were incubated with hybrid gold (Au)-iron oxide (Fe_3O_4)-nanoparticles, coupled to TPP (TPP-PEG4-FeAuNPs) or NGL (NGL-PEG4-FeAuNPs) and irradiated at a dose of 2 Gy, 4 Gy, and 6 Gy. TPP is an antibody that specifically targets membrane Hsp70 on malignantly transformed cells. The present work aims to determine a possible toxicity of TPP-PEG4-FeAuNPs and NGL-PEG4-FeAuNPs for MDA-MB-231 in the absence of irradiation, as well as determine the concentration at which AuNPs become toxic and coincidentally, which concentrations are safe for use in vitro. Furthermore, the aim is to rule out any possible toxicity of the citrate buffer in which the nanoparticles are suspended. Finally, the objective is to combine the established radiation treatment for TNBC with the irradiation-enhancing effect of AuNPs. By incubating MDA-MB-231 cells with TPP-PEG4-FeAuNPs at a concentration of 0.5 and 1.0 µg/ml, the objective is to increase the radiosensitivity of the tumour cells towards photon-radiation at 200 keV. The goal is to achieve an increased cell death compared to cells irradiated in the absence of AuNPs. Moreover, to increase cell death by employing TPP-coupled AuNPs, which specifically target mHsp70 compared to NGL-AuNPs.

The long-term aim is first to establish mHsp70 as a universal target protein for malignantly transformed cells and metastases, and second, to attain more specific dose delivery in ‘in vivo’ models using AuNPs targeting mHsp70. This would represent a significant advancement in cancer treatment.

3 Material and methods

3.1 Material

Medium and Supplements	
RPMI-1640	Roswell Park Memorial Institute (RPMI)-1640 Medium With L-glutamine and sodium bicarbonate, liquid, sterile-filtered Sigma life science, Sigma-Aldrich, St. Louis, MO 63103, USA
FBS	Foetal Bovine Serum Sigma life science, Sigma-Aldrich, St. Louis, MO 63103, USA
Penicillin/ Streptomycin	Penicillin-Streptomycin 10,000 units penicillin, 10 mg streptomycin per ml in 0.9% NaCl, Sigma life science, Sigma-Aldrich, St. Louis, MO 63103, USA
L-Glutamine	L-Glutamine solution – 200 mM, solution Sigma life science, Sigma-Aldrich, St. Louis, MO 63103, USA
Na-Pyruvate	Sodium pyruvate solution – 100 mM Sigma life science, Sigma-Aldrich, St. Louis, MO 63103, USA

Cell culture Reagents and Kits	
PBS	Dulbecco's Phosphate Buffered Saline Modified, without calcium chloride and magnesium chloride Sigma life science, Sigma-Aldrich, St. Louis, MO 63103, USA
Trypsin	Trypsin-EDTA Solution – 1X Sigma life science, Sigma-Aldrich, St. Louis, MO 63103, USA
Trypan Blue	Trypan Blue Solution – 0.4% Sigma-Aldrich, St. Louis, MO 63103, USA
DMSO	Dimethyl sulfoxide (DMSO) HYBRI-MAX® Sigma-Aldrich, St. Louis, MO 63103, USA
Crystal Violet	Crystal violet solution – 1% aqueous solution Sigma life science, Sigma-Aldrich, St. Louis, MO 63103, USA
Mycoplasma Test Kit	MycoAlert™ Mycoplasma Detection Kit Lonza Group Ltd, CH-4002 Basel, Switzerland

Culture flasks	
T175	Cellstar cell culture flasks – 550 ml, 175 cm^2 Greiner Bio-One GmbH, Maybachstr. 2, 72636 Frickenhausen, Germany
T75	Cellstar cell culture flasks – 250 ml, 75 cm^2 Greiner Bio-One GmbH, Maybachstr. 2, 72636 Frickenhausen, Germany
T25	Cellstar cell culture flasks – 50 ml, 25 cm^2 Greiner Bio-One GmbH, Maybachstr. 2, 72636 Frickenhausen, Germany
12-well Plate	Corning Incorporated Costar – Cell Culture Plate 12-well Corning Incorporated, 2 Alfred Rd., Kennebunk, ME 04043 USA
96-well Plate	Tissue Culture Testplate 96F TPP Techno Plastic Products AG, Zollstraße 7, 8219 Trasadingen, Switzerland

Consumables	
Pipette 1–10 µl	Pipetman L P10L, 1 – 10 µl, metal ejector Gilson Incorporated, Global Headquarters, 3000 Parmenter Street, P.O. Box 620027, Middleton, WI 53562-0027, USA
Pipette 10–100 µl	Pipetman L P100L, 10 – 100 µl, metal ejector Gilson Incorporated, Global Headquarters, 3000 Parmenter Street, P.O. Box 620027, Middleton, WI 53562-0027, USA
Pipette 20–200 µl	Pipetman L P200L, 20 – 200 µl, metal ejector Gilson Incorporated, Global Headquarters, 3000 Parmenter Street, P.O. Box 620027, Middleton, WI 53562-0027, USA
Pipette 100–1000 µl	Pipetman L P1000L, 100 – 1000 µl, metal ejector Gilson Incorporated, Global Headquarters, 3000 Parmenter Street, P.O. Box 620027, Middleton, WI 53562-0027, USA
Pipette Tips 10 µl	Eppendorf Tips 0.1 – 10 µL Eppendorf AG, 22331 Hamburg, Germany
Pipette Tips 200 µl	200 µl Tip Volume Range 2 – 200 µl Gilson Incorporated, Global Headquarters, 3000 Parmenter Street, P.O. Box 620027, Middleton, WI 53562-0027, USA
Pipette Tips 1000 µl	Pipette Tip 1000 µl Sarstedt AG & Co. KG, Sarstedtstr. 1, D-51588 Nümbrecht, Germany
Stripettor	Corning® Stripettor™ Ultra Pipet Controller Corning Incorporated, One Riverfront Plaza, Corning, NY 14831, USA
Pipette Tip 1 ml	Cellstar serological pipette, sterile – 1 ml Greiner Bio-One GmbH Maybachstr. 2, 72636 Frickenhausen, Germany
Pipette Tip 2 ml	Cellstar serological pipette, sterile – 2 ml Greiner Bio-One GmbH Maybachstr. 2, 72636 Frickenhausen, Germany
Pipette Tip 5 ml	Cellstar serological pipette, sterile – 5 ml Greiner Bio-One GmbH Maybachstr. 2, 72636 Frickenhausen, Germany
Pipette Tip 10 ml	Cellstar serological pipette, sterile – 10 ml Greiner Bio-One GmbH Maybachstr. 2, 72636 Frickenhausen, Germany
Pipette Tip 25 ml	Cellstar serological pipette, sterile – 25 ml Greiner Bio-One GmbH Maybachstr. 2, 72636 Frickenhausen, Germany
Pipette Tip 50 ml	Cellstar serological pipette, sterile – 50 ml Greiner Bio-One GmbH Maybachstr. 2, 72636 Frickenhausen, Germany
Safe-lock tubes 0.5 ml	Safe-Lock Tubes 0.5 ml – Eppendorf Tubes Eppendorf AG, 22331 Hamburg, Germany
Safe-lock tubes 1.5 ml	Micro tube 1.5 ml SARSTEDT AG & Co. KG, Sarstedtstr. 1, D-51588 Nümbrecht, Germany
Safe-lock tubes 2.0 ml	SafeSeal micro tube 2 ml, SARSTEDT AG & Co. KG, Sarstedtstr. 1, D-51588 Nümbrecht, Germany
Falcon Tube	CELLSTAR ® Tubes – 15 ml,

15 ml	Greiner Bio One Maybachstr. 2, 72636 Frickenhausen, Germany
Falcon Tube 50 ml	CELLSTAR ® Tubes – 50 ml, Greiner Bio One Maybachstr. 2, 72636 Frickenhausen, Germany
FACS Tubes	Falcon® 5 mL Round Bottom Polystyrene Test Tube Corning Incorporated, One Riverfront Plaza, Corning, NY 14831 USA
Filter Unit 500 ml	Thermo Scientific™ Nalgene™ Rapid-Flow™ 75 mm Filter Unit – 500 ml Thermo Fisher Scientific Inc., Waltham, MA, USA
Filter Unit 250 ml	Thermo Scientific™ Nalgene™ Rapid-Flow™ 50 mm Filter Unit 250 ml Thermo Fisher Scientific Inc., Waltham, MA, USA
Filter Bottle 500 ml	Filter receiver and storage Bottle Thermo Scientific Nalgene Receiver Bottle – 500 ml Ref: 455-0500 Thermo Fisher Scientific Inc., Waltham, MA, USA
Filter Bottle 250 ml	Filter receiver and storage Bottle Thermo Scientific Nalgene Receiver Bottle – 250 ml Thermo Fisher Scientific Inc., Waltham, MA, USA
Cryovials 2 ml	Cryo Tube 20, 2 ml TPP Techno Plastic Products AG Zollstraße 7, 8219 Trasadingen, Switzerland
Cryobox Mr Freeze	Freezing container Mr. Frosty™ Thermo Fisher Scientific Inc., Waltham, MA, USA

Instruments/ Equipment	
FACSCalibur	BD Biosciences, Heidelberg,
Incubator	Heracell™ 240i CO_2 Incubator Thermo Fisher Scientific Inc., Waltham, MA, USA
Incubator	Heraeus BBD 6220 CO_2 Incubator Thermo Fisher Scientific Inc., Waltham, MA, USA
Workbench	ENVAIReco Safe Comfort Plus ENVAIR Deutschland GmbH, Emmendingen, Deutschland
Centrifuge	HERAEUS™ MEGAFUGE™ 16R Centrifuge Thermo Fisher Scientific Inc., Waltham, MA, USA
Centrifuge	HERAUES ™ FRESCO™ 17 Centrifuge Thermo Fisher Scientific Inc., Waltham, MA, USA
Microscope	Microscope Primo Vert Zeiss, Oberkochen, Germany
Neubauer counting chamber	Neubauer improved Counting Chamber Marienfeld Superior, Lauda-Königshofen, Germany
Gulmay RS225A	Gulmay Medical Ltd. Camberly, UK
Bioreader	Bioreader ® – 3000 Bio-Sys GmbH, 61184 Karben, Germany
Liquid nitrogen tank	Cryotherm BIOSAFE® Cryotherm GmbH & Co. KG 57548 Kirchen (Sieg), Germany

Autoclave	Systec VX-150 Systec GmbH Konrad-Adenauer-Str. 15, 35440 Linden, Germany
Faxitron®	CellRad® by Faxitron® Tucson, Arizona, USA 85706

FACS Reagents	
FACS Flow	BD FACSFlow™ Becton, Dickinson and Company, BD BioScience, San Jose, CA 95131, USA
FACS Rinse	BD™ FACSRinse Becton, Dickinson and Company, BD BioScience, San Jose, CA 95131, USA
FACS Clean	BD™ FACSClean Becton, Dickinson and Company, BD BioScience, San Jose, CA 95131, USA

FACS Antibodies	
cmHsp70.1	FITC (fluorescein isothiocyanante)-conjugated mouse monoclonal antibody specific for mHsp70.1, IgG1 [2 mg/ml] contains 0.06% NaAzid Lot: 04/13 multimmune GmbH, Munich, Germany
Mouse IgG1	FITC-labelled isotype matched IgG- negative control antibody Clone: X40 (CE/IVD), Mouse BALB/c IgG1, Lot: 9274955 Ref: 345815 BD Biosciences; (Becton, Dickinson & Co.) San Jose, California, USA
MHC HLA Human	Monoclonal Anti-HLA Class I Antigen FITC antibody produced in mouse clone W6/32 purified immunoglobulin buffered aqueous solution Clone: W6/32 Lot: 127M4877V Sigma life science, St. Louis, MO, USA
Propidium Iodide (PI)	Propidium iodide Sigma-Aldrich, St. Louis, MO 63103, USA

Gold Nanoparticles (AuNP)	
TPP-PEG4-FeAuNPs	Functionalised Spherical Gold Nanoparticles Product Nr.: CP1M1-2-1-PEP1-CIT-50-1 Lot: K7311 Form: Gold colloid Functionalisation: Fe_3O_4:Au-CYS-NHS-PEG4-MAL-PEP(CTKDNNLLGRFELSG) Solution: 5 mM Citrate Source: J7034 Diameter: 4 nm - Diameter Fe_3O_4: 2.0 nm - Diameter Au coating: 1.0 nm Wt-Conc.: 2.3 µg/ml

	Nanopartz ™ Inc., Loveland, Colorado, USA
NGL-PEG4-FeAuNPs	Functionalised Spherical Gold Nanoparticles Product Nr.: CP1M1-2-1-PEP2-CIT-50-1 Lot: K7312 Form: Gold colloid Functionalisation: Fe_3O_4:Au-CYS-NHS-PEG4-MAL-PEP(CNGLTLKNDFSRLEG) Solution: 5 mM Citrate Source: J7034 Diameter: 4 nm - Diameter Fe_3O_4: 2.0 nm - Diameter Au coating: 1.0 nm Wt-Conc.: 2.7 µg/ml Nanopartz ™ Inc., Loveland, Colorado, USA

Chemicals	
Methanol	Methanol Merck KGaA, 64271 Darmstadt, Germany
Ethanol	Alkopharm 80, Ethanol 80% Brüggemann Alcohol Heilbronn GmbH, Salzstr. 129, 74076 Heilbronn, Germany
Isopropanol	Otto Fischar GmbH & Co. KG Kaiserstr. 221, D-66133 Saarbrücken
Bacillol	Bacillol ® AF Bacillol ® AF BODE Chemie GmbH, Hamburg, Germany
Incidin	Incidin™ Plus Ecolab, Saint Paul, Minnesota, USA

Software	
FACSCalibur	BD CellQuest Pro Becton/ Dickinson Labware, Franklin Lakes, USA
Sigma Plot	Systat Software Inc. Chicago, Illinois, USA
EndNote	EndNote™ 19130, Philadelphia, PA, USA
MS Office	Microsoft Corporation Redmond, WA, USA
PubMed	http://www.ncbi.nlm.nih.gov/pubmed

MDA-MB-231 (ATCC® CRM HTB26™)(Collection, 2016)	
Organism	*Homo sapiens*, human
Tissue	Mammary gland/breast; derived from metastatic site: Pleural effusion
Disease	Adenocarcinoma
Cell Type	Epithelial cell (KRAS CRM)
Morphology	Epithelial
Growth Properties	Adherent

Medium and Reagent composition	
Full medium: RPMI-1640 plus supplements	500 ml RPMI-1640 50 ml FBS 5 ml Penicillin/ Streptomycin [100 IU/ml penicillin, 100 µg/ml Streptomycin] 5 ml Sodium-pyruvate [1 mM] 5 ml L-Glutamine [2 mM]
Myoplasma-test medium: RPMI-1640 plus supplements Penicillin/ Streptomycin free	500 ml RPMI-1640 50 ml FBS 5 ml Sodium-pyruvate 5 ml L-Glutamine
Freezing medium (100 ml)	70 ml RPMI-1640 20 ml FBS 10 ml DMSO
FACS Buffer	500 ml PBS 50 ml FBS

3.1.1 Antibodies

The cmHsp70.1 mouse monoclonal antibody (mAb) (multimmune GmbH, Munich, Germany) is specific for the major stress-inducible Hsp70 of both human and mouse tumours (Multhoff & Hightower, 2011). It is directed against the lipid-associated, membrane-bound Hsp70 on viable tumour cells with an intact cell membrane (Stangl, Gehrmann, Dressel, et al., 2011). The IgG1 antibody cmHsp70.1 is produced by immunising mice with a 14-mer peptide sequence TKDNNLLGRFELSG termed ‘TKD’ in the C-terminal oligomerisation domain of Hsp70 which is exposed to the extracellular milieu in its membrane-bound form (Stangl, Gehrmann, Dressel, et al., 2011; Stangl, Gehrmann, Riegger, et al., 2011). The antibody recognises an 8-mer epitope NNLLGRFE (453–460) within the C-terminus of Hsp70 (Botzler, Li, et al., 1998; Stangl, Gehrmann, Dressel, et al., 2011). Other available antibodies are not able to recognize integral membrane Hsp70 but rather detect Hsp70 in its receptor-bound form (Multhoff & Hightower, 2011).

The tumour cell-penetrating peptide (TPP) is an amino acid sequence from the C-terminal oligomerisation domain of Hsp70, which specifically binds membrane-bound Hsp70 (Stangl et al., 2014). NGL is a scavenger peptide of equal size with a shuffled amino acid sequence and unspecific binding. This way, the shape, size, surface charge, and assembling of the various components are comparable.

3.2 Methods

3.2.1 Cell culture

MDA-MB-231 is a human epithelial TNBC cell line isolated in 1973 from pleural effusions from a 51-year-old Caucasian woman by R. Cailleau et al. (1974). The mean chromosome number of these cells is between 65 and 69 (Cailleau, Young, et al., 1974). Morphologically, MDA-MB-231 cells appear spindle-shaped or round, with a granular character due to numerous lysosomes present in the cytoplasm (Cailleau, Mackay, et al., 1974). The cells exhibit a rapid growth pattern with a doubling time of around one day.

3.2.2 Cell cultivation and harvest

This work was performed in a safety level 2 laboratory following the Genetic Engineering Act (Federal Office of Consumer Protection and Food Safety, 1990) under sterile conditions at a workbench. According to current knowledge, genetic work assigned to safety level 2 poses a low risk to human health and the environment. The workbench was used for sterile work only, disinfected before and after each use, and illuminated with UV light for two hours post-usage. All instruments used under the workbench had previously been sterilised by autoclaving and disinfected with 70% alcohol. All components and reagents used were stored at the conditions recommended by the manufacturer.

The cells were cultivated in 15 ml of Roswell Park Memorial Institute 1640 (RPMI) medium supplemented with 10% heat-inactivated Foetal Bovine Serum (FBS), 1% Penicillin/ Streptomycin to inhibit the growth of bacteria, 1% L-Glutamine, and 1% Sodium-pyruvate to provide the ideal nutrients, in T75 (75 cm^2) culture flasks. The heat inactivation of the FBS was completed in a water bath at 56 °C for 45 minutes. All cells were grown in an incubator at 37 °C with 5% CO^2 and 95% humidity to best mimic the in vivo conditions. These conditions were regularly controlled.

Cells were split two to three times a week upon reaching 70–80% confluence to avoid growth stops and to replace nutrients to ensure optimal growing conditions. Before commencing, the culture was examined under a microscope at a magnification of 4–40x to ensure optimal colonisation density, evaluate the number of dead cells in suspension, and judge the overall morphology and condition of the culture. All reagents were warmed up to room temperature or 37 °C. The cells were collected as follows: The RPMI-1640 medium was removed, and the T75 flask with adherent cells was carefully washed with 4–6 ml PBS to

remove medium residues. The PBS was then removed and 2 ml Trypsin/EDTA was added for 2–3 minutes at 37 °C. Trypsin is a serine protease that specifically hydrolyses peptide bonds after the amino acids lysine and arginine (Sigma-Aldrich, 2020b), disconnecting cells from each other and detaching them from the surface of the culture flask. After this time, the cells would appear small and round, at which point gently tapping the flask completely detached the remaining cells and ensured all cells were in suspension. 8 ml of RPMI-1640 was then added to the cell suspension. The serum contained in the medium stopped the protease activity of the trypsin.

To determine the cell count, 30 µl of cell suspension was mixed with 30 µl of Trypane-blue in a 96-well plate (1:2 dilution). A small amount was transferred to a Neubauer counting chamber. Cells with a damaged membrane take up the dye, appearing blue under the microscope, and thus, can be distinguished from intact cells. Viable cells, in turn, appear round, colourless, and bright. Viable cells in all four quadrants were counted, and the cell number per millilitre was calculated with the following formula:

$$\text{Cell count/ml} = \frac{\text{number of cells counted}}{\text{number of squares counted}} \text{ x dilution x } 10^4.$$

The factor 10^4 results from the size of the counting chamber (0.1 mm^3 = 0.1 µl = 10^{-4} ml). The ideal seeding density in a T75 culture flask was between 0.4 and 0.5 million cells in around 15 ml of RPMI-1640 medium.

Every three months, the cells were tested for mycoplasma contamination. 200,000 cells were seeded in T25 culture flasks and grown in Penicillin/ Streptomycin-free RPMI-1640 medium for at least two passages. The supernatant of the culture was then tested. All cells were negative throughout the experiment series.

3.2.3 Freezing and thawing of cells

Cells were kept in liquid nitrogen at -196 °C to allow long-term storage. At the start of the experiments, the cell line was expanded in T175 culture flasks and collected upon reaching a confluence of around 70–80%. After the medium was removed, the adherent cells were washed and collected as described above. Cells were counted, and a defined number of cells was centrifuged at 300 g at 4 °C for 5 minutes. The supernatant was discarded and cells were resuspended in freezing medium at a concentration of around one million cells per millilitre. The freezing medium contained 20% FBS, 70% RPMI-1640 medium plus supplements, and

10% Dimethyl sulfoxide (DMSO). DMSO, as a cryoprotectant, was added to protect cells from mechanical injury caused by ice crystal formation during freezing (Sigma-Aldrich, 2020a). The cell suspension was then aliquoted into cryovials containing around two million cells in 1.5 millilitres of medium and labelled accordingly. The cryovials were placed into a 'Mr. Freeze' container and placed in a -80 °C freezer overnight, from which they were transferred to the liquid nitrogen tank the following day. The lining of the 'Mr. Freeze' container was filled with isopropanol, ensuring a gradual yet quick lowering of the temperature of around one degree per millilitre per minute. Freezing a cell stock ensured that all experiments could be completed from an identical stock.

When the cells had undergone 15–20 passages, new cells were thawed from the selection of previously frozen vials. The frozen vial was removed from the liquid nitrogen tank, thawed in a 37 °C water bath, and the cell suspension was transferred to a 50 ml falcon tube filled with 10 ml of RPMI-1640 medium. Cells were centrifuged at 300 g and 4 °C for 5 minutes, and the supernatant containing the cytotoxic DMSO was discarded. The cell pellet was taken up in 15 ml of RPMI-1640 medium plus supplements and sown in a T75 cell culture flask. The cells were split as described above upon reaching 70–80% confluence and left to rest and grow for at least three passages before commencing new experiments.

3.2.4 Flow cytometry

3.2.4.1 Principle of flow cytometry

Fluorescent-activated cell sorting (FACS) is a specialised form of flow cytometry. Flow cytometry is used to analyse individual cell parameters from a heterogeneous population (Picot et al., 2012), such as geometric properties (size, volume, etc.), physiological properties (vitality, membrane potential, etc.), and quantitative properties (surface antigens, enzymes, proteins, etc.) (Buscher, 2019).

A flow cytometer consists of three parts: First, a fluid system responsible for transporting the cells from the sample into the sheath fluid, where they are aligned in a laminar sample flow via hydrodynamic focusing (Menon et al., 2014); second, an optical system with lasers that illuminate the cells as they file past, wavelength filters, and detectors (Picot et al., 2012); and third, an electrical system, which converts the measured signals into digital data which can then be analysed on a computer with according software (Menon et al., 2014; Picot et al., 2012).

The cells' laminar flow intersects with the optical system's laser beam, causing a scattering of light. This light scattering can either be measured by a detector in the same plane as the laser direction, forward scatter (FSC), or by a detector perpendicular to the laser beam, side scatter (SSC) (Menon et al., 2014). FSC provides information about the size of the cell, while SSC reflects the granularity and complexity of said cell (Menon et al., 2014; Picot et al., 2012).

Furthermore, the expression of surface or intercellular proteins and structures can be quantified with the help of fluorochromes (Abcam, 2020). Often, these fluorochromes are bound to antibodies, which specifically target proteins of interest. When excited by a laser with the corresponding wavelength (Argon laser 488 nm, Helium-neon laser 633 nm), these fluorochromes emit light, meaning stained cells can be detected separately (Abcam, 2020). Such fluorochromes include Fluorescein Isothiocyanate (FITC), emitting light at a wavelength of around 530 nm; Phycoerythrin (PE), emitting light at about 575 nm wavelength, Propidium Iodide (PI), with emission of about 613 nm wavelength, and Allophycocyanin (APC) at a wavelength of 665 nm (Alvarez et al., 2010). This light emission is filtered and channelled so each sensor, called a photomultiplier tube, detects the fluorescence of a specific wavelength, converting this information into a voltage pulse correlating to the intensity of the fluorescence signal (Abcam, 2020). This information (i.e., FSC, SSC, fluorescent marker, etc.) is then displayed as an ‘event’ in a diagram, where the cell population of interest can be gated and further analysis can be completed.

3.2.4.2 Flow cytometry of Hsp70

To quantify the membrane bound Hsp70 (mHsp70), the FACSCalibur flow cytometry by BD Biosciences, Heidelberg, was used. It contains an Argon-Ion-Laser (488 nm), SSC and FSC detectors. Cells were seeded at 0.5 million in a T75 culture flask with 15 ml of RPMI-1640 with supplements and left to grow for 48 hours in the incubator. For the FACS analysis of cells after irradiation, 0.25 million cells were seeded two days before irradiation with 0, 2, 4, or 6 Gy, then left in the incubator for another 24 or 48 hours. After this time, the flask was inspected under a microscope to ensure the growing density did not exceed 80%. The cells were collected as described above and counted. From here onward, all steps were completed on ice. Single-cell suspension of 0.2 million cells per FACS-tube was transferred into a 50 ml Falcon tube and centrifuged at 300–500 g for 5 minutes at 4 °C. The medium was discarded, and the cells were washed in cold 10% FACS buffer consisting of 500 ml Dulbecco's Phosphate

Buffered Saline (PBS) and 50 ml FBS. The cell suspension was equally distributed into 1.5 ml safe lock tubes, labelled, and centrifuged at 300–500 g for 5 minutes at 4 °C.

In the meantime, the 1:20 dilution of the cmHsp70.1 antibody was prepared using pure PBS and a FITC-conjugated cmHsp70.1 antibody stock suspension with a concentration of 2 mg/ml. The supernatant was removed from the safe-lock tubes using a vacuum pump, leaving a dry pellet. All FACS-buffer must be removed to avoid further dilution of the antibody. In the next step, the antibodies were added, distributed evenly, and incubated for 30 minutes on ice in the dark. Table 1 summarises the Hsp70 flow cytometry experimental setup:

Tube 1	Mouse IgG Iso-FITC	5 µl
Tube 2	HLA	5 µl
Tube 3	cmHsp70.1 (2 mg/ml) 1:20	20 µl

Table 1 – Membrane Hsp70 and HLA FACS

After 30 minutes, 1 ml of 10% FACS Buffer was added to each safe lock tube. The cells were resuspended to ensure sufficient washing of all cells and centrifuged for another 5 minutes at 300–500 g at 4 °C. The supernatant was removed using a vacuum pump, the cells were resuspended in 100–500 µl of 10% FACS buffer (depending on the pellet size), and transferred into FACS-Tubes. Shortly before measuring, PI was added to the FACS-Tube, 1 µl per 100 µl of 10% FACS buffer used, giving a final concentration of 1 µg/ml. PI binds to the DNA in necrotic or dead cells, allowing the distinction between viable and non-viable cells seeing PI cannot penetrate into the cell when the cell membrane is intact (van Engeland et al., 1998).

The same measuring mask and instrument settings were used for each experiment. For each tube, 50,000 counts were measured. Upon finishing, the FACSCalibur machine was disconnected and cleaned for 5 minutes with each of the following solutions: FACS-Clean/ Rinse/ Flow, and distilled water.

3.2.4.3 Analysis of the flow cytometry data

For the flow cytometry data analysis, FSC (linear) versus SSC (linear), FSC versus PI (logarithmic), and the FITC (logarithmic) signal intensity were plotted against each other. Looking at the fluorescent and scatter dot-plot illustrated in Figure 4 (FSC vs. PI and SSC vs. FSC), the regions R1 and R2 were defined to include all cells of the right size and granularity, which were coincidentally PI negative (Gate 3 = R1 and R2). This usually yielded between

20,000 and 40,000 analysed events. For simplicity and to ensure a standardized procedure, the regions were placed around the light blue contour line in the contour plot (as shown in Figure 4).

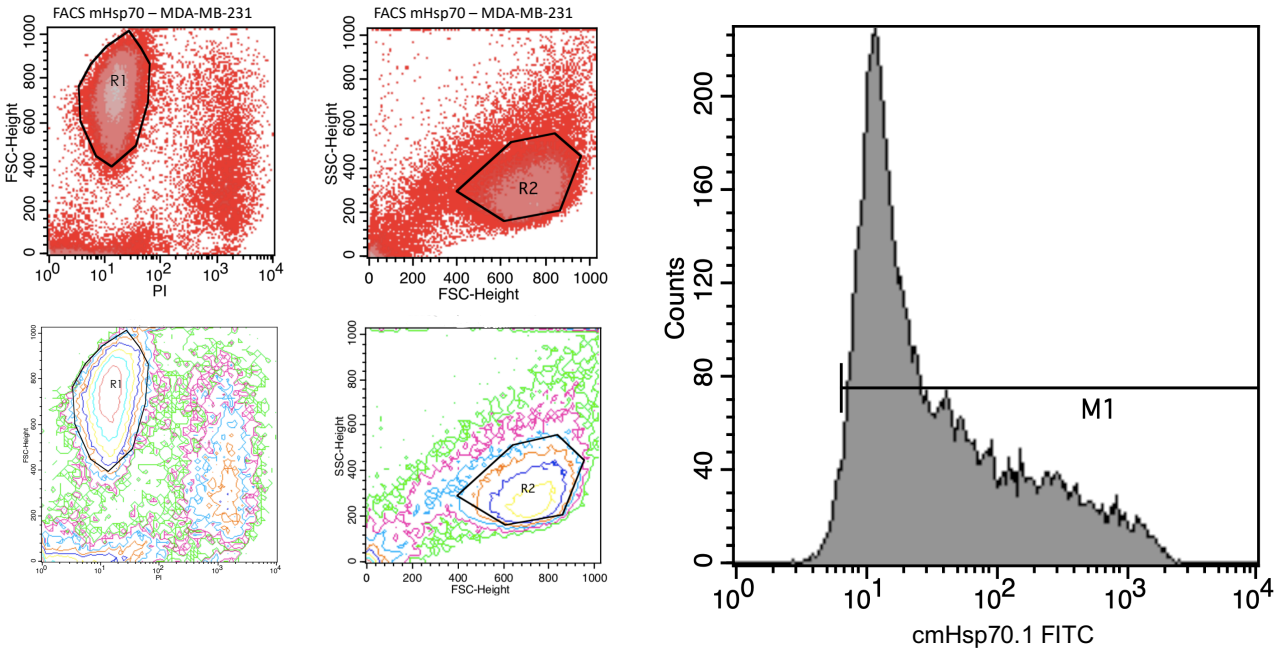

Figure 4 – Hsp70 FACS analysis of MDA-MB-231 cells

Next, the FITC signal intensity for G3 (G3 = R1 and R2) was determined. The mouse IgG-FITC-Isotype control in Tube 1 (see Table 1) was used to determine the unspecific binding of the antibody, where unspecific binding of under 5% was considered an evaluable experiment. A marker M1, as shown in Figure 4 (right), was set at the x-axis intercept with the tangent of the steepest part of the IgG1 control curve and used to measure the mean fluorescent intensity (MFI) of mHsp70, as well as the percentage of FITC-mHsp70 positive cells in Tube 3 (see Table 1).

3.2.5 Colony forming assay

The colony forming assay (CFA) is considered the gold standard for determining the effect of cell irradiation in vitro. The cells' ability to form colonies is evaluated and used to assess the radiosensitivity of the cells, as well as the toxic effect of the irradiation treatment. After irradiation and lesions to the cells' DNA, a series of possible outcomes exist. Smaller genome damage may be repaired, resulting in possible misrepair. Unrepaired breaks, however, may lead to chromosomal aberrations and cell death after several cell cycles (Ross, 1999). This is known as mitotic or clonogenic cell death and is considered the predominant mechanism to prevent tumour cell growth (Ross, 1999).

To determine the number of cells seeded in each well, colony forming assays were performed testing the cell densities of 200, 400, and 800 cells per well in a 12-well plate containing 1.1 ml RPMI medium with supplements. These were irradiated at 2, 4, and 6 Gy, or left to grow without irradiation 24 hours after seeding. The cells were then left to grow for another 5–7 days and later fixated, stained, and analysed as described in sections 3.2.9, "Fixation and staining", and 3.2.10, "Analysis of CFA".

The concentration range used was based on previous work from Gehrmann et al. (2015), who showed that at concentrations of 0.1–10 µg/ml, no toxic effects could be seen in 4T1 and CT26 cells (a murine TNBC and colon carcinoma cell line). In addition, they determined that the best working concentration with the optimal uptake of nanoparticles was 1 µg/ml (Gehrmann et al., 2015). With the help of bright field microscopy, they proved an accumulation of nanoparticle clusters in the perinuclear region after an incubation time of 24 hours at 37 °C (Gehrmann et al., 2015). The incubation period was chosen based on work by Stangl et al. (2011). After in vivo imaging of fluorescently labelled cmHsp70.1, Stangl et al. (2011) saw a rapid turnover rate and accumulation of mHsp70, reaching a maximum after 24 hours.

3.2.6 Toxicity assays

Colony forming assays were performed, to prove that neither the citrate buffer in which the nanoparticles were suspended nor the nanoparticles by their lonesome had independent toxic effects on the cells. For this purpose, 400 cells were seeded from a single cell suspension into 12-well plates with 1.1 ml RPMI-1640 medium until adherend. Increasing volumes (2 µl–250 µl) of 5 mM citrate buffer at pH 6.2 were added, and the cells were left to grow in the incubator for 5–7 days. In parallel, 12-well plates with 400 cells and 1.1 ml RPMI plus supplements were set up and, upon adherence, incubated with varying concentrations from 0.1 µg/ml to 20.0 µg/ml of both TPP- and NGL-coupled gold-coated nanoparticles (TPP-PEG4-FeAuNPs and NGL-PEG4-FeAuNPs) to determine AuNP toxicity. Working concentrations of 0.5 µg/ml and 1.0 µg/ml were chosen.

3.2.7 Main experiment

The cells were collected from a regular culture flask, resuspended, and carefully counted with a Neubauer counting chamber. 0.5 million cells from the single cell suspension were transferred into a 50 ml Falcon tube and filled to 5 ml with culture-medium to give a concentration of 100,000 cells/ml. The cells were diluted until a final concentration of 400 cells

per 1.1 ml, carefully pipetted into the wells and swayed. The distribution within the well was checked under the microscope. Upon adherence around 6–12 hours later, the TPP-PEG4-FeAuNPs and NGL-PEG4-FeAuNPs at a concentration of 0.5 µg/ml and 1.0 µg/ml, as well as a control group were added for incubation. Triplicates of each concentration were performed. The exact amount to be added was calculated based on the concentrations determined by the manufacturer (for the TPP-PEG4-FeAuNPs: 2.3 µg/ml, for the NGL-PEG4-FeAuNPs: 2.7 µg/ml), using:

$$\text{concentration} = \frac{\text{mass}}{\text{volume}}.$$

The amounts added can be seen in Table 2. To reduce the risk of error, 1:100 dilutions of the AuNP-solutions were made with RPMI.

Aimed concentration [µg/ml]	Dilution used	Volume TPP-AuNP [µl] of [2.3µg/ml]	Volume NGL-AuNP [µl] of [2.7µg/ml]
0.5	1:100	23.9	20.4
1.0	1:100	47.8	40.7

Table 2 – Dilution of AuNPs

The AuNPs used had a diameter of 4 nm. The inner 2 nm were made of iron oxide, which, due to its paramagnetic properties, can increase the MRI relaxation rates (Wood & Ghugre, 2008; Wu et al., 2023), giving the nanoparticles significant theranostic capabilities.

3.2.8 Irradiation

The cells were irradiated with the Gulmay RS225A (Gulmay Medical Ltd., UK) device machine, which was operating at 200 keV and 15 mA. The cells were irradiated for 2 minutes and 14 seconds to receive a dose of 2 Gy, 4 minutes and 18 seconds for 4 Gy, and finally 6 minutes and 42 seconds for 6 Gy. Irradiation took place 24 hours after incubation with the TPP- and NGL-PEG4-FeAuNPs with 2 Gy, 4 Gy, and 6 Gy, as well as the unirradiated sham group. Before irradiation, a warm-up of the machine was completed to ensure constant and accurate doses were delivered to the cells. The 12-well plates were placed symmetrically on a rotating tray table in the irradiation chamber. After the irradiation was completed, the cells were left to grow in the incubator at 37 °C, 5% CO_2, and 95% humidity for 5–7 days until colonies of 50 cells or more had formed.

3.2.9 Fixation and staining

Around 5–7 days post-irradiation, after 5–6 cell divisions had taken place, the colonies of the sham cells (i.e., unirradiated, untreated group) had reached a size of around 50 cells or more without reaching confluence. The medium was removed, and the individual wells were carefully rinsed with PBS to remove the supernatant and cell residues. The wells were left to fully dry before proceeding with the following steps to reduce the risk of rinsing off colonies. Next, the cells were fixated with ice-cold methanol at minus 20 °C for 5 minutes. The methanol was then removed, the wells dried, and the cells stained with 0.1% aqueous crystal violet solution for two minutes. Finally, the wells were washed with distilled water and left to dry overnight. The stained plates were read out and measured using Bioreader® (Bio-Sys GmbH, Karben, Germany). The measuring mask was explicitly created for the cell line with direct control under the microscope to measure colonies larger than 50 cells with a defined roundness, colour intensity, and size. Survival curves were fitted to the linear-quadratic model using Sigmaplot (Systat Software Inc).

3.2.10 Analysis of CFA

First, the plating efficiency (PE) was calculated as follows:

$$\mathrm{PE} = \frac{\text{mean colony count of sham (0 Gy)}}{\text{number of cells seeded}}.$$

Next, the survival fraction (SF) for each irradiation dose and concentration was determined:

$$\mathrm{SF} = \frac{\text{(mean colony count for each irradiation dose and concentration / PE)}}{\text{number of cells seeded}}.$$

To calculate the survival fraction of each nanoparticle and concentration at each irradiation dose, the mean colony count of that condition was divided by the PE of the equivalent sham group and then by 400 (number of cells seeded). For the graphic representation of the data, the SF was plotted with a logarithmic scale on the y-axis. The linear-quadratic-model (Fowler, 1989; Kellerer & Rossi, 1973) was used to describe the line of best fit for a survival curve. The following formula describes this model:

$$\ln \mathrm{SF} = -\alpha \mathrm{D} - \beta \mathrm{D}^2,$$

whereby SF is the natural logarithm of the survival fraction, D is the applied dose, α and β the cell and tissue-specific constants. At low irradiation doses, a linear component (- αD) can be

seen, with a quadratic decline (βD2) as the dose increases (Herrmann et al., 2006; Kellerer & Rossi, 1973; Sauer, 2010b; Schulz-Ertner et al., 2006). The theory behind this model states, that as the frequency of damages increases, the effectivity of the repair systems decreases; that is, the more pronounced the linear component, the better the cell's ability to repair damages (Herrmann et al., 2006; Kellerer & Rossi, 1973; Sauer, 2010b; Schulz-Ertner et al., 2006).

3.2.11 Statistics

The mHsp70 data was performed 9–12 times, and the CFA data was completed three times. For the toxicity controls for the AuNPs, two repetitions were performed due to the high cost, whereas the rest of the toxicity assays were repeated three times.

For statistical analysis, the SF of the treated cells was compared to the untreated sham group. For the toxicity assays, the SF of the cells incubated with TPP- and NGL-PEG4-FeAuNPs at various concentrations or cells incubated with different amounts of citrate buffer was compared to the SF of untreated sham cells. For the seeding controls, the SF after 2 Gy, 4 Gy, and 6 Gy was compared to the SF of the unirradiated sham group. For the main experiments, the SF of cells incubated with TPP- and NGL-PEG4-FeAuNPs irradiated with 2 Gy, 4 Gy, and 6 Gy was compared to the SF of the sham group irradiated with the same dose without nanoparticles. Furthermore, to detect an increased radiosensitivity for TPP-PEG4-FeAuNPs, the SF of cells incubated with TPP-PEG4-FeAuNPs at various irradiation doses was plotted against NGL-PEG4-FeAuNPs at the same irradiation dose.

The statistical analysis was completed in Microsoft Excel. To determine statistical significance, the Student's t-test was performed with a 95% confidence interval, assuming a normal data distribution using two groups and two tails. In line with prior research, significance levels were determined as follows: $p \leq .05$ * (significant), $p \leq .01$ ** (very significant), and $p \leq .001$ *** (highly significant).

4 Results

4.1 Preliminary results

4.1.1 Membrane Hsp70

As stated in existing literature, Hsp70 is expressed on the membrane of breast cancer cells (Botzler, Schmidt, et al., 1998; Hantschel et al., 2000; Pfister et al., 2007). Flow cytometry was performed on the MDA-MB-231, a human TNBC cell line, to quantify the mHsp70. MDA-MB-231 cells were seeded two days prior to the FACS analysis, with a confluence not exceeding 80%, to ensure that experiments were completed during the exponential growth phase.

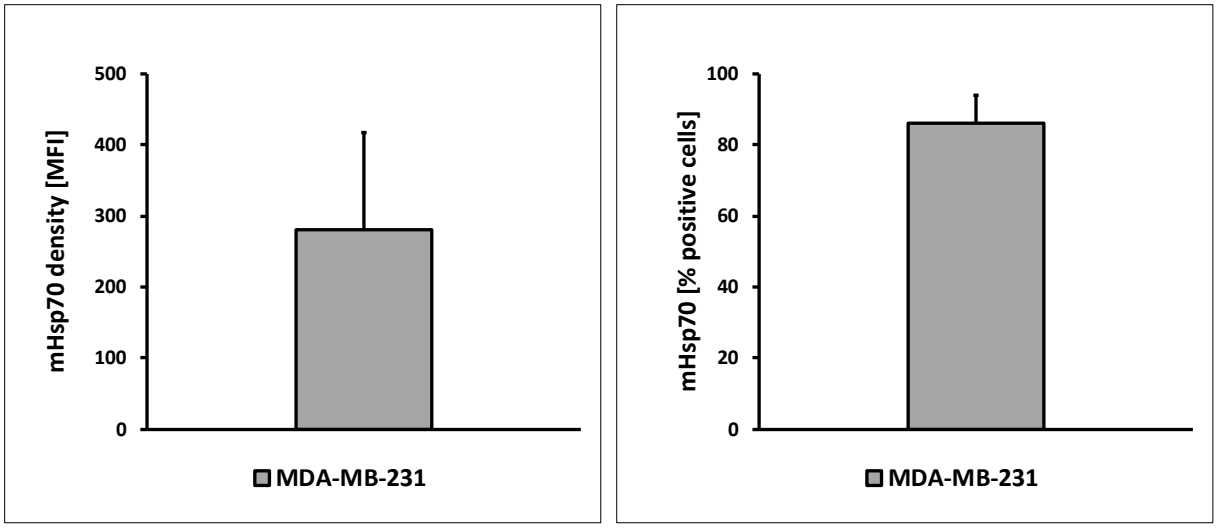

Figure 5A and 5B – Hsp70 FACS results for MDA-MB-231 cells

Left (A): MFI of Hsp70 on MDA-MB-231 cells. Right (B): Percentage of Hsp70 positive cells. Dilution of Hsp70 1:20.

Figure 5A (left) shows the mean fluorescent intensity (MFI), the average expression quantity of the fluorescent dye of the population of interest at a 1:20 dilution. As described above, only PI negative cells and of the appropriate size and granularity were included. The data shows a 1:20 dilution of the FITC-labelled cmHsp70.1 antibody. The MFI had a mean of 280.54 with a standard deviation of 136.14. Figure 5B (right) illustrates the percentage of positive cells for the fluorescent FITC dye from the whole sample. As described previously, the unspecific binding of the antibody was subtracted. As expected, 86.01% of cells with a standard deviation of 8.06 were positive for membrane bound Hsp70. This experiment was repeated 12 times. Interestingly, the cells did not always express a single peak for Hsp70 but occasionally showed a triple peak constellation: Some cells expressed lower Hsp70, others medium, and

higher Hsp70 densities. In Figures 5 and 6 the average MFI are shown. Several parameters that might have influenced the Hsp70 expression, including a new medium, new thawing, different incubator, different confluence, or different experimenters, were tested to determine the cause for fluctuations in Hsp70 expression without conclusions. A possible explanation might be an intrinsic precaution to increase heterogeneity amongst cells brought about by intercellular communication, thus augmenting survival chances.

4.1.2 Membrane Hsp70 after irradiation

Hsp70 is subject to an upregulation following cellular stress, such as electromagnetic irradiation (Gehrmann et al., 2005). Additionally, the established clinical radiation routine involves a cumulative treatment plan with fractionated irradiation of around 2 Gy per session. To mimic later clinical regimes more closely, experiments were performed to test whether pre-irradiating cells would lead to a significant upregulation in the membrane Hsp70 expression. For this purpose, cells were seeded two days prior to irradiation and left to grow for another 24 or 48 hours, after which the membrane Hsp70 was analysed via flow cytometry.

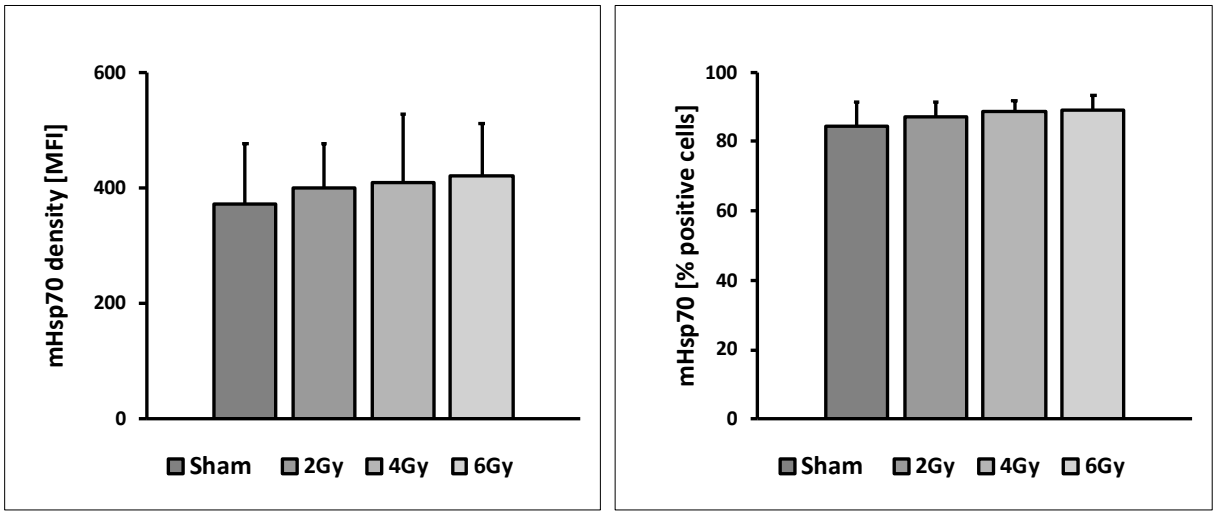

Figure 6A and 6B – Hsp70 post irradiation

Left (A): MFI of Hsp70 on MDA-MB-231 cells 24 hours post irradiation. Right (B): Percentage of Hsp70 positive cells 24 hours post irradiation. Dilution of Hsp70 1:20.

Figure 6A (left) shows a trend towards an increase in the MFI levels of Hsp70 on the cell membrane, from 371.40 (SD = 105.93) at sham, 400.99 (SD = 74.98) at 2 Gy, 409.45 (SD = 116.99) at 4 Gy, and 421.19 (SD = 90.12) at 6 Gy, 24 hours after irradiation of cells with 2, 4, and 6 Gy. Forty-eight hours after irradiation, a similar trend could be seen (data not shown). However, at neither timepoint the upregulation of Hsp70 was significant. Figure

6B (right) shows, that the percentage of Hsp70 positive cells barely changes with increasing irradiation, with 84.45% (SD = 7.08) of Hsp70 positive cells at sham, 87.03% (SD = 4.27) at 2 Gy, 88.54% (SD = 3.30) at 4 Gy, and 89.01% (SD = 4.28) at 6 Gy. Therefore, cells were not pre-irradiated prior to incubation with the AuNPs. This experiment was repeated six times – all results remained robust.

The unirradiated cells were exposed to the same conditions as the irradiated cells. Distortions in the Hsp70 levels due to temperature changes, location changes, and mobilisation of the flasks could therefore be avoided. Alterations in the Hsp70 levels which could not be traced back solely to the irradiation should be excluded as far as possible by this procedure.

4.1.3 Human leukocyte antigen after irradiation

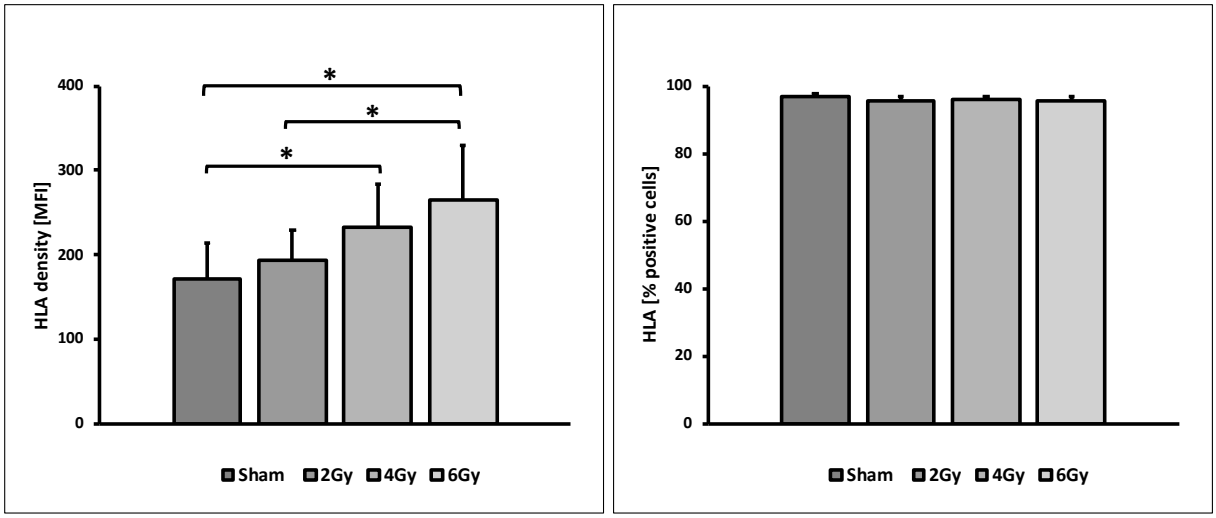

Figure 7A and 7B – Human leukocyte antigen after irradiation

Left (A): MFI of HLA on MDA-MB-231 cells 24 hours post irradiation. Right (B): Percentage of HLA positive cells 24 hours post irradiation.

Figures 7A and 7B show the human leukocyte antigen (HLA) expression of MDA-MB-231 cells 24 hours after irradiation with sham, 2, 4, and 6 Gy. Figure 7A (left) shows the significant increase of the MFI of HLA expression on the MDA-MB-231 cells after irradiation, ranging on average from 170.87 (SD = 42.60) in the sham group, 193.09 (SD = 36.25) at 2 Gy, 232.84 (SD = 51.45) at 4 Gy, and 264.89 (SD = 64.89) after irradiation with 6 Gy. Figure 7B (right) shows that over 95% of cells are positive for HLA. All cells were positive for HLA; however, subtracting the unspecific binding (≤ 5.0%) rendered the values above. The increase in MFI from sham to 4 Gy was significant *(p = .046)*. There was a significant increase from

2 Gy to 6 Gy *(p = .040)* and from sham to 6 Gy *(p = .014)*. The HLA antibody was used as an internal positive control to show the human origin of the MDA-MB-231 cell line.

4.1.4 Seeding density

Before performing the clonogenic assays, the optimal cell seeding density needed to be determined. Ideally, the cells in the 12-well plate should not be confluent after 5–7 days, and the error caused by minor fluctuations in the exact number of cells seeded should be as small as possible. Figure 8 shows, that the larger the seeding density, the smaller the standard deviation and the more accurate and significant the results were. However, when seeding 800 cells, many colonies were confluent and had merged. Therefore, a seeding density of 400 cells per well for all doses was chosen.

Additionally, Figure 8 shows the significant increase in cell death after 4 and 6 Gy irradiation. The survival fractions were calibrated to the sham group, which was set to a survival rate of 1.0. At a seeding density of 200 (Figure 8A), the SF at 2 Gy was 0.76 (SD = 0.16), at 4 Gy, 0.40 (SD = 0.19), and at 6 Gy, 0.32 (SD = 0.12). There was a significant decrease in SF from sham to 4 Gy *(p = .047)* and from sham to 6 Gy *(p = .015)*. After seeding 400 cells per well (Figure 8B), the survival fraction at 2 Gy was 0.69 (SD = 0.15), at 4 Gy 0.25 (SD = 0.06), and at 6 Gy 0.12 (SD = 0.05), with significant values between sham and 4 Gy *(p = .003),* and between sham and 6 Gy *(p = .001)*. There was also a significant decrease in the SF from 2 Gy to 6 Gy *(p = .034)*. With the seeding density of 800 cells (Figure 8C), most colonies were beginning to become confluent. The SF for 2, 4, and 6 Gy were 0.60 (SD = 0.08), 0.24 (SD = 0.06), and 0.12 (SD = 0.03), respectively, with significant results from sham to 2 Gy *(p = .021)*, from sham to 4 Gy *(p = .003)*, and from sham to 6 Gy *(p < .001)*. There was also a significant decrease in the SF from 2 Gy to 4 Gy *(p = .038)* and 2 Gy to 6 Gy *(p = .017)*. The results for 400 and 800 cells were very similar and comparable.

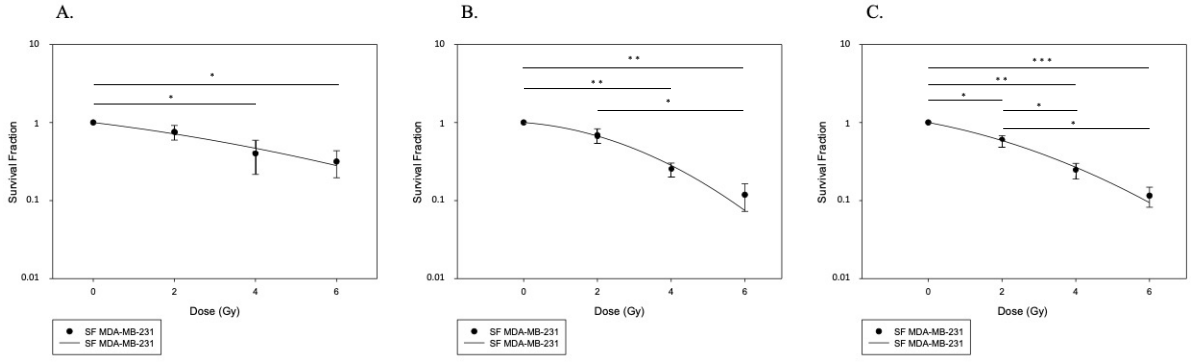

Figure 8 – Control CFA of MDA-MB-231 cells

CFA of MDA-MB-231 5-7 days post irradiation with sham, 2 Gy, 4 Gy, and 6 Gy at a seeding density of A. 200 cells, B. 400 cells, and C. 800 cells.

4.1.5 Toxicity assay – buffer

After determining the ideal cell seeding density, the possible toxicities of the reagents and solutions were determined. The TPP-PEG4-FeAuNPs and NGL-PEG4-FeAuNPs were delivered suspended in a buffer solution of 5 mM of citrate buffer at pH 6.2. Various volumes of the citrate buffer without nanoparticles in suspension (namely 2 µl, 5 µl, 10 µl, 20 µl, 50 µl, 100 µl, 200 µl, and 250 µl) were added to the wells containing 400 MDA-MB-231 cells and 1.1 ml RPMI-1640 medium. The cells were then left to grow for another 5–7 days. This enabled the exclusion of possible toxicity of the stock solution, even in the absence of nanoparticles. After 5–7 days, the cells were fixated and stained as described in section 3.2.9, and the SF of each condition was calculated as described in section 3.2.10. This experiment was repeated three times. Figure 9 shows the SF after each volume was added, with sham set to a SF of 1.0. Between 2 and 20 µl of citrate buffer no significant decrease in cell viability could be seen. The SF were 0.99 (SD = 0.08) for 2 µl, 0.91 (SD = 0.11) for 5 µl, 0.85 (SD = 0.14) for 10 µl, and 0.92 (SD = 0.09) for 20 µl. When adding 50 µl or more, a significant decrease in the cells' survival could be seen compared to the untreated sham group. After adding 50 µl, the SF was 0.75 (SD = 0.02) *($p < .001$)*. The SF at 100 µl was 0.76 (SD = 0.07) *($p = .004$)*, at 200 µl 0.65 (SD = 0.11) *($p = .006$)*, and at 250 µl, 0.50 (SD = 0.11) *($p = .001$)*.

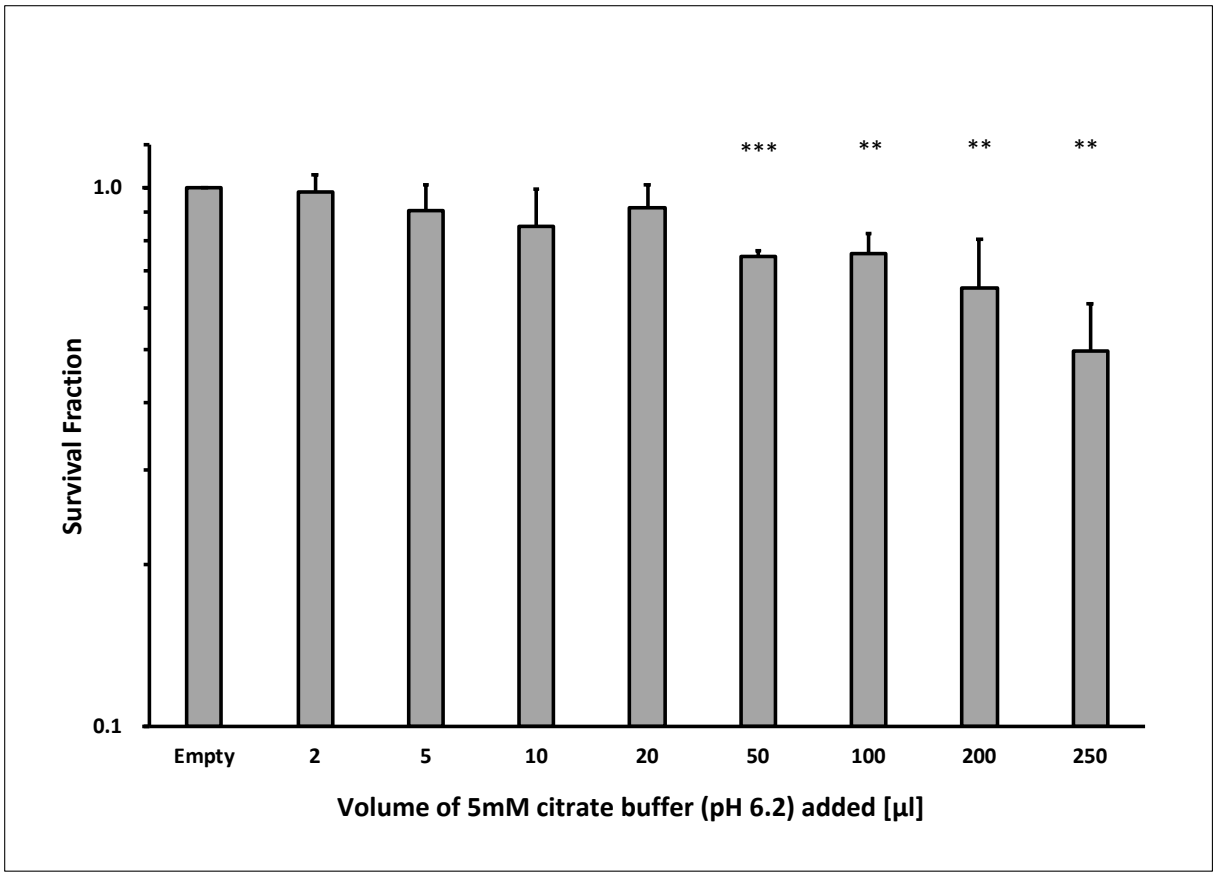

Figure 9 – CFA – Toxicity assay – Citrate buffer

CFA of the SF of MDA-MB-231 after adding 2–250 µl of 5 mM citrate buffer (pH 6.2).

When performing the toxicity assays with the TPP-PEG4-FeAuNPs and NGL-PEG4-FeAuNPs to determine the working concentrations, to reach a concentration of 1.0 µg/ml in a 1.1 ml well using a 2.3 µg/ml concentrated AuNP, a total volume of around 0.5 µl of the stock-solution would be needed – a volume much lower than the volumes tested above in Figure 9.

4.1.6 Toxicity assay – gold nanoparticles

The final preliminary experiment was aimed at ruling out the potential toxicity of the TPP-PEG4-FeAuNPs and NGL-PEG4-FeAuNPs before irradiation. The aim of the experimental setup was to examine the effect of radiation on cells with Hsp70 specifically binding TPP-PEG4-FeAuNPs. Therefore, a possible toxicity of the AuNPs on the unirradiated sham cells needed to be ruled out. For this purpose, 400 cells were seeded in each well of a 12-well plate. After adhesion, various concentrations of AuNPs were added and the cells were left to grow for another 5–7 days before fixation and analysis of the CFA, according to sections 3.2.9 and 3.2.10. The concentrations used were 0.1 µg/ml, 0.25 µg/ml, 0.5 µg/ml, 0.75 µg/ml, 1.0 µg/ml, 2.5 µg/ml, 5.0 µg/ml, and 10.0 µg/ml (not all data shown).

Table 3 and Figure 10 show the survival fraction of the unirradiated sham cells to determine the toxicity of the AuNPs. For simplicity, only the concentrations 0.5 µg/ml, 1.0 µg/ml, 2.5 µg/ml, 5.0 µg/ml, and 10.0 µg/ml are shown. Cells left untreated without AuNP are labelled 'Empty', and cells incubated with TPP-PEG4-FeAuNPs and NGL-PEG4-FeAuNPs are labelled 'TPP' and 'NGL', respectively. Up to a concentration of 2.5 µg/ml, no trend towards an increased cell-killing could be seen. At a concentration of 5.0 µg/ml, a strong trend towards increased toxicity and decreased cell survival could be seen, albeit not significant *(p = .093* for TPP and *p = .11* for NGL*)*. At a concentration of 10 µg/ml, a significant decrease in cell viability could be seen for TPP *(p = .026)* and NGL *(p = .032).* Figure 10 shows the SF of unirradiated sham (Empty) and various concentrations of AuNPs. The SF of the sham group was defined to be 1.0.

	Concentration				
	0.5 µg/ml	**1.0 µg/ml**	**2.5 µg/ml**	**5.0 µg/ml**	**10.0 µg/ml**
Empty	1.00	1.00	1.00	1.00	1.00
TPP	1.03 ± 0.03	1.00 ± 0.10	0.99 ± 0.09	0.59 ± 0.19	0.49 ± 0.12
NGL	1.02 ± 0.03	0.95 ± 0.17	0.90 ± 0.10	0.51 ± 0.25	0.43 ± 0.15

Table 3 – CFA – Toxicity Assay – AuNPs

Survival fraction and standard deviation of unirradiated MDA-MB-231 incubated at various AuNP concentrations of TPP-PEG4-FeAuNPs and NGL-PEG4-FeAuNPs compared to the empty sham group.

In addition to looking at the possible toxicity of the nanoparticles, an experiment was set up to determine, at which concentrations an increased cell killing could be seen. For this purpose, 400 cells were seeded per well in a 12-well plate, incubated with both TPP-PEG4-FeAuNPs and NGL-PEG4-FeAuNPs, irradiated at 2 Gy, 4 Gy, and 6 Gy 24 hours after incubation, and left to grow for another 5–7 days. The concentrations used were 0.1 µg/ml, 0.25 µg/ml, 0.5 µg/ml, 0.75 µg/ml, 1.0 µg/ml, 2.5 µg/ml, 5.0 µg/ml, and 10.0 µg/ml (not all data shown). This experiment showed that for low concentrations of AuNPs (0.1 µg/ml and 0.25 µg/ml) no trend towards increased toxicity after irradiation with AuNPs compared to sham could be seen. At concentrations of 0.5 µg/ml and higher, a trend towards increased cell killing when using AuNPs compared to untreated sham cells could be seen, setting 0.5 µg/ml as the lower working concentration and 1.0 µg/ml as the higher working concentration.

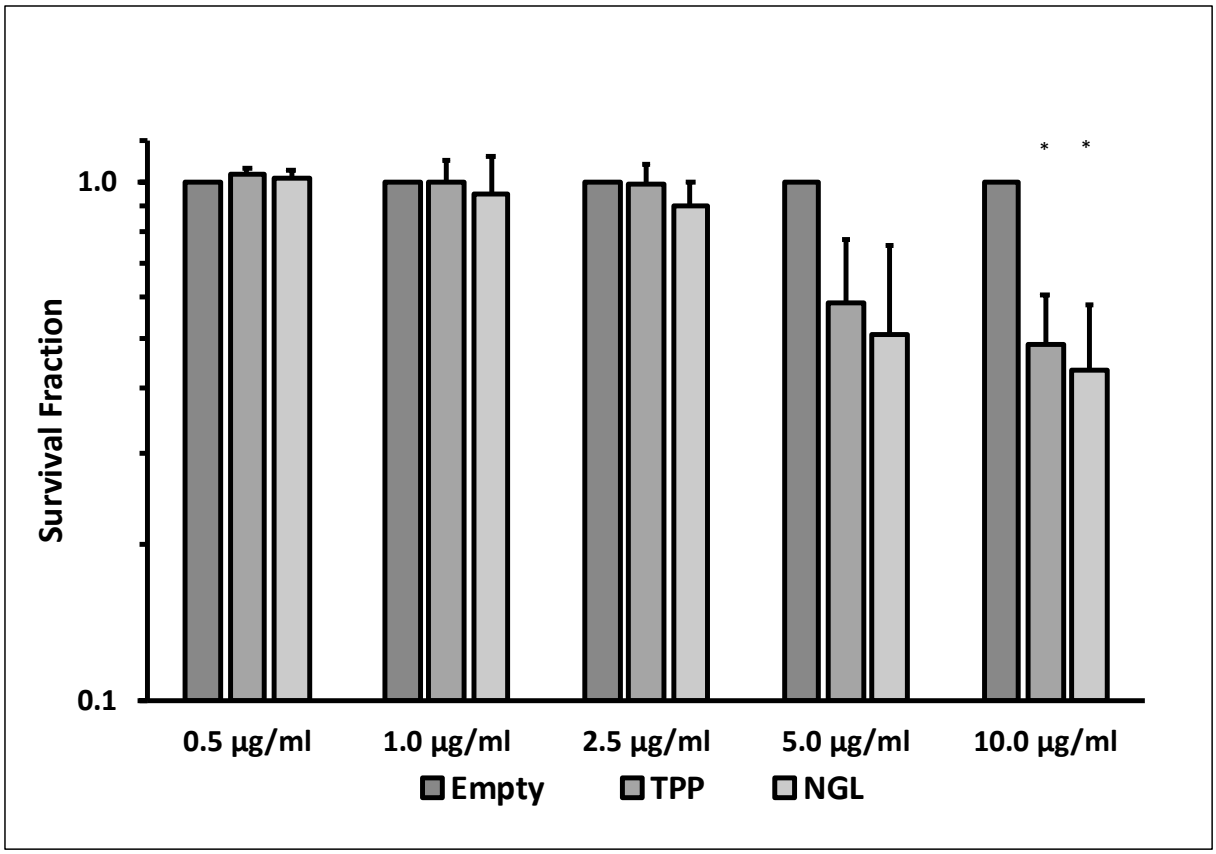

Figure 10 – CFA – Toxicity Assay – AuNPs

Survival fraction of unirradiated MDA-MB-231 cells incubated at various AuNP concentrations of TPP-PEG4-FeAuNPs and NGL-PEG4-FeAuNPs compared to the "Empty" sham group.

At neither one of these concentrations (i.e., 0.5 or 1.0 µg/ml), a tendency towards increased toxicity at sham could be seen, as shown in Figure 10. At a concentration of 5.0 µg/ml or higher, there is a strong tendency towards increased cell killing, and at concentrations of 10.0 µg/ml statistically significant increase in cell death was observed, making these unsuitable working concentrations.

4.2 Colony forming assays – AuNPs and irradiation

Figure 11 and Figure 12 show dose-effect curves for the treatment of cells with TPP-PEG4-FeAuNPs and NGL-PEG4-FeAuNPs at irradiation doses of 0 Gy, 2 Gy, 4 Gy, and 6 Gy. Sham represents the cells which were left untreated, meaning without AuNPs (Empty).

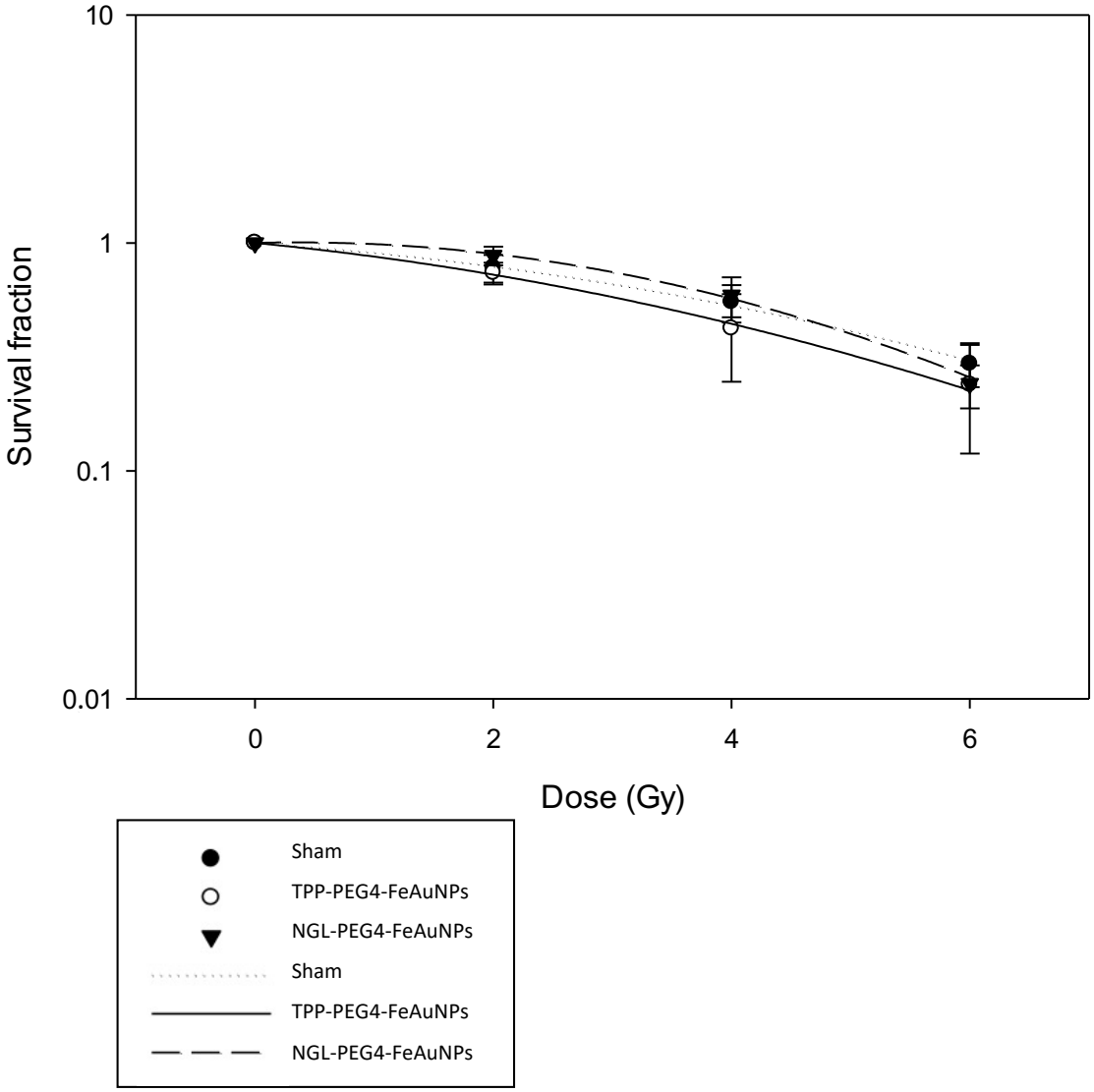

Figure 11 – CFA – Survival of MDA-MB-231 with AuNPs (0.5 µg/ml)

CFA – Survival fraction of MDA-MB-231 incubated with 0.5 µg/ml TPP-PEG4-FeAuNPs vs. 0.5 µg/ml NGL-PEG4-FeAuNPs vs. Empty (untreated) 5–7 days post irradiation with sham (0 Gy), 2 Gy, 4 Gy, and 6 Gy.

After seeing no toxic effects at a concentration of 0.5 and 1.0 µg/ml in the unirradiated group, the survival fraction at sham (0 Gy) was set to 1.0. The x-axis represents the radiation dose ranging from 0 Gy to 6 Gy, while the y-axis shows the SF plotted on a logarithmic scale. The dotted line represents the linear-quadratic survival curve for sham. The dashed line shows the survival curve for cells treated with NGL-PEG4-FeAuNPs, and the continuous line shows the survival curve for cells treated with TPP-PEG4-FeAuNPs. Figure 11 shows a trend towards decreased cell survival when comparing TPP-PEG4-FeAuNP with NGL-PEG4-FeAuNPs or

the untreated (Empty) cells, albeit the decrease is not significant. This trend is most visible around 4 Gy. Table 4 shows the data visualised in Figure 11.

		Dose (Gy)			
		0 Gy	2 Gy	4 Gy	6 Gy
Concentration 0.5 µg/ml	Empty (sham)	1.00	0.778 ± 0.108	0.550 ± 0.103	0.295 ± 0.062
	TPP-AuNPs	1.00	0.738 ± 0.081	0.421 ± 0.175	0.239 ± 0.051
	NGL-AuNPs	1.00	0.880 ± 0.083	0.589 ± 0.117	0.241 ± 0.122

Table 4 – CFA – Survival fraction and standard deviation of MDA-MB-231 with AuNPs (0.5 µg/ml).

Survival fraction and standard deviation of Empty (untreated) MBA-MB-231 cells and cells treated with TPP- and NGL-PEG4-FeAuNPs at a concentration of 0.5 µg/ml at different irradiation doses (0 Gy, 2 Gy, 4 Gy, and 6 Gy).

In Figure 12, a concentration of 1.0 µg/ml AuNPs was used. The trend towards decreased cell viability is more visible at this higher concentration. At higher irradiation doses, the dotted sham line and the continuous TPP-AuNP line diverge more noticeably. The TPP-AuNP and the NGL-AuNP show a parallel progression, where the TPP-AuNP is shifted downwards, suggesting a more considerable cell death. Table 5 shows the data visualised in Figure 12.

		Dose (Gy)			
		0 Gy	2 Gy	4 Gy	6 Gy
Concentration 1.0 µg/ml	Empty (sham)	1.00	0.778 ± 0.108	0.550 ± 0.103	0.295 ± 0.062
	TPP-AuNP	1.00	0.785 ± 0.140	0.370 ± 0.178	0.183 ± 0.139
	NGL-AuNP	1.00	0.883 ± 0.172	0.453 ± 0.073	0.199 ± 0.079

Table 5 – CFA – Survival fraction and standard deviation of MDA-MB-231 with AuNPs (1.0 µg/ml).

Survival fraction and standard deviation of Empty (untreated) MBA-MB-231 cells and cells treated with TPP- and NGL-PEG4-FeAuNPs at a concentration of 1.0 µg/ml at different irradiation doses (0 Gy, 2 Gy, 4 Gy, and 6 Gy).

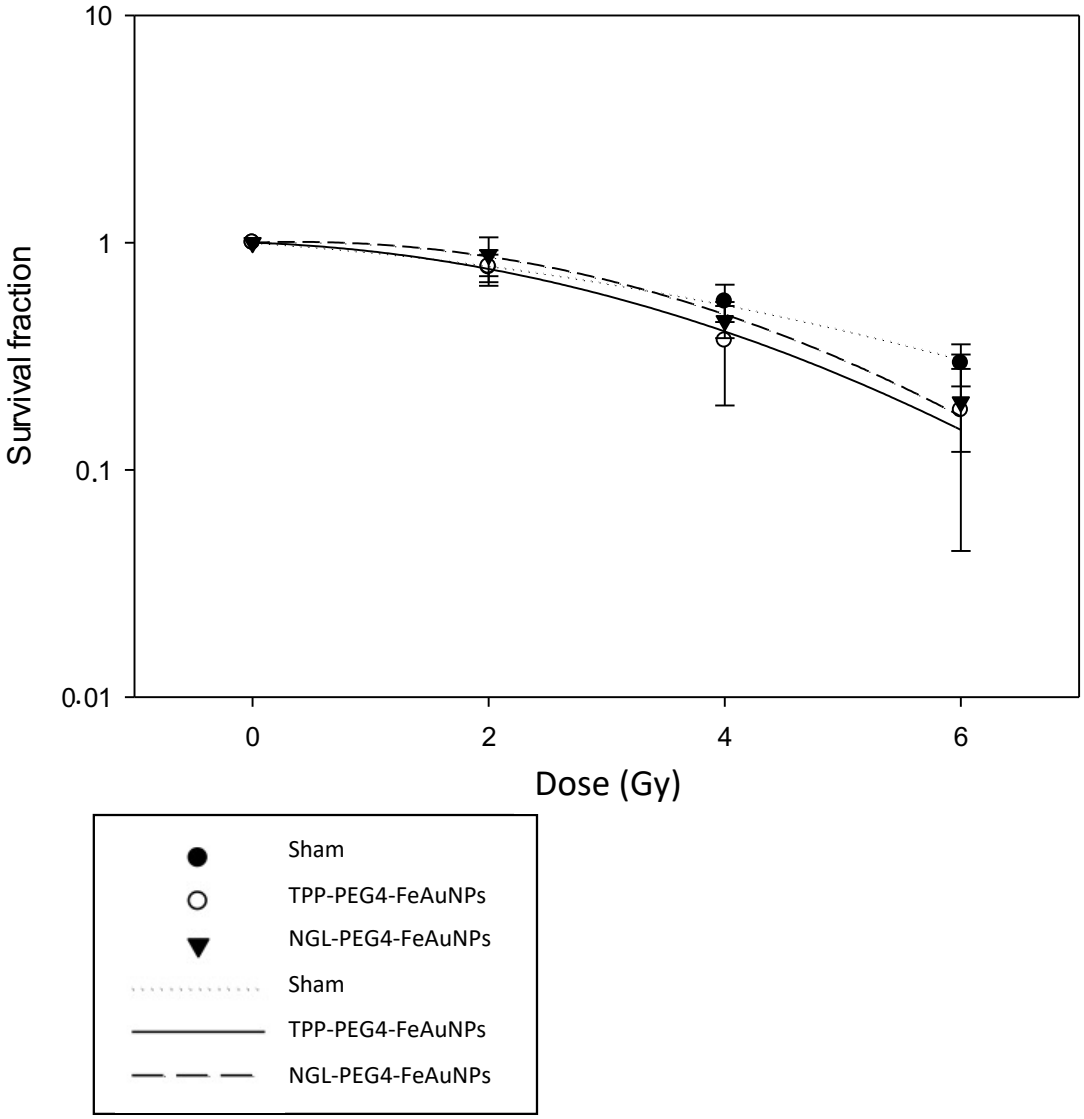

Figure 12 – CFA – Survival of MDA-MB-231 with AuNPs (1.0 µg/ml)

CFA – Survival fraction of MDA-MB-231 incubated with 1.0 µg/ml TPP-PEG4-FeAuNPs vs 1.0 µg/ml NGL-PEG4-FeAuNPs vs. Empty (untreated) 5–7 days post irradiation with sham (0 Gy), 2 Gy, 4 Gy, and 6 Gy.

The increase in radiosensitivity can be measured using the DEF, which describes the ratio of radiation absorbed in the presence of AuNPs to the dose absorbed without nanoparticles (Muddineti et al., 2015; Shahhoseini et al., 2018). It is dependent on the AuNPs' characteristics,

concentration, and localisation (Butterworth et al., 2012; Hossain & Su, 2012). It measures chromosome aberrations, DNA damage, or clonogenic cell survival (Kong et al., 2008). The DEF is calculated using the following equation:

$$DEF50 = \frac{\mathrm{D50}\ (sham)}{D50\ (AuNPs)},$$

where D50 (sham) represents the dose required to reduce the viability of cells by 50% in cells irradiated without nanoparticles, and D50 (AuNPs) represents the dose required to reduce the viability of cells by 50% in cells irradiated with nanoparticles. For both 0.5 and 1.0 μg/ml of the TPP-PEG4-FeAuNPs, an increase in the DEF could be seen of 1.10 and 1.13, respectively. For the NGL-PEG4-FeAuNPs, the DEF was at 0.97 and 1.0 for 0.5 and 1.0 μg/ml, respectively.

5 Discussion

An increasing focus is set on research aimed at improving cancer treatments. A novel technique being studied is the use of AuNPs combined with conventional radiation treatments, a concept known as 'gold nanoparticle assisted radiation therapy' (Cooper et al., 2014; Li et al., 2020; Zygmanski & Sajo, 2016). In this work, the human TNBC cell line MDA-MB-231 was incubated with different concentrations of hybrid gold (Au)-iron oxide (Fe_3O_4)-nanoparticles coupled to either TPP (TPP-PEG4-FeAuNPs) or NGL (NGL-PEG4-FeAuNPs), using PEG4 as a linker to hinder aggregation. MDA-MB-231 cells are highly positive for mHsp70, which operated as the target protein for the TPP-PEG4-FeAuNPs. TPP is a 14 amino acid sequence from the C-terminal oligomerisation domain of Hsp70 which specifically binds membrane Hsp70 expressed exclusively on tumours and metastases but not on normal tissue (Multhoff, Botzler, Wiesnet, Muller, et al., 1995). TPP shows a high affinity to mHsp70 both in vivo and in vitro, expressing good in vivo biodistribution and no toxic effects on the organism (Stangl et al., 2014). NGL is a scavenger peptide consisting of a shuffled amino acid sequence with unspecific protein binding (Gehrmann et al., 2014) that served as a control. Upon binding to mHsp70, TPP is rapidly internalised by tumour cells as opposed to scrambled, unspecific peptides (Gehrmann et al., 2014; Wu et al., 2023) and features a maximum accumulation in the perinuclear region 24 hours after incubation (Gehrmann et al., 2015; Stangl et al., 2014; Wu et al., 2023). These findings regarding maximum accumulation 24 hours after administration were confirmed by Goel et al. (2009) using 33 nm-sized AuNPs conjugated with PEG and tumour necrosis factor-alpha (TNF-α). Melancon et al. (2008) also showed a maximum accumulation of AuNPs after 24 hours, where only 10% of the AuNP dose, however, accumulated in the tumour (Khlebtsov & Dykman, 2011; Melancon et al., 2008). Considering this data, the timepoint for irradiation following incubation with TPP-PEG4-FeAuNPs and NGL-PEG4-FeAuNPs was chosen after 24 hours for the abovementioned experiments.

The nanoparticles used in this work consisted of a 2 nm iron oxide core coated with a 1 nm gold shell, resulting in an overall diameter of 4 nm. The iron core enables additional diagnostic purposes due to its paramagnetic properties increasing MRI relaxation times (Wood & Ghugre, 2008; Wu et al., 2023), which will be helpful in everyday clinical practice. To quantify the cell death following irradiation, clonogenic assays were performed using MDA-MB-231 cells incubated with 0.5 and 1.0 µg/ml of TPP-PEG4-FeAuNPs or NGL-PEG4-FeAuNPs. 24 hours post incubation the cells were irradiated with 2 Gy, 4 Gy, or 6 Gy and left

to grow until colonies of over 50 cells had formed. This study used a seeding density of 400 cells per well considering the optimal growing conditions as shown in Figure 8.

The CFA results showed a decrease in cell viability and an increase in clonogenic cell death in the cells incubated with the TPP-PEG4-FeAuNPs compared to the cells irradiated without nanoparticle incubation, in line with existing literature. Moreover, a strong trend towards increased cell death could be seen in cells treated with the TPP-PEG4-FeAuNPs compared to the NGL-PEG4-FeAuNPs even at low concentrations, suggesting the specific targeting of membrane-bound Hsp70 could prove a promising hallmark in the future of cancer diagnostics and therapies. Wu et. al (2023) tested AuNP concentrations of 2.5 µg/ml of TPP-PEG4-FeAuNPs and NGL-PEG4-FeAuNPs and were able to show similar, corresponding results with a significant radiosensitisation of TNBC cell lines MDA-MB-231 and 4T1, a murine TNBC line (Wu et al., 2023), strengthening the findings above.

In this study mHsp70 was used as the target protein on MDA-MB-231 cells. As reviewed by Ciocca and Calderwood (2005), Hsp70 poses a valuable marker for carcinogenesis, differentiation, and aggressiveness for certain tumour entities. High Hsp70 levels correlate with poor tumour differentiation, increased proliferation, higher clinical stage, and tendency to metastasize in tumours such as breast, uterine, colon, and lung (Ciocca & Calderwood, 2005). Concomitantly, Hsp70 has a negative influence on the prognosis and survival (Ciocca & Calderwood, 2005). Interestingly, Hsp70 can be used as a predictor for treatment response, where high levels mean lower response to, for instance, radiation and chemotherapy (Ciocca & Calderwood, 2005; Gehrmann, Radons, et al., 2008; Murakami et al., 2015). In some tumours, metastases expressed higher levels of membrane Hsp70 than the corresponding primary tumours, supporting the correlation between high Hsp70 levels and a more aggressive, treatment-resistant phenotype (Botzler, Schmidt, et al., 1998; Farkas et al., 2003). As discussed earlier, Hsp70 is selectively expressed on the surface membrane of tumours but not on corresponding healthy tissue (Hantschel et al., 2000; Multhoff, Botzler, Wiesnet, Muller, et al., 1995; Pfister et al., 2007). This selective expression may be used as a diagnostic and therapeutic target (Ciocca & Calderwood, 2005; Murphy, 2013; Pfister et al., 2007), for instance, for intraoperative and near infrared fluorescence (NIRF) imaging of Hsp70-positive tumours in mice (Stangl, Gehrmann, Dressel, et al., 2011), positron emission tomography (PET)-tracer (TPP-PEG24-DFO [89Zr]), or as the results of this work emphasize, the potential of mHsp70 as a target protein in future cancer treatments to deliver AuNPs, increasing the affinity of tumour cells towards radiation, and enabling more efficient radiotherapy treatments.

The results above mark a significant advancement in the search for a therapeutic agent that may both increase radiosensitivity and be safe for use to treat breast cancer. First, I could show that the citrate buffer in which the TPP- and NGL-AuNPs were suspended does not exert any toxic effects on MDA-MB-231 cells at volumes of 20 µl and under, suggesting it is safe for in vitro use. This lack of toxicity needs to be confirmed in further in vivo models. Second, I could show no significant toxicity of TPP-PEG4-FeAuNPs and NGL-PEG4-FeAuNPs at concentrations of 5 µg/ml or less. Toxicity of AuNPs at high concentrations in the absence of irradiation might render useful in later therapeutic regimes; however, this requires a specific uptake into tumour cells, with a proven lack of toxicity in healthy surrounding cells, as well as cells of the liver and spleen, where accumulation will most likely occur. A possible experimental setup to confirm this safety would be to test the uptake and toxicity of TPP-PEG4-FeAuNPs and NGL-PEG4-FeAuNPs on, for instance, peripheral blood lymphocytes (PBL) or liver cells. Wu et al. (2023) were already able to show no AuNP uptake into mHsp70 negative PBL cells. Third, I was able to show a superiority of TPP-PEG4-FeAuNPs compared to NGL-PEG4-FeAuNPs even at low concentrations of 0.5 µg/ml and 1.0 µg/ml, achieving an increased radiosensitivity in the presence of TPP-PEG4-FeAuNPs, in line with previous findings. This superiority of TPP-PEG4-FeAuNPs becomes more visible and significant at AuNP concentrations of 2.5 µg/ml (Wu et al., 2023), strengthening the findings above.

An efficacy and lack of toxicity in vitro must be shown to design and establish a therapeutic agent. The primary aim of this work was to prove a lack of toxicity of the AuNPs in question, determine the ideal working concentration of AuNPs at which an effect can be seen but where no toxicity is exerted, and show the superiority of the TPP- compared to the NGL-PEG4-FeAuNPs following incubation and irradiation of the AuNPs with MDA-MB-231 cells. These aims were thus achieved. The next step when working towards a clinical translation involves a series of individual intermediate steps, starting with determining the optimal administration pathways, biodistribution, cellular uptake, elimination, tumour targeting, and potential systemic toxicity (Cui, Her, Borst, et al., 2017), which we will discuss in the following sections. The experiments above were performed in vitro. To achieve the anticipated radiosensitisation by AuNPs in vivo, the nanoparticles first need to reach their target, in this case, the tumour cells. The first step in this journey commences with the administration route. Four major administration pathways have been studied, namely intravenous, intraperitoneal, oral, and intratumoural application. Intratumoural application achieves the highest local concentration of nanoparticles with the lowest systemic toxicity (Cui, Her, Borst, et al., 2017). Furthermore, the administered nanoparticles will remain at the desired site days and weeks after

application (Cui, Her, Borst, et al., 2017). Intraperitoneal administration is helpful for loco-regional tumours, including gastric malignancies and ovarian cancers (Cui, Her, Borst, et al., 2017). Studies have shown increased survival for patients with ovarian cancer treated with radioactive AuNPs. However, only small amounts of the AuNPs remained on site, while a more significant fraction accumulated in extraperitoneal organs such as the heart and lungs (Cui, Her, Borst, et al., 2017). Intravenous application is by far the most common and unequivocal method of drug administration. It renders high systemic distribution and availability with the disadvantage of lower concentrations of the drug at the desired sites (0.7–7.0%) due to high blood clearance, in addition to potentially higher systemic toxicity of non-target organs (Cui, Her, Borst, et al., 2017). Hillyer and Albrecht (2001) tested the uptake of 4 to 58 nm AuNPs through the alimentary track and found it to be inversely proportional to the particle size. A study performed by Zhang et al. (2010) compared the toxicity of oral, intraperitoneal, and intravenous administration in vivo using 13.5 nm AuNPs in mice, controlling body weight, blood samples, and spleen changes. Interestingly, they found the highest toxicity for both the oral and intraperitoneal routes, whilst intravenous administration was best tolerated (Zhang et al., 2010). These factors need to be considered when designing a patient's treatment plan, where nanoparticles are to be used, keeping not only the optimal uptake or potential toxicity in mind, but also the patient's quality of life. In the case of localised breast cancer, such as in this study, intratumoural injections prior to surgical removal or intraoperative application into the tumour bed following resection might be considered efficient routes. Furthermore, if a sufficient intratumoural concentration can be achieved, an intravenous application might prevail as a long-term solution in parallel with postoperative irradiation therapy.

The second step in reaching the target focuses on bioavailability. The bioavailability of nanoparticles strongly depends on blood clearance, circulation time, and particle size (Singh et al., 2018). Upon entering a living organism, a protein coating known as 'corona' envelopes the nanoparticles, forming a nanoparticle-protein complex (Singh et al., 2018). These circulating nanoparticle-protein complexes are recognised as foreign material, opsonised by cells of the RES, and eliminated from the bloodstream (Chen et al., 2020; Wolfram et al., 2015), hindering them from reaching their target. This issue can be circumvented by coating and conjugating nanoparticles with various proteins and linkers (Haume et al., 2016). PEG is a commonly used surface coat hindering aggregation, opsonisation, recognition, and premature clearance by mononuclear phagocytes of the spleen and liver, enabling longer blood circulation times (Alexis et al., 2008; Aminabad et al., 2019; Chen et al., 2020; Gao et al., 2021; Gerosa et al., 2020; Haume et al., 2016; Liu et al., 2010; Mieszawska et al., 2013; Otsuka et al., 2003; Owens &

Peppas, 2006; Singh et al., 2018; Yu et al., 2020). Consequently, to prevent aggregation and premature elimination in future in vivo models, PEG4 coating was used on the hybrid gold (Au)-iron oxide (Fe_3O_4)-nanoparticles used in this study.

As mentioned before, particle size also influences blood circulation times. Zhang et al. (2009) studied size-dependent blood circulation times for various nanoparticle sizes. Nanoparticles sized 80 nm showed a half-life clearance of under one minute; particles sized 40 nm showed a half-life clearance of ten minutes, and the longest half-life clearance and blood circulation time of around half an hour was achieved by 20 nm-sized particles (G. Zhang et al., 2009). As would be expected, the higher circulation time of half an hour achieved by 20 nm-sized particles showed the highest nanoparticle accumulation in tumour tissue (Khlebtsov & Dykman, 2011; G. Zhang et al., 2009). Using PEG as a surface coat, Cho et al. (2009) successfully achieved even longer blood circulation times of 30 hours. By prolonging blood circulation times and concomitantly bioavailability, passive targeting and intratumoural accumulation through the EPR can be increased (Chen et al., 2020; Cui, Her, Borst, et al., 2017; de Lazaro & Mooney, 2020; Gerosa et al., 2020; Tudda et al., 2022; Zhu et al., 2013), aiding the goal of optimising tumour accumulation and increasing radiosensitisation.

The use of PEG for clinical intravenous application has already been approved (Gao et al., 2021). The coating of nanoparticles with PEG, however, also has downsides. First, studies suggest, that PEG-coating might reduce the uptake of AuNPs into tumour cells once these have reached the tumour site (Alhussan et al., 2021; Cruje et al., 2015). To counteract this, Cruje et al. (2015) proposed the addition of an arginine-glycine-aspartic acid (RGD) sequence to increase uptake. Second, the repeated administration of PEG-coating has been shown to promote the formation of anti-PEG antibodies, resulting in the ‘accelerated blood clearance’ (ABC) phenomenon with reduced blood circulation times (Gao et al., 2021; Wolfram et al., 2015). Third, due to the shielding of the AuNP surface from radiolytic processes, PEG-coated AuNPs may produce fewer hydroxyl radicals than naked AuNPs (Cui, Her, Borst, et al., 2017). Lastly, some studies even suggested protective effects due to the thiol group of the PEG, scavenging free radicals, reactive oxygen species, and low energy electrons (Cui, Her, Borst, et al., 2017). These findings must be considered when designing the ideal nanoparticle, and advantages and disadvantages must be weighed.

The third step focuses on cellular uptake and subsequent intracellular localisation of AuNPs. This step is influenced by various nanoparticle properties including size, shape, surface

charge, functionalisation (Sabella et al., 2014), and cell cycle (Chen et al., 2020; Cui, Her, Borst, et al., 2017; Zhu et al., 2013). Several uptake pathways into a cell are known. These include: A passive uptake across the cellular membrane, predominantly for small AuNPs sized 4–10 nm; an endocytic uptake, including phagocytosis and micropinocytosis, mainly for larger AuNPs and conglomerates; clathrin-coated-endocytosis for functionalised AuNPs between 10 and 100 nm in size; caveolin-dependent endocytosis for charged AuNPs 10–100 nm in size; and clathrin- and caveolin-independent uptake for functionalised, charged, or neutral AuNPs smaller than 100 nm (Darweesh et al., 2019; Zhu et al., 2013). In most cases, the AuNP uptake is via receptor-mediated endocytosis (RME) (Alhussan et al., 2021; Surapaneni et al., 2018). Sindhwani et al. (2020) showed, that the passive uptake of AuNPs through endothelial gaps in tumour vessels accounts for only 3–25%, varying with nanoparticle size, proving that the main uptake pathway is via the trans-endothelial pathway. Studies performed by Chithrani et al. (2006) showed the highest uptake for nanoparticles sized 50 nm compared to 14 nm and 74 nm.

As seen in the previous sections, uptake and intracellular localisation vary largely between different particles. Therefore, we need to better understand the path the AuNPs used in this work take upon entry into the cell. Stangl et al. (2011) showed a translocation of cmHsp70.1 monoclonal antibody into early endosomes and lysosomes after internalisation into tumour cells. Gehrmann et al. (2014) showed a time-dependent uptake via an endolysosomal pathway for TPP. Using confocal microscopy, they showed the co-localisation of carboxy-fluorescein (CF) labelled TPP with Rab5, Rab7, and lysosomal-associated membrane protein-1 (LAMP1), marker proteins for early endosomes, late endosomes, and lysosomes, respectively (Gehrmann et al., 2014). TPP was localised in early endosomes (Rab5) within 30 minutes after uptake. After 30 minutes, TPP was found in late endosomes (Rab7), and after 60 minutes, TPP could be seen in LAMP1-positive lysosomes (Gehrmann et al., 2014). The small Rab5 stained vesicles could be found near the plasma membrane, late endosomes expressing Rab7, between the nucleus and plasma membrane, and the large lysosomes expressing LAMP1, in the perinuclear region (Gehrmann et al., 2014). Other studies support these findings: Jain et al. (2011) showed a significant uptake of AuNPs into cytoplasmic lysosomes of MDA-MB-231 cells, where accumulation and aggregation seemed to occur. Lee et al. (2014) saw receptor-mediated endocytosis dependent AuNP-uptake in MDA-MB-231 cells, where the vesicles later fused into lysosomes and autophagosomes. Additionally, a proportion of intracellular TPP was shown to co-localise with mitochondria in breast cancer cell lines (Gehrmann et al., 2015). In summary, the findings above strongly suggest, that the 4 nm-sized TPP-PEG4-FeAuNPs used

in this study are taken up via the endocytic pathway and accumulate in lysosomes in the perinuclear region.

In order to maximise the damage inflicted on the DNA after irradiation, nuclear localisation of AuNPs was long believed necessary, since low energy electrons only dispose of a short travelling range (Chen et al., 2020; Hainfeld et al., 2008; Kuncic & Lacombe, 2018; Li et al., 2020). Nanoparticles smaller than 10 nm in size, positively charged nanoparticles, or those with specific nuclear localisation signals (NLS), have been shown to be able to penetrate the nuclear membrane (Chen et al., 2020; Cui, Her, Borst, et al., 2017; Nunez et al., 2018; Ozcelik & Pratx, 2020; Zhu et al., 2013). Fan et al. (2020) showed a nuclear uptake for AuNPs of 2 nm and 6 nm in size. However, most nanoparticles used in previous studies were trapped in endosomes or lysosomes hindering nuclear penetration (Chen et al., 2020; Zhu et al., 2013). The same holds true for the 4 nm-sized hybrid gold (Au)-iron oxide (Fe_3O_4)-nanoparticles used in this study, where TPP-PEG4-FeAuNPs showed a uniform, perinuclear localisation 24 hours after incubation (Wu et al., 2023). Although lysosomes are predominantly located surrounding the nucleus, no internalisation into the nuclear region occurs (Cui, Her, Borst, et al., 2017). Most likely, this is due to the nuclear double membrane (Pernodet et al., 2006). Polyethylenimine (PEI) or cell penetrating-peptides (CPP) can be used to escape these compartments into the cellular cytoplasm (Zhu et al., 2013). However, against prior assumptions, nanoparticles can enhance the radiation effect without nuclear localisation, suggesting nuclear penetration is superfluous (Cui, Her, Borst, et al., 2017; Janic et al., 2021; Tudda et al., 2022). This emphasises the possibility of enhancing radiosensitisation by TPP-PEG4-FeAuNPs, regardless of their perinuclear localisation within lysosomes.

Before administering nanoparticles in vivo, potential toxic effects on the organism besides the targeted tumour must be considered. Thus, the properties necessary for optimal therapeutic effects at the same time need to be balanced with potential toxic side effects. In the experiments performed above, a significant decrease in cell survival for the unirradiated control group could be seen at 10 µg/ml and above, suggesting an in vitro toxicity of AuNPs at higher concentrations. At a concentration of 5 µg/ml, there was a strong trend towards increased cell killing, however, it was not statistically significant. The lower concentrations of 0.5 µg/ml, 1.0 µg/ml, and 2.5 µg/ml showed no toxicity. These findings held true for both TPP-PEG4-FeAuNPs and NGL-PEG4-FeAuNPs, albeit NGL does not actively target tumour cells. As seen before, however, nanoparticles smaller than 10 nm may experience a degree of passive uptake

across the cellular membrane (Darweesh et al., 2019; Zhu et al., 2013), explaining this toxicity of nanoparticles lacking specific targeting.

Furthermore, as opposed to the generally accepted view that gold is predominantly inert, increasing evidence is arising, that suggests gold can catalyse chemical reactions through surface interactions (Ionita et al., 2005; Mikami et al., 2013; Tao, 2018; Wang et al., 2017). AuNPs can create superoxide radicals by transferring surface-bound electrons to O_2 (Chen et al., 2020; Her et al., 2017; Wang et al., 2017). This was mainly observed in small AuNPs under 5 nm with high curvature (Her et al., 2017; Wang et al., 2017) due to increased catalytic activity (Alkilany & Murphy, 2010; Chen et al., 2020; Falagan-Lotsch et al., 2016; Khlebtsov & Dykman, 2011; Pernodet et al., 2006). Other studies suggest a contrary position, showing increased cytotoxicity for larger AuNPs, possibly due to greater physical damage to cell organelles (Khlebtsov & Dykman, 2011; Mironava et al., 2010). Exceptionally high toxicity was shown for positively charged nanoclusters sized 1–2 nm, similar in size to B-form DNA (Semmler-Behnke et al., 2008). This suggests, that these AuNPs can bind DNA and other key biomolecules irreversibly, altering cellular processes, and causing increased cellular toxicity (Khlebtsov & Dykman, 2011; Semmler-Behnke et al., 2008; Wang et al., 2017).

These findings of metal toxicity have been published by several groups with various possible explanations. Sharma et al. (2009) suggested the toxicity of metal in a biological system may be due to three reasons: First, the formation of ROS with consecutive oxidative stress and modification of anti-oxidant mechanisms; second, the expulsion of cations from protein binding sites resulting in loss of function; and third, the direct interaction with protein end-groups, influencing protein structures and cellular transport or metabolism (Sharma & Dietz, 2009). Sabella et al. (2014) found, that the acidic conditions in lysosomes, where nanoparticles are predominantly located after internalisation into the cell, cause degradation and corrosion of nanoparticles with lysosomal membrane permeabilization and the subsequent release of toxic ions into the intracellular space (Sabella et al., 2014). This mechanism was termed the ‘lysosome-enhanced Trojan horse effect’ by Sabella et al. (2014). A significantly lower cell toxicity was found when nanoparticles entered the cell in an energy-independent pathway (Sabella et al., 2014). Other studies suggest that smaller nanoparticles’ highly curved surface leads to crystal structure defects and electron configuration disruption (Cui, Her, Borst, et al., 2017). This results in the formation of reactive electron donating and accepting locations as well as an increase in the number of chemical reactions (Cui, Her, Borst, et al., 2017; Nel et al., 2006). Misawa et al. (2011) agreed with this hypothesis, as they showed an inverse

correlation between the AuNP size and the ROS formation, where smaller-sized nanoparticles generated more ROS than larger AuNPs with a smaller surface-to-volume ratio. This formation of ROS, catalysed by AuNPs, may cause damage to cell organelles, proteins, mitochondria, and DNA, resulting in cellular harm (Jain et al., 2011; Pan et al., 2009; Wolfram et al., 2015). In turn, a series of cell-death pathways such as apoptosis, autophagy, and necrosis may ignite (Jain et al., 2011; Pan et al., 2009; Wolfram et al., 2015). I speculate, that these factors play a role in the in vitro toxicity of TPP- and NGL-PEG4-FeAuNPs at concentrations above 10 µg/ml in the unirradiated sham group.

In addition to intracellular toxicity, an effect on systemic oxidative stress and inflammation has been reported (Lopez-Chaves et al., 2018; Sabella et al., 2014). The metallic nature of AuNPs can establish interactions with cellular components, such as proteins and nucleotides, possibly causing an oxidative imbalance and impairing molecular function (Lopez-Chaves et al., 2018). Genes involved in DNA repair and the genomic stability of cells also seem to be affected (Lopez-Chaves et al., 2018). Surapaneni et al. (2018) showed a cytotoxic effect of AuNPs on MDA-MB-231 and MDA-MB-468 cells as a result of induced oxidative stress, leading to increased cell death and epigenetic mutations.

Finally, the exposure time plays an important role when determining toxicity. Falagan-Lotsch et al. (2016) studied the long-term effects of various AuNPs and the difference between one-time acute exposure and continuous, chronic exposure. They found that acute, one-time exposure to AuNPs in human dermal fibroblasts (HDFs) had a greater effect on gene expression after 20 weeks than chronic exposure (Falagan-Lotsch et al., 2016).

The previous sections discussed the different factors influencing the biodistribution and bioavailability of AuNPs in vivo, the various methods in which AuNPs are taken up into cells, and their intracellular localisation with the ensuing impact. The process by which nanoparticles are removed from cells and the organism, as well as any possible side effects, will be covered in the following section. Gold, as a non-biodegradable material, can either accumulate in or be eliminated by an organism (Zhu et al., 2013). The first studies on this topic were completed in the 1970s and 1980s and found, that after parenteral application, nanoparticles were predominantly taken up by hepatocytes (Khlebtsov & Dykman, 2011). Exocytosis is believed to be the predominant pathway in which cells later clear nanoparticles (Zhu et al., 2013). Thereby, particle size, charge, and coating influence elimination rates and pathways.

Some studies suggest, nanoparticles sized below 6–10 nm are typically renally eliminated, while larger particles sized 50–100 nm are recognised and opsonised by the mononuclear phagocyte system (MPS) and removed from the bloodstream to the liver or spleen (Almeida et al., 2011; Chen et al., 2020; Cui, Her, Borst, et al., 2017; Fan et al., 2020; Haume et al., 2016; Lopez-Chaves et al., 2018; Yu et al., 2020). Generally, the larger the nanoparticle, the more likely they will accumulate in the spleen, suggesting that the spleen is one of the key organs in the metabolism of AuNPs (Lopez-Chaves et al., 2018; Singh et al., 2018).

Most studies agree that nanoparticle accumulation will predominantly occur in the liver and spleen. Research, however, is inconclusive on whether accumulation occurs in other organs. Sadauskas et al. (2007) showed an assembly of nanoparticles in macrophages of the liver, so-called Kupffer cells, and spleen in a relation of 10:1, where the nanoparticles would persist in lysosomes for several months. Little accumulation could be seen in other organs, such as the kidneys, lungs, brain, or ovaries (Sadauskas et al., 2007). De Jong et al. (2008) studied the biodistribution of nanoparticles sized 10–250 nm in rats after intravenous injection. They found 10 nm-sized nanoparticles in the testes, thymus, kidney, and brain in addition to the liver and spleen (De Jong et al., 2008). Goel et al. (2009) used 33 nm-sized AuNPs conjugated with PEG and TNF-α. They showed a maximum accumulation in the liver and spleen of mice 24 hours after administration with little decrease over the next four months (Goel et al., 2009; Khlebtsov & Dykman, 2011). Melancon et al. (2008) showed a nanoparticle distribution of around 20% of the dose each in the liver, spleen, and kidney, with only 10% accumulation in the tumour (Khlebtsov & Dykman, 2011; Melancon et al., 2008). Liver biopsies of patients who underwent treatment with CYT-6091, a human recombinant TNF (rhTNF)-conjugated AuNP, contained AuNPs, while biopsies of other tissues (skin and breast) did not (Libutti et al., 2010).

Whether penetration of the blood-brain barrier (BBB) or nanoparticle accumulation in the brain occurs is still a large discussion topic. Several authors listed in the preceding paragraphs could detect nanoparticles in the brain. Hillyer and Albrecht (2001) showed a crossing of the BBB for AuNPs sized 4 nm but not for larger AuNPs. A possible explanation for the difference in BBB penetration lies in the fact, that the astrocyte endfeet and the capillary endothelium are approximately 20 nm apart, suggesting nanoparticles smaller in size may penetrate the gap (Khlebtsov & Dykman, 2011). For future research and practical application, this should be considered when choosing a nanoparticle as a therapeutic agent.

The accumulation alone, however, does not prove a harmful toxicity. Cho et al. (2009) showed an accumulation of 13 nm PEG-coated AuNPs in the liver and spleen over the course of a week. The localisation was predominantly in lysosomes and vesicles in Kupffer cells of the liver and macrophages of the spleen (Cho, Cho, et al., 2009). This uptake into liver cells induced apoptosis and inflammation in the organ with increased cytokine and chemokine levels (Cho, Cho, et al., 2009). The liver toxicity showed two peaks: The first immediately following administration and the second several days later, when the particles had cleared from the bloodstream (Cho, Cho, et al., 2009). In addition, Cho et al. (2009) demonstrated dose-dependent toxicity, where higher nanoparticle concentrations (4.26 mg/kg body weight) showed increased toxicity compared to lower concentrations (0.17 and 0.85 mg/kg body weight). Other organs, such as kidneys, lungs, and the brain, showed slow elimination but were no primary targets (Cho, Cho, et al., 2009). Non-PEG-coated nanoparticles were found in other organs, suggesting PEG-coated AuNPs spread to organs containing phagocytic cells (Cho, Cho, et al., 2009). Hwang et al. (2012) were also able to demonstrate an accumulation in lysosomes of liver Kupffer cells. This accumulation of AuNPs caused no damage in healthy livers and the Kupffer cells remained resting (Hwang et al., 2012). In pre-damaged livers or those under stressful conditions, however, the application of AuNPs caused activation of Kupffer cells with recruitment and upregulation of immunological cells, secretion of cytokines, as well as increased ROS production, apoptosis, and necrosis (Hwang et al., 2012). Abdelhalim and Jarrar (2011, 2012), who administered 10, 20, and 50 nm sized AuNPs at different concentrations intraperitoneally to rats also reported this toxicity and alteration in liver cells. The livers of treated rats showed cloudy swelling, vacuolisation of hepatocytes, nuclear changes, and signs of chronic inflammation (Abdelhalim & Jarrar, 2011, 2012). According to these results, using AuNPs in vivo may result in an unintentional accumulation in liver cells, inflammation, and apoptosis, which could exacerbate liver damage and have an undesirable toxic effect on the organism. (Abdelhalim & Jarrar, 2011, 2012; Cho, Cho, et al., 2009; Hwang et al., 2012).

Looking at the possible long-term effects of nanoparticle utilisation, Cho et al. (2009) showed genetic alterations in mice after intravenous administration of 4 nm and 100 nm PEG-coated nanoparticles at a dose of 4.26 mg/kg weight. The affected genes were involved in metabolic processes, apoptosis, cell cycle, inflammation, and signal transduction (Cho, Cho, et al., 2009). Vecchio et al. (2012) showed a mutagenic effect of AuNPs on *Drosophila melanogaster*. The administration of 15 nm citrate AuNPs resulted in a lower number of laid eggs, a decrease in the number of organisms developed, and aberrant phenotypes (Vecchio et al., 2012). This strongly indicates DNA damage and genotoxicity induced by nanoparticles

possibly through increased levels of ROS (Vecchio et al., 2012). Chen et al. (2009) showed, that nanoparticles sized 8 to 37 nm administered intraperitoneally in mice induced loss in appetite and weight, fur change, fatigue, and premature death compared to the control group. Interestingly, smaller nanoparticles and those over 50 nm in size showed no increased toxicity (Chen et al., 2009). All these elements need to be considered when designing a future treatment plan for patients involving the application of nanoparticles. Consequently, practitioners should weigh up the many advantages with the possible drawbacks, such as aggravation of pre-existing organ damage and the potential long-term adverse side effects.

Naturally, it is difficult to predict the effect and behaviour of nanomedicine in humans from 'in vitro' and 'in vivo' experiments. In addition to the potential obstacles outlined in the previous sections, the administered dose of nanoparticles in vivo is essential. The studies cited here show a large discrepancy in the nanoparticle dose tested, ranging from fragments of micrograms to over 2,000 µg per gram of animal weight (Khlebtsov & Dykman, 2011). As reviewed by Khlebtsov and Dykman (2011) and agreed upon by most in vitro studies, the optimal dose lies between 0.1 and 10 µg/g of animal weight. In an average human of around 70 kg, this would amount to 7–700 mg of AuNPs. The upper concentration of particles should not exceed 10^{12} particles per ml (Khlebtsov & Dykman, 2011). As reviewed by Cui, Her, and Borst (2017), the concentration needed to accomplish a significant delay in tumour growth ranges from around 0.250 µg to 74.24 mg gold per gram of tumour weight. These values need to be considered when translating these pre-clinical experiments into future in vivo models in the next step of this project. The concentrations used in this work are congruent with the recommended concentrations from existing literature.

Summarising existing research and the findings of this project, the following conclusions can be drawn: First, AuNPs are able to enhance radiation effects by producing secondary electrons (Hainfeld et al., 2008; Kuncic & Lacombe, 2018; Li et al., 2020), catalysing chemical reactions, and producing ROS (Ionita et al., 2005; Mikami et al., 2013). These cause damage to the DNA, proteins, and threaten the stability of membranes and organelles (Cui, Her, Borst, et al., 2017; Haume et al., 2016), ultimately leading to cell death (Her et al., 2017; Pan et al., 2009; Xia et al., 2006). Second, AuNPs sized between 10 and 100 nm will primarily target and accumulate in organs of the RES, namely the liver and spleen (Almeida et al., 2011; Chen et al., 2020; Cui, Her, Borst, et al., 2017; Fan et al., 2020; Haume et al., 2016; Lopez-Chaves et al., 2018; Yu et al., 2020), while smaller AuNPs may be renally excreted (Cui, Her, Borst, et al., 2017). The clearing and excretion largely depend on the hepatobiliary system and

may take several months (Sadauskas et al., 2007). Third, the smaller the particle, the more uniform the distribution (G. Zhang et al., 2009). This includes a possible penetration of the BBB with accumulation in the brain, restricted to particles smaller than 15–20 nm (Khlebtsov & Dykman, 2011). Where and to what extent distribution and accumulation occurs strongly correlates with the administration method and functionalisation (Khlebtsov & Dykman, 2011). Fourth, the smaller the nanoparticle, the more toxic it seems to be (Lopez-Chaves et al., 2018), where ultrasmall nanoparticles, less than 2 nm, wide show particularly high toxicity due to irreversible binding properties to DNA and other vital biomolecules (Semmler-Behnke et al., 2008). Lastly, surface coating and active targeting can strongly influence blood circulation time, targeting, and accumulation (Haume et al., 2016). Hence, reflecting on the research described above and assuming in vitro qualities can be transferred to an in vivo model, the AuNPs used in this study are universally applicable: With a size of 4 nm, the TPP-PEG4-FeAuNPs would show an even distribution in the organism with maximum accumulation in the tumour 24 hours post application. Due to their conjugation to TPP, active targeting and uptake would be expected into malignant cells which express mHsp70 on their surface membrane. Furthermore, a degree of unspecific uptake may take place with the help of the EPR. Their small size of less than 6 nm might grant the TPP-PEG4-FeAuNPs access through the BBB, qualifying them as therapeutic agents for central nervous system malignancies. Accumulation should primarily occur in the liver and spleen due to the PEG-coating and coupling to peptides. Nonetheless, their small size might enable partial renal clearing, possibly lowering the accumulation in other organs. Lastly, one would expect a maximum toxicity for target cells due to their ideal size and short PEG-linker coating.

In this study, irradiation of 200 keV was used. In a clinical setting, MeV radiation is applied for deeply seated tumours (Alhussan et al., 2021; Rahman et al., 2009; Yogo et al., 2022). In modern radiotherapy, the gamma- or X-rays typically have an energy of 8 to 18 MeV, ranging from 80 keV to 25 MeV (Haume et al., 2016). At these energy levels the Compton effect is dominant (Cui, Her, Borst, et al., 2017). MeV energies have the advantage of greater matter penetration, dose uniformity, and less dose deposition in the surrounding tissue (Alhussan et al., 2021; Huang et al., 2015). At keV radiation energies, AuNPs have been shown to enhance radiosensitisation due to the difference in the absorption coefficient between gold and the surrounding tissue, with subsequent photoelectric effect and emission of Auger electrons (Her et al., 2017; Jain et al., 2011; Kuncic & Lacombe, 2018; Yogo et al., 2022).

Monte Carlo simulations (MC) are algorithms used to model the physical and chemical effects of radiation when interacting with biological structures (Kuncic & Lacombe, 2018). When these MC simulations were first applied, they predicted little dose enhancement effects of AuNPs at MeV radiation since gold was believed to only influence the physical stage with photoelectric absorption, a phenomenon with minimal contribution at MeV energies (Chen et al., 2020; Douglass et al., 2013; Sarria et al., 2019; Yogo et al., 2022). However, when in vitro studies were performed to test this hypothesis, the effect rendered significantly higher than in previous simulations, suggesting an involvement of AuNPs in all three stages, namely physical, chemical, and biological (Chen et al., 2020; Cui, Her, Borst, et al., 2017; Yogo et al., 2022). Chithrani et al. (2010) tested various radiation energies (105 kVp–6 MeV). While seeing a decrease in radiosensitisation and DEF with increasing radiation energies, significant radioenhancement was still achieved at 6 MeV (Chithrani et al., 2010). Similar observations were made by Jain et al. (2011) and Rahman et al. (2009), proving a significant radiosensitisation at 6 MeV, 12 MeV, and 15 MeV using MDA-MB-231 cells and 1.9 nm AuNPs. Huang et al. (2015) showed a significant enhancement in cell death in MDA-MB-231 cells using hollow AuNPs which was much larger than the theory-based predictions for MeV sources. Geng et al. (2011) reported increased radiation-induced ROS formation after irradiation with 90 kVp and 6 MeV. Yogo et al. (2022) proved increased DNA damage for 1.4 nm sized AuNPs at MeV energies. Ferrero et al. (2017) then suggested a novel approach for the prediction of radiation effects using an alteration of the local effect model (LEM) in combination with MC simulations, stating that at MeV energies, the nanoparticle contribution to dose deposition is negligible, nonetheless, the deposition of inhomogeneous dose in close nanoparticle proximity following a single ionisation event would suffice to trigger a series of lethal consequences (Ferrero et al., 2017).

The exact mechanism by which AuNPs influence the dose enhancement effect has not been fully understood. However, it is widely accepted that the surface chemistry of AuNPs plays an important role (Cui, Her, Borst, et al., 2017). Seeing radiation enhancement occurs at MeV energies suggests additional underlying biological and chemical mechanisms contributing to radiosensitisation (Chen et al., 2020; Cui, Her, Borst, et al., 2017). Such mechanisms include the production of secondary photons of keV energies and secondary electrons from the primary MeV photons (Tudda et al., 2022), the formation of ROS or the radiolysis of water catalysed by AuNPs, mitochondria dysfunction, alteration of the cell membrane and cycle, DNA repair mechanisms, as well as direct damage to the DNA (Jain et al., 2011; Yogo et al., 2022). I showed an increased radiosensitivity in vitro for TNBC cells at an irradiation energy of

200 keV. Seeing that existing literature was previously able to reproduce significant radioenhancement also at MeV energies has meaningful implications for the radioenhancement shown in this work. Specifically, I assume that the radioenhancement will also be detectable at MeV energies in future in vivo experiments and in the final application of AuNPs in patients.

5.1 Clinical translation

The long-term aim shared by all the groups and studies mentioned is the clinical translation of theoretical laboratory findings to functional technology safe for human application. In this regard, currently established irradiation regimes and logistics must be considered when establishing a radiation plan in a clinical setting. Evidence suggests that the application of AuNPs in combination with fractioned irradiation results in significantly higher radiation enhancement (Cui, Her, Borst, et al., 2017), fitting with existing guidelines. Furthermore, the timing of the AuNP application, dosing schedule, and irradiation type must be calculated (Cui, Her, Borst, et al., 2017). According to current knowledge, the optimal administration of AuNPs is 24 hours prior to radiation therapy, as this achieves optimal distribution in the tumour cells (Cui, Her, Borst, et al., 2017). A limitation in the translation of preclinical research into in vivo success is believed to be hypoxia (Cui et al., 2014; Jain et al., 2014), where the data from monolayer cell culture to 3D-tumours in a living organism are not transferrable. This is due to hypoxic cells' tendency to be radioresistant in the absence of oxygen and its radicals, crucial mediators of the radiation response (Her et al., 2017). Tumour hypoxia poses a major challenge for radiotherapy, increasing the risk of tumour recurrence and poor prognosis (Her et al., 2017). Cui et al. (2014) and Jain et al. (2014) looked at the effect of radiation in the presence of AuNPs for hypoxic cell conditions. They found, that under various hypoxic conditions, the radiosensitising effects of AuNPs were reduced compared to normoxic conditions (Jain et al., 2014). This suggests a lower effect of radiosensitisation in vivo than in vitro should be expected.

More pre-clinical studies, especially in vivo studies, are needed to achieve this long-term goal. Primarily, these studies should aim at an enhanced understanding of the cell cycle dependent uptake, hypoxia and reoxygenation, safe administration pathways, and short- and long-term toxicity on the organism. Several AuNPs are currently being evaluated in Phase 0 to 2 clinical studies in the battle against cancer:

- A phase 1 trial completed with CYT-6091, rhTNF conjugated PEGylated AuNPs (Aurimune ®) sized 27 nm for treating primary, advanced, and metastatic solid tumours

has shown selective delivery to the tumour without major toxicities (NCT00356980 and NCT00436410) (Alhussan et al., 2021; Chen et al., 2020; Cui, Her, Borst, et al., 2017; Lee et al., 2014; Libutti et al., 2010). The 108 individuals included in the study received 50–600 $\mu g/m^2$; the only side effects identified were fever and mild hypotension (Yu et al., 2020). In 2020, a Phase 2 trial was announced by CytImmune (Sibuyi et al., 2021; Yu et al., 2020).

- AuroShell®, a PEGylated AuNP with a silica shell used for photothermal therapy in lung, head and neck tumours (NCT00848042 and NCT02680535) (Alhussan et al., 2021; Chen et al., 2020; Cui, Her, Borst, et al., 2017; Her et al., 2017; Libutti et al., 2010), as well as prostate cancer (NCT04240639) (Zhang et al., 2023).
- Another nanoparticle undergoing Phase 2 and 3 trials is the NBTXR3, a hafnium-oxide nanoparticle being administered to patients with locally advanced head and neck squamous cell carcinoma (LA-HNSCC) in combination with radiotherapy (Cui, Her, Borst, et al., 2017). It has shown decent efficacy as a radiosensitiser as well as minor toxicity thus far (NCT04892173) (Cui, Her, Borst, et al., 2017).
- NU-0129, a drug based on small interfering RNA (siRNA) conjugated to spherical AuNPs targeting the Bcl2-L12 gene found in glioblastoma multiforme, is being tested in patients with gliosarcoma or glioblastoma multiforme recurrence in an early Phase 1 trial (NCT03020017) (Chen et al., 2020; Zhang et al., 2023).

5.2 Limitations and outlook

In the next section we will discuss possible limitations, strengths, and weaknesses of this work. First, one cell line of a solid tumour, namely MDA-MB-231, was tested. The degree of transferability of the data collected is variable and other cell lines may react differently to radiation and AuNP exposure. To further corroborate the data collected, testing on other cell lines with various Hsp70 levels would be beneficial: It might render promising results, considering the tumour entities that may qualify for this type of treatment. This might be especially interesting for other highly malignant cell lines with high mHsp70 levels, which are resistant to conventional treatments. Furthermore, a second, healthy cell line, which does not express mHsp70, as an additional negative control could be advantageous.

Second, further concentrations of AuNPs should be tested. Prof. Multhoff's group expanded the experimental setup testing a higher AuNP concentration of 2.5 µg/ml and a second cell line, 4T1. They achieved a significant increase in cell death at higher nanoparticle concentrations of 2.5 µg/ml when treated with Hsp70-targetting-TPP-PEG4-FeAuNPs (Wu et al., 2023), strengthening the data collected above. In this work, statistically significant toxicity of the AuNPs was only seen at a concentration of 10 µg/ml or higher, leaving a variety of concentrations that may be further examined.

Third, a higher number of cases (n) may be beneficial to improve statistical significance and predictability. A greater number of samples minimises the influence of random variants, more so in biological samples, thereby increasing statistical power. Partly, this limitation is due to the high material costs of the AuNPs. Nonetheless, in the samples carried out of n=3, a clear tendency towards increased cell killing of MDA-MB-231 cells following incubation with TPP-PEG4-FeAuNPs and irradiation can be seen.

Fourth, to ensure a reproducible, objective evaluation method the CFA data and colony count were analysed using *Bioreader®-3000* which showed a minor system error inversely proportional to the colony count and size – higher error with decreasing colony count and size. A possible approach to tackle this issue could be using different seeding densities as proposed by Huang et al. (2015), where MDA-MB-231 cells were seeded at different densities, namely 100, 100, 400, and 4000 cells for 0 Gy, 2 Gy, 4 Gy, and 6 Gy, respectively, depending on the irradiation dose to be administered. At the point of fixation and staining, similar colony densities could thus be counted. However, this alternative seeding protocol poses limitations seeing the initial growing conditions and incubation conditions of the cells are no longer equal

and comparable. I thus chose the approach described above, noting that the error would be equal for all samples tested and, therefore, comparable.

Fifth, in vitro and in vivo experiments with fractioned radiation regimes based on clinical workflow should be tested to better mimic and predict everyday irradiation regimes. During in vitro experiments, due to the vulnerability of cells in culture, this might further increase the source of errors, so I suggest this be carried out in in vivo models.

Finally, further in vivo testing is necessary. Before entering a clinical phase, the application of AuNPs must be approved as safe for human use. To guarantee this, in vivo testing on the safety of AuNP delivery, distribution, possible systemic side effects, and foremost long-term toxicity must be completed. TPP-coupled AuNPs specifically target membrane-bound Hsp70 expressed exclusively on the surface of malignant cells but not on corresponding healthy cells. This work shows, that after the internalisation of TPP-AuNPs into MDA-MB-231 cells, an increase in radiosensitivity of the tumour cells can be achieved. This represents a breakthrough in the rapidly growing domain of nanomedicine, where TPP-coupled AuNPs targeting mHsp70 prove their potential as universal diagnostic and therapeutic agents to improve both the quality of life and chances of survival of affected patients.

6 Bibliography

Abcam. (2020). *Introduction to flow cytometry*. https://www.abcam.com/protocols/introduction-to-flow-cytometry#measurement%20of%20scsattered%20light%20and%20fluorescence

Abdelhalim, M. A., & Jarrar, B. M. (2011). Gold nanoparticles induced cloudy swelling to hydropic degeneration, cytoplasmic hyaline vacuolation, polymorphism, binucleation, karyopyknosis, karyolysis, karyorrhexis, and necrosis in the liver. *Lipids Health Dis*, *10*, 166. https://doi.org/10.1186/1476-511X-10-166

Abdelhalim, M. A., & Jarrar, B. M. (2012). Histological alterations in the liver of rats induced by different gold nanoparticle sizes, doses, and exposure duration. *J Nanobiotechnology*, *10*, 5. https://doi.org/10.1186/1477-3155-10-5

Adams, G. E. (1973). Chemical radiosensitization of hypoxic cells. *British Medical Bulletin*, *29*(1), 48-53. https://doi.org/10.1093/oxfordjournals.bmb.a070956

Akhter, S., Ahmad, M. Z., Ahmad, F. J., Storm, G., & Kok, R. J. (2012). Gold nanoparticles in theranostic oncology: Current state-of-the-art. *Expert Opin Drug Deliv*, *9*(10), 1225-1243. https://doi.org/10.1517/17425247.2012.716824

Albanese, A., Tang, P. S., & Chan, W. C. (2012). The effect of nanoparticle size, shape, and surface chemistry on biological systems. *Annu Rev Biomed Eng*, *14*, 1-16. https://doi.org/10.1146/annurev-bioeng-071811-150124

Alexis, F., Pridgen, E., Molnar, L. K., & Farokhzad, O. C. (2008). Factors affecting the clearance and biodistribution of polymeric nanoparticles. *Mol Pharm*, *5*(4), 505-515. https://doi.org/10.1021/mp800051m

Alhussan, A., Bozdogan, E. P. D., & Chithrani, D. B. (2021). Combining gold nanoparticles with other radiosensitizing agents for unlocking the full potential of cancer radiotherapy. *Pharmaceutics*, *13*(4). https://doi.org/10.3390/pharmaceutics13040442

Alkilany, A. M., & Murphy, C. J. (2010). Toxicity and cellular uptake of gold nanoparticles: What we have learned so far? *J Nanopart Res*, *12*(7), 2313-2333. https://doi.org/10.1007/s11051-010-9911-8

Almeida, J. P., Chen, A. L., Foster, A., & Drezek, R. (2011). In vivo biodistribution of nanoparticles. *Nanomedicine (Lond)*, *6*(5), 815-835. https://doi.org/10.2217/nnm.11.79

Alric, C., Miladi, I., Kryza, D., Taleb, J., Lux, F., Bazzi, R., Billotey, C., Janier, M., Perriat, P., Roux, S., & Tillement, O. (2013). The biodistribution of gold nanoparticles designed for renal clearance. *Nanoscale*, *5*(13), 5930-5939. https://doi.org/10.1039/c3nr00012e

Alvarez, D. F., Helm, K., Degregori, J., Roederer, M., & Majka, S. (2010). Publishing flow cytometry data. *Am J Physiol Lung Cell Mol Physiol*, *298*(2), L127-130. https://doi.org/10.1152/ajplung.00313.2009

Aminabad, N. S., Farshbaf, M., & Akbarzadeh, A. (2019). Recent advances of gold nanoparticles in biomedical applications: State of the art. *Cell Biochem Biophys*, *77*(2), 123-137. https://doi.org/10.1007/s12013-018-0863-4

Arnold-Schild, D., Hanau, D., Spehner, D., Schmid, C., Rammensee, H. G., de la Salle, H., & Schild, H. (1999). Cutting edge: Receptor-mediated endocytosis of heat shock proteins by professional antigen-presenting cells. *J Immunol*, *162*(7), 3757-3760. https://www.ncbi.nlm.nih.gov/pubmed/10201889

Babaei, M., & Ganjalikhani, M. (2014). The potential effectiveness of nanoparticles as radio sensitizers for radiotherapy. *Bioimpacts*, *4*(1), 15-20. https://doi.org/10.5681/bi.2014.003

Basu, S., & Srivastava, P. K. (2000). Heat shock proteins: The fountainhead of innate and adaptive immune responses. *Cell Stress Chaperones*, *5*(5), 443-451. https://doi.org/10.1379/1466-1268(2000)005<0443:hsptfo>2.0.co;2

Beddoes, C. M., Case, C. P., & Briscoe, W. H. (2015). Understanding nanoparticle cellular entry: A physicochemical perspective. *Adv Colloid Interface Sci*, *218*, 48-68. https://doi.org/10.1016/j.cis.2015.01.007

Beere, H. M., Wolf, B. B., Cain, K., Mosser, D. D., Mahboubi, A., Kuwana, T., Tailor, P., Morimoto, R. I., Cohen, G. M., & Green, D. R. (2000). Heat-shock protein 70 inhibits apoptosis by preventing recruitment of procaspase-9 to the Apaf-1 apoptosome. *Nat Cell Biol*, *2*(8), 469-475. https://doi.org/10.1038/35019501

Begg, A. C. (1990). Cisplatin and radiation: Interaction probabilities and therapeutic possibilities. *Int J Radiat Oncol Biol Phys*, *19*(5), 1183-1189. https://doi.org/10.1016/0360-3016(90)90226-a

Bertrand, N., & Leroux, J. C. (2012). The journey of a drug-carrier in the body: An anatomo-physiological perspective. *J Control Release*, *161*(2), 152-163. https://doi.org/10.1016/j.jconrel.2011.09.098

Bertz, J., Dahm, S., Haberland, J., Kraywinkel, K., Kurth, B.-M., & Wolf, U. (2010). Verbreitung von Krebserkrankungen in Deutschland. In: Robert Koch-Institut.

Bhutia, S. K., Mukhopadhyay, S., Sinha, N., Das, D. N., Panda, P. K., Patra, S. K., Maiti, T. K., Mandal, M., Dent, P., Wang, X. Y., Das, S. K., Sarkar, D., & Fisher, P. B. (2013). Autophagy: Cancer's friend or foe? *Adv Cancer Res*, *118*, 61-95. https://doi.org/10.1016/B978-0-12-407173-5.00003-0

Blachere, N. E., Li, Z., Chandawarkar, R. Y., Suto, R., Jaikaria, N. S., Basu, S., Udono, H., & Srivastava, P. K. (1997). Heat shock protein-peptide complexes, reconstituted in vitro, elicit peptide-specific cytotoxic T lymphocyte response and tumor immunity. *J Exp Med*, *186*(8), 1315-1322. https://doi.org/10.1084/jem.186.8.1315

Böcker, W., Denk, H., Heitz, P. U., & Moch, H. (2008). *Repetitorium Pathologie* (2 ed.). Elsevier.

Botzler, C., Issels, R., & Multhoff, G. (1996). Heat-shock protein 72 cell-surface expression on human lung carcinoma cells in associated with an increased sensitivity to lysis mediated by adherent natural killer cells. *Cancer Immunol Immunother*, *43*(4), 226-230. https://doi.org/10.1007/s002620050326

Botzler, C., Li, G., Issels, R. D., & Multhoff, G. (1998). Definition of extracellular localized epitopes of Hsp70 involved in an NK immune response. *Cell Stress Chaperones*, *3*(1), 6-11. https://doi.org/10.1379/1466-1268(1998)003<0006:doeleo>2.3.co;2

Botzler, C., Schmidt, J., Luz, A., Jennen, L., Issels, R., & Multhoff, G. (1998). Differential Hsp70 plasma-membrane expression on primary human tumors and metastases in mice with severe combined immunodeficiency. *Int J Cancer*, *77*(6), 942-948. https://doi.org/10.1002/(sici)1097-0215(19980911)77:6<942::aid-ijc25>3.0.co;2-1

Buscher, M. (2019). Flow cytometry instrumentation - An overview. *Curr Protoc Cytom*, *87*(1), e52. https://doi.org/10.1002/cpcy.52

Butterworth, K. T., McMahon, S. J., Currell, F. J., & Prise, K. M. (2012). Physical basis and biological mechanisms of gold nanoparticle radiosensitization. *Nanoscale*, *4*(16), 4830-4838. https://doi.org/10.1039/c2nr31227a

Cailleau, R., Mackay, B., Young, R. K., & Reeves, W. J., Jr. (1974). Tissue culture studies on pleural effusions from breast carcinoma patients. *Cancer Res*, *34*(4), 801-809. https://www.ncbi.nlm.nih.gov/pubmed/4592574

Cailleau, R., Young, R., Olive, M., & Reeves, W. J., Jr. (1974). Breast tumor cell lines from pleural effusions. *J Natl Cancer Inst*, *53*(3), 661-674. https://doi.org/10.1093/jnci/53.3.661

Calcinotto, A., Kohli, J., Zagato, E., Pellegrini, L., Demaria, M., & Alimonti, A. (2019). Cellular senescence: Aging, cancer, and injury. *Physiol Rev*, *99*(2), 1047-1078. https://doi.org/10.1152/physrev.00020.2018

Carter, J. D., Cheng, N. N., Qu, Y., Suarez, G. D., & Guo, T. (2007). Nanoscale energy deposition by X-ray absorbing nanostructures. *J Phys Chem B*, *111*(40), 11622-11625. https://doi.org/10.1021/jp075253u

Chattopadhyay, N., Cai, Z., Kwon, Y. L., Lechtman, E., Pignol, J. P., & Reilly, R. M. (2013). Molecularly targeted gold nanoparticles enhance the radiation response of breast cancer cells and tumor xenografts to X-radiation. *Breast Cancer Res Treat*, *137*(1), 81-91. https://doi.org/10.1007/s10549-012-2338-4

Chattopadhyay, N., Cai, Z., Pignol, J. P., Keller, B., Lechtman, E., Bendayan, R., & Reilly, R. M. (2010). Design and characterization of HER-2-targeted gold nanoparticles for enhanced X-radiation treatment of locally advanced breast cancer. *Mol Pharm*, *7*(6), 2194-2206. https://doi.org/10.1021/mp100207t

Chen, Y., Yang, J., Fu, S., & Wu, J. (2020). Gold nanoparticles as radiosensitizers in cancer radiotherapy. *Int J Nanomedicine*, *15*, 9407-9430. https://doi.org/10.2147/IJN.S272902

Chen, Y. S., Hung, Y. C., Liau, I., & Huang, G. S. (2009). Assessment of the in vivo toxicity of gold nanoparticles. *Nanoscale Res Lett*, *4*(8), 858-864. https://doi.org/10.1007/s11671-009-9334-6

Chithrani, B. D., Ghazani, A. A., & Chan, W. C. (2006). Determining the size and shape dependence of gold nanoparticle uptake into mammalian cells. *Nano Lett*, *6*(4), 662-668. https://doi.org/10.1021/nl052396o

Chithrani, B. D., Stewart, J., Allen, C., & Jaffray, D. A. (2009). Intracellular uptake, transport, and processing of nanostructures in cancer cells. *Nanomedicine*, *5*(2), 118-127. https://doi.org/10.1016/j.nano.2009.01.008

Chithrani, D. B., Jelveh, S., Jalali, F., van Prooijen, M., Allen, C., Bristow, R. G., Hill, R. P., & Jaffray, D. A. (2010). Gold nanoparticles as radiation sensitizers in cancer therapy. *Radiat Res*, *173*(6), 719-728. https://doi.org/10.1667/RR1984.1

Cho, W. S., Cho, M., Jeong, J., Choi, M., Cho, H. Y., Han, B. S., Kim, S. H., Kim, H. O., Lim, Y. T., Chung, B. H., & Jeong, J. (2009). Acute toxicity and pharmacokinetics of 13 nm-sized PEG-coated gold nanoparticles. *Toxicol Appl Pharmacol*, *236*(1), 16-24. https://doi.org/10.1016/j.taap.2008.12.023

Cho, W. S., Kim, S., Han, B. S., Son, W. C., & Jeong, J. (2009). Comparison of gene expression profiles in mice liver following intravenous injection of 4 and 100 nm-sized PEG-coated gold nanoparticles. *Toxicol Lett*, *191*(1), 96-102. https://doi.org/10.1016/j.toxlet.2009.08.010

Ciocca, D. R., & Calderwood, S. K. (2005). Heat shock proteins in cancer: Diagnostic, prognostic, predictive, and treatment implications. *Cell Stress Chaperones*, *10*(2), 86-103. https://doi.org/10.1379/csc-99r.1

Collection, A. A. T. C. (2016). *MDA-MB-231 (ATCC® HTB-26™)*. https://www.lgcstandards-atcc.org/products/all/HTB-26.aspx?geo_country=de#

Cooper, D. R., Bekah, D., & Nadeau, J. L. (2014). Gold nanoparticles and their alternatives for radiation therapy enhancement. *Front Chem*, *2*, 86. https://doi.org/10.3389/fchem.2014.00086

Coulter, J. A., Hyland, W. B., Nicol, J., & Currell, F. J. (2013). Radiosensitising nanoparticles as novel cancer therapeutics – pipe dream or realistic prospect? *Clin Oncol (R Coll Radiol)*, *25*(10), 593-603. https://doi.org/10.1016/j.clon.2013.06.011

Cruje, C., Yang, C., Uertz, J., van Prooijen, M., & Chithrani, B. D. (2015). Optimization of PEG coated nanoscale gold particles for enhanced radiation therapy [10.1039/C5RA19104A]. *RSC Advances*, *5*(123), 101525-101532. https://doi.org/10.1039/C5RA19104A

Cui, L., Her, S., Borst, G. R., Bristow, R. G., Jaffray, D. A., & Allen, C. (2017). Radiosensitization by gold nanoparticles: Will they ever make it to the clinic? *Radiother Oncol*, *124*(3), 344-356. https://doi.org/10.1016/j.radonc.2017.07.007

Cui, L., Her, S., Dunne, M., Borst, G. R., De Souza, R., Bristow, R. G., Jaffray, D. A., & Allen, C. (2017). Significant radiation enhancement effects by gold nanoparticles in combination with Cisplatin in triple negative breast cancer cells and tumor xenografts. *Radiat Res*, *187*(2), 147-160. https://doi.org/10.1667/RR14578.1

Cui, L., Tse, K., Zahedi, P., Harding, S. M., Zafarana, G., Jaffray, D. A., Bristow, R. G., & Allen, C. (2014). Hypoxia and cellular localization influence the radiosensitizing effect of gold nanoparticles (AuNPs) in breast cancer cells. *Radiat Res*, *182*(5), 475-488. https://doi.org/10.1667/RR13642.1

da Rocha, E. L., Caramori, G. F., & Rambo, C. R. (2013). Nanoparticle translocation through a lipid bilayer tuned by surface chemistry. *Phys Chem Chem Phys*, *15*(7), 2282-2290. https://doi.org/10.1039/c2cp44035k

Darweesh, R. S., Ayoub, N. M., & Nazzal, S. (2019). Gold nanoparticles and angiogenesis: Molecular mechanisms and biomedical applications. *Int J Nanomedicine*, *14*, 7643-7663. https://doi.org/10.2147/IJN.S223941

Daugaard, M., Kirkegaard-Sorensen, T., Ostenfeld, M. S., Aaboe, M., Hoyer-Hansen, M., Orntoft, T. F., Rohde, M., & Jaattela, M. (2007). Lens epithelium-derived growth factor is an Hsp70-2 regulated guardian of lysosomal stability in human cancer. *Cancer Res*, *67*(6), 2559-2567. https://doi.org/10.1158/0008-5472.CAN-06-4121

Daugaard, M., Rohde, M., & Jaattela, M. (2007). The heat shock protein 70 family: Highly homologous proteins with overlapping and distinct functions. *FEBS Lett*, *581*(19), 3702-3710. https://doi.org/10.1016/j.febslet.2007.05.039

De Jong, W. H., Hagens, W. I., Krystek, P., Burger, M. C., Sips, A. J., & Geertsma, R. E. (2008). Particle size-dependent organ distribution of gold nanoparticles after intravenous administration. *Biomaterials*, *29*(12), 1912-1919. https://doi.org/10.1016/j.biomaterials.2007.12.037

de Lazaro, I., & Mooney, D. J. (2020). A nanoparticle's pathway into tumours. *Nat Mater*, *19*(5), 486-487. https://doi.org/10.1038/s41563-020-0669-9

De Maio, A. (1999). Heat shock proteins: Facts, thoughts, and dreams. *Shock*, *11*(1), 1-12. https://doi.org/10.1097/00024382-199901000-00001

De Maio, A. (2011). Extracellular heat shock proteins, cellular export vesicles, and the stress observation system: A form of communication during injury, infection, and cell damage. It is never known how far a controversial finding will go! Dedicated to Ferruccio Ritossa. *Cell Stress Chaperones*, *16*(3), 235-249. https://doi.org/10.1007/s12192-010-0236-4

Diagaradjane, P., Shetty, A., Wang, J. C., Elliott, A. M., Schwartz, J., Shentu, S., Park, H. C., Deorukhkar, A., Stafford, R. J., Cho, S. H., Tunnell, J. W., Hazle, J. D., & Krishnan, S. (2008). Modulation of in vivo tumor radiation response via gold nanoshell-mediated vascular-focused hyperthermia: Characterizing an integrated antihypoxic and localized vascular disrupting targeting strategy. *Nano Lett*, *8*(5), 1492-1500. https://doi.org/10.1021/nl080496z

Dokladny, K., Myers, O. B., & Moseley, P. L. (2015). Heat shock response and autophagy--cooperation and control. *Autophagy*, *11*(2), 200-213. https://doi.org/10.1080/15548627.2015.1009776

Douglass, M., Bezak, E., & Penfold, S. (2013). Monte Carlo investigation of the increased radiation deposition due to gold nanoparticles using kilovoltage and megavoltage photons in a 3D randomized cell model. *Med Phys*, *40*(7), 071710. https://doi.org/10.1118/1.4808150

Dreaden, E. C., Gryder, B. E., Austin, L. A., Tene Defo, B. A., Hayden, S. C., Pi, M., Quarles, L. D., Oyelere, A. K., & El-Sayed, M. A. (2012). Antiandrogen gold nanoparticles dual-target and overcome treatment resistance in hormone-insensitive prostate cancer cells. *Bioconjug Chem*, *23*(8), 1507-1512. https://doi.org/10.1021/bc300158k

Dreaden, E. C., Mwakwari, S. C., Sodji, Q. H., Oyelere, A. K., & El-Sayed, M. A. (2009). Tamoxifen-poly(ethylene glycol)-thiol gold nanoparticle conjugates: Enhanced potency and selective delivery for breast cancer treatment. *Bioconjug Chem*, *20*(12), 2247-2253. https://doi.org/10.1021/bc9002212

Elston, C. W., & Ellis, I. O. (1991). Pathological prognostic factors in breast cancer. I. The value of histological grade in breast cancer: Experience from a large study with long-term follow-up. *Histopathology*, *19*(5), 403-410. https://doi.org/10.1111/j.1365-2559.1991.tb00229.x

Erdmann, F., Spix, C., Katalinic, A., Christ, M., Folkerts, J., Hansmann, J., Kranzhöfer, K., Kunz, B., Manegold, K., Penzkofer, A., Treml, K., Vollmer, G., Weg-Remers, S., Barnes, B., Buttmann-Schweiger, N., Dahm, S., Fiebig, J., Franke, M., Gurung-Schönfeld, I., . . . Wienecke, A. (2021). Krebs in Deutschland für 2017/2018. In (pp. 172): Robert Koch-Institut.

Falagan-Lotsch, P., Grzincic, E. M., & Murphy, C. J. (2016). One low-dose exposure of gold nanoparticles induces long-term changes in human cells. *Proc Natl Acad Sci U S A*, *113*(47), 13318-13323. https://doi.org/10.1073/pnas.1616400113

Fan, M., Han, Y., Gao, S., Yan, H., Cao, L., Li, Z., Liang, X. J., & Zhang, J. (2020). Ultrasmall gold nanoparticles in cancer diagnosis and therapy. *Theranostics*, *10*(11), 4944-4957. https://doi.org/10.7150/thno.42471

Farkas, B., Hantschel, M., Magyarlaki, M., Becker, B., Scherer, K., Landthaler, M., Pfister, K., Gehrmann, M., Gross, C., Mackensen, A., & Multhoff, G. (2003). Heat shock protein 70 membrane expression and melanoma-associated marker phenotype in primary and metastatic melanoma. *Melanoma Res*, *13*(2), 147-152. https://doi.org/10.1097/00008390-200304000-00006

Federal Office of Consumer Protection and Food Safety. (1990, 27.9.2021). *Gesetz zur Regelung der Gentechnik (Gentechnikgesetz - GenTG)*. https://www.gesetze-im-internet.de/gentg/GenTG.pdf

Ferrarini, M., Heltai, S., Zocchi, M. R., & Rugarli, C. (1992). Unusual expression and localization of heat-shock proteins in human tumor cells. *Int J Cancer*, *51*(4), 613-619. https://doi.org/10.1002/ijc.2910510418

Ferrero, V., Visona, G., Dalmasso, F., Gobbato, A., Cerello, P., Strigari, L., Visentin, S., & Attili, A. (2017). Targeted dose enhancement in radiotherapy for breast cancer using gold nanoparticles, part 1: A radiobiological model study. *Med Phys*, *44*(5), 1983-1992. https://doi.org/10.1002/mp.12180

Flaherty, K. M., DeLuca-Flaherty, C., & McKay, D. B. (1990). Three-dimensional structure of the ATPase fragment of a 70K heat-shock cognate protein. *Nature*, *346*(6285), 623-628. https://doi.org/10.1038/346623a0

Fowler, J. F. (1989). The linear-quadratic formula and progress in fractionated radiotherapy. *Br J Radiol*, *62*(740), 679-694. https://doi.org/10.1259/0007-1285-62-740-679

Fowler, J. F., Adams, G. E., & Denekamp, J. (1976). Radiosensitizers of hypoxic cells in solid tumors. *Cancer Treat Rev*, *3*(4), 227-256. https://doi.org/10.1016/s0305-7372(76)80012-6

Freeman, B. C., Myers, M. P., Schumacher, R., & Morimoto, R. I. (1995). Identification of a regulatory motif in Hsp70 that affects ATPase activity, substrate binding, and interaction with HDJ-1. *EMBO J*, *14*(10), 2281-2292. https://www.ncbi.nlm.nih.gov/pubmed/7774586

Gabai, V. L., Meriin, A. B., Yaglom, J. A., Volloch, V. Z., & Sherman, M. Y. (1998). Role of Hsp70 in regulation of stress-kinase JNK: Implications in apoptosis and aging. *FEBS Lett*, *438*(1-2), 1-4. https://doi.org/10.1016/s0014-5793(98)01242-3

Gao, Q., Zhang, J., Gao, J., Zhang, Z., Zhu, H., & Wang, D. (2021). Gold nanoparticles in cancer theranostics. *Front Bioeng Biotechnol*, *9*, 647905. https://doi.org/10.3389/fbioe.2021.647905

Garcia Calavia, P., Bruce, G., Perez-Garcia, L., & Russell, D. A. (2018). Photosensitiser-gold nanoparticle conjugates for photodynamic therapy of cancer. *Photochem Photobiol Sci*, *17*(11), 1534-1552. https://doi.org/10.1039/c8pp00271a

Gastpar, R., Gehrmann, M., Bausero, M. A., Asea, A., Gross, C., Schroeder, J. A., & Multhoff, G. (2005). Heat shock protein 70 surface-positive tumor exosomes stimulate migratory and cytolytic activity of natural killer cells. *Cancer Res*, *65*(12), 5238-5247. https://doi.org/10.1158/0008-5472.CAN-04-3804

Gehrmann, M., Liebisch, G., Schmitz, G., Anderson, R., Steinem, C., De Maio, A., Pockley, G., & Multhoff, G. (2008). Tumor-specific Hsp70 plasma membrane localization is enabled by the glycosphingolipid Gb3. *PLoS One*, *3*(4), e1925. https://doi.org/10.1371/journal.pone.0001925

Gehrmann, M., Marienhagen, J., Eichholtz-Wirth, H., Fritz, E., Ellwart, J., Jaattela, M., Zilch, T., & Multhoff, G. (2005). Dual function of membrane-bound heat shock protein 70 (Hsp70), Bag-4, and Hsp40: Protection against radiation-induced effects and target structure for natural killer cells. *Cell Death Differ*, *12*(1), 38-51. https://doi.org/10.1038/sj.cdd.4401510

Gehrmann, M., Pfister, K., Hutzler, P., Gastpar, R., Margulis, B., & Multhoff, G. (2002). Effects of antineoplastic agents on cytoplasmic and membrane-bound heat shock protein 70 (Hsp70) levels. *Biol Chem*, *383*(11), 1715-1725. https://doi.org/10.1515/BC.2002.192

Gehrmann, M., Radons, J., Molls, M., & Multhoff, G. (2008). The therapeutic implications of clinically applied modifiers of heat shock protein 70 (Hsp70) expression by tumor cells. *Cell Stress Chaperones*, *13*(1), 1-10. https://doi.org/10.1007/s12192-007-0006-0

Gehrmann, M., Schmetzer, H., Eissner, G., Haferlach, T., Hiddemann, W., & Multhoff, G. (2003). Membrane-bound heat shock protein 70 (Hsp70) in acute myeloid leukemia: A tumor specific recognition structure for the cytolytic activity of autologous NK cells. *Haematologica*, *88*(4), 474-476. https://www.ncbi.nlm.nih.gov/pubmed/12681978

Gehrmann, M., Stangl, S., Foulds, G. A., Oellinger, R., Breuninger, S., Rad, R., Pockley, A. G., & Multhoff, G. (2014). Tumor imaging and targeting potential of an Hsp70-derived 14-mer peptide. *PLoS One*, *9*(8), e105344. https://doi.org/10.1371/journal.pone.0105344

Gehrmann, M. K., Kimm, M. A., Stangl, S., Schmid, T. E., Noel, P. B., Rummeny, E. J., & Multhoff, G. (2015). Imaging of Hsp70-positive tumors with cmHsp70.1 antibody-conjugated gold nanoparticles. *Int J Nanomedicine*, *10*, 5687-5700. https://doi.org/10.2147/IJN.S87174

Geng, F., Song, K., Xing, J. Z., Yuan, C., Yan, S., Yang, Q., Chen, J., & Kong, B. (2011). Thio-glucose bound gold nanoparticles enhance radio-cytotoxic targeting of ovarian cancer. *Nanotechnology*, *22*(28), 285101. https://doi.org/10.1088/0957-4484/22/28/285101

Gerosa, C., Crisponi, G., Nurchi, V. M., Saba, L., Cappai, R., Cau, F., Faa, G., Van Eyken, P., Scartozzi, M., Floris, G., & Fanni, D. (2020). Gold nanoparticles: A new golden era in oncology? *Pharmaceuticals (Basel)*, *13*(8). https://doi.org/10.3390/ph13080192

Goel, R., Shah, N., Visaria, R., Paciotti, G. F., & Bischof, J. C. (2009). Biodistribution of TNF-alpha-coated gold nanoparticles in an in vivo model system. *Nanomedicine (Lond)*, *4*(4), 401-410. https://doi.org/10.2217/nnm.09.21

Greish, K. (2007). Enhanced permeability and retention of macromolecular drugs in solid tumors: A royal gate for targeted anticancer nanomedicines. *J Drug Target*, *15*(7-8), 457-464. https://doi.org/10.1080/10611860701539584

Haas, I. G. (1994). BiP (GRP78), an essential hsp70 resident protein in the endoplasmic reticulum. *Experientia*, *50*(11-12), 1012-1020. https://doi.org/10.1007/bf01923455

Hainfeld, J. F., Dilmanian, F. A., Slatkin, D. N., & Smilowitz, H. M. (2008). Radiotherapy enhancement with gold nanoparticles. *J Pharm Pharmacol*, *60*(8), 977-985. https://doi.org/10.1211/jpp.60.8.0005

Hainfeld, J. F., O'Connor, M. J., Dilmanian, F. A., Slatkin, D. N., Adams, D. J., & Smilowitz, H. M. (2011). Micro-CT enables microlocalisation and quantification of Her2-targeted gold nanoparticles within tumour regions. *Br J Radiol*, *84*(1002), 526-533. https://doi.org/10.1259/bjr/42612922

Hainfeld, J. F., Slatkin, D. N., & Smilowitz, H. M. (2004). The use of gold nanoparticles to enhance radiotherapy in mice. *Phys Med Biol*, *49*(18), N309-315. https://doi.org/10.1088/0031-9155/49/18/n03

Hantschel, M., Pfister, K., Jordan, A., Scholz, R., Andreesen, R., Schmitz, G., Schmetzer, H., Hiddemann, W., & Multhoff, G. (2000). Hsp70 plasma membrane expression on primary tumor biopsy material and bone marrow of leukemic patients. *Cell Stress Chaperones*, *5*(5), 438-442. https://doi.org/10.1379/1466-1268(2000)005<0438:hpmeop>2.0.co;2

Harbeck, H., & Heywang-Köbrunner, S. (2011). Veränderungen und Tumoren der Mamma. In M. Kiechle (Ed.), *Gynäkologie und Geburtshilfe* (pp. 475-501). Elsevier Health Sciences Germany.

Hartl, F. U. (1996). Molecular chaperones in cellular protein folding. *Nature*, *381*(6583), 571-579. https://doi.org/10.1038/381571a0

Hartl, F. U., & Hayer-Hartl, M. (2002). Molecular chaperones in the cytosol: From nascent chain to folded protein. *Science*, *295*(5561), 1852-1858. https://doi.org/10.1126/science.1068408

Haume, K., Rosa, S., Grellet, S., Smialek, M. A., Butterworth, K. T., Solov'yov, A. V., Prise, K. M., Golding, J., & Mason, N. J. (2016). Gold nanoparticles for cancer radiotherapy: A review. *Cancer Nanotechnol*, *7*(1), 8. https://doi.org/10.1186/s12645-016-0021-x

Helmbrecht, K., Zeise, E., & Rensing, L. (2000). Chaperones in cell cycle regulation and mitogenic signal transduction: A review. *Cell Prolif*, *33*(6), 341-365. https://doi.org/10.1046/j.1365-2184.2000.00189.x

Her, S., Jaffray, D. A., & Allen, C. (2017). Gold nanoparticles for applications in cancer radiotherapy: Mechanisms and recent advancements. *Adv Drug Deliv Rev*, *109*, 84-101. https://doi.org/10.1016/j.addr.2015.12.012

Herrmann, T., Baumann, M., & Dörr, W. (2006). *Klinische Strahlenbiologie* (4 ed.). Elsevier - Urban & Fischer.

Hightower, L. E., & Guidon, P. T., Jr. (1989). Selective release from cultured mammalian cells of heat-shock (stress) proteins that resemble glia-axon transfer proteins. *J Cell Physiol*, *138*(2), 257-266. https://doi.org/10.1002/jcp.1041380206

Hillyer, J. F., & Albrecht, R. M. (2001). Gastrointestinal persorption and tissue distribution of differently sized colloidal gold nanoparticles. *J Pharm Sci*, *90*(12), 1927-1936. https://doi.org/10.1002/jps.1143

Hossain, M., & Su, M. (2012). Nanoparticle location and material dependent dose enhancement in X-ray radiation therapy. *J Phys Chem C Nanomater Interfaces*, *116*(43), 23047-23052. https://doi.org/10.1021/jp306543q

Howlader, N., Altekruse, S. F., Li, C. I., Chen, V. W., Clarke, C. A., Ries, L. A., & Cronin, K. A. (2014). US incidence of breast cancer subtypes defined by joint hormone receptor and HER2 status. *J Natl Cancer Inst*, *106*(5). https://doi.org/10.1093/jnci/dju055

Huang, C. W., Kearney, V., Moeendarbari, S., Jiang, R. Q., Christensen, P., Tekade, R., Sun, X. K., Mao, W. H., & Hao, Y. W. (2015). Hollow gold nanoparticals as biocompatible radiosensitizer: An in vitro proof of concept study. *Journal of Nano Research (Vol. 32,*

pp. 106–112). Trans Tech Publications, Ltd. . https://doi.org/https://doi.org/10.4028/www.scientific.net/jnanor.32.106

Huang, K., Ma, H., Liu, J., Huo, S., Kumar, A., Wei, T., Zhang, X., Jin, S., Gan, Y., Wang, P. C., He, S., Zhang, X., & Liang, X. J. (2012). Size-dependent localization and penetration of ultrasmall gold nanoparticles in cancer cells, multicellular spheroids, and tumors in vivo. *ACS Nano*, *6*(5), 4483-4493. https://doi.org/10.1021/nn301282m

Hwang, J. H., Kim, S. J., Kim, Y. H., Noh, J. R., Gang, G. T., Chung, B. H., Song, N. W., & Lee, C. H. (2012). Susceptibility to gold nanoparticle-induced hepatotoxicity is enhanced in a mouse model of nonalcoholic steatohepatitis. *Toxicology*, *294*(1), 27-35. https://doi.org/10.1016/j.tox.2012.01.013

Ionita, P., Gilbert, B. C., & Chechik, V. (2005). Radical mechanism of a place-exchange reaction of Au nanoparticles. *Angew Chem Int Ed Engl*, *44*(24), 3720-3722. https://doi.org/10.1002/anie.200500518

Jaattela, M. (1999). Escaping cell death: Survival proteins in cancer. *Exp Cell Res*, *248*(1), 30-43. https://doi.org/10.1006/excr.1999.4455

Jain, S., Coulter, J. A., Butterworth, K. T., Hounsell, A. R., McMahon, S. J., Hyland, W. B., Muir, M. F., Dickson, G. R., Prise, K. M., Currell, F. J., Hirst, D. G., & O'Sullivan, J. M. (2014). Gold nanoparticle cellular uptake, toxicity, and radiosensitisation in hypoxic conditions. *Radiother Oncol*, *110*(2), 342-347. https://doi.org/10.1016/j.radonc.2013.12.013

Jain, S., Coulter, J. A., Hounsell, A. R., Butterworth, K. T., McMahon, S. J., Hyland, W. B., Muir, M. F., Dickson, G. R., Prise, K. M., Currell, F. J., O'Sullivan, J. M., & Hirst, D. G. (2011). Cell-specific radiosensitization by gold nanoparticles at megavoltage radiation energies. *Int J Radiat Oncol Biol Phys*, *79*(2), 531-539. https://doi.org/10.1016/j.ijrobp.2010.08.044

Jäkel, O., & Karger, C. P. (2006). Physikalische Grundlagen. In M. Reiser, F. P. Kuhn, & J. Debus (Eds.), *Radiologie* (4 ed., pp. 15-36). Georg Thieme Verlag.

Janic, B., Brown, S. L., Neff, R., Liu, F., Mao, G., Chen, Y., Jackson, L., Chetty, I. J., Movsas, B., & Wen, N. (2021). Therapeutic enhancement of radiation and immunomodulation by gold nanoparticles in triple negative breast cancer. *Cancer Biol Ther*, *22*(2), 124-135. https://doi.org/10.1080/15384047.2020.1861923

Jindal, S. (1996). Heat shock proteins: Applications in health and disease. *Trends Biotechnol*, *14*(1), 17-20. https://doi.org/10.1016/0167-7799(96)80909-7

Joza, N., Pospisilik, J. A., Hangen, E., Hanada, T., Modjtahedi, N., Penninger, J. M., & Kroemer, G. (2009). AIF: Not just an apoptosis-inducing factor. *Ann N Y Acad Sci*, *1171*, 2-11. https://doi.org/10.1111/j.1749-6632.2009.04681.x

Kampinga, H. H., Hageman, J., Vos, M. J., Kubota, H., Tanguay, R. M., Bruford, E. A., Cheetham, M. E., Chen, B., & Hightower, L. E. (2009). Guidelines for the nomenclature of the human heat shock proteins. *Cell Stress Chaperones*, *14*(1), 105-111. https://doi.org/10.1007/s12192-008-0068-7

Kastan, M. B., & Bartek, J. (2004). Cell-cycle checkpoints and cancer. *Nature*, *432*(7015), 316-323. https://doi.org/10.1038/nature03097

Kaur, P., Hurwitz, M. D., Krishnan, S., & Asea, A. (2011). Combined hyperthermia and radiotherapy for the treatment of cancer. *Cancers (Basel)*, *3*(4), 3799-3823. https://doi.org/10.3390/cancers3043799

Kavanagh, J. N., Redmond, K. M., Schettino, G., & Prise, K. M. (2013). DNA double strand break repair: A radiation perspective. *Antioxid Redox Signal*, *18*(18), 2458-2472. https://doi.org/10.1089/ars.2012.5151

Kellerer, A. M., & Rossi, H. H. (1973). The biophysical properties of 3.9-GeV nitrogen ions. VI. Interpretation of results. *Radiat Res*, *55*(3), 447-456. https://www.ncbi.nlm.nih.gov/pubmed/4743244

Khlebtsov, N., & Dykman, L. (2011). Biodistribution and toxicity of engineered gold nanoparticles: A review of in vitro and in vivo studies. *Chem Soc Rev*, *40*(3), 1647-1671. https://doi.org/10.1039/c0cs00018c

Kiang, J. G., & Tsokos, G. C. (1998). Heat shock protein 70 kDa: Molecular biology, biochemistry, and physiology. *Pharmacol Ther*, *80*(2), 183-201. https://doi.org/10.1016/s0163-7258(98)00028-x

Kleinjung, T., Arndt, O., Feldmann, H. J., Bockmuhl, U., Gehrmann, M., Zilch, T., Pfister, K., Schonberger, J., Marienhagen, J., Eilles, C., Rossbacher, L., & Multhoff, G. (2003). Heat shock protein 70 (Hsp70) membrane expression on head-and-neck cancer biopsy-a target for natural killer (NK) cells. *Int J Radiat Oncol Biol Phys*, *57*(3), 820-826. https://doi.org/10.1016/s0360-3016(03)00629-1

Kobayashi, K., Usami, N., Porcel, E., Lacombe, S., & Le Sech, C. (2010). Enhancement of radiation effect by heavy elements. *Mutat Res*, *704*(1-3), 123-131. https://doi.org/10.1016/j.mrrev.2010.01.002

Kong, T., Zeng, J., Wang, X., Yang, X., Yang, J., McQuarrie, S., McEwan, A., Roa, W., Chen, J., & Xing, J. Z. (2008). Enhancement of radiation cytotoxicity in breast-cancer cells by localized attachment of gold nanoparticles. *Small*, *4*(9), 1537-1543. https://doi.org/10.1002/smll.200700794

Krpetic, Z., Anguissola, S., Garry, D., Kelly, P. M., & Dawson, K. A. (2014). Nanomaterials: Impact on cells and cell organelles. *Adv Exp Med Biol*, *811*, 135-156. https://doi.org/10.1007/978-94-017-8739-0_8

Kumar, A., Ma, H., Zhang, X., Huang, K., Jin, S., Liu, J., Wei, T., Cao, W., Zou, G., & Liang, X. J. (2012). Gold nanoparticles functionalized with therapeutic and targeted peptides for cancer treatment. *Biomaterials*, *33*(4), 1180-1189. https://doi.org/10.1016/j.biomaterials.2011.10.058

Kuncic, Z., & Lacombe, S. (2018). Nanoparticle radio-enhancement: Principles, progress and application to cancer treatment. *Phys Med Biol*, *63*(2), 02TR01. https://doi.org/10.1088/1361-6560/aa99ce

Lee, J., Chatterjee, D. K., Lee, M. H., & Krishnan, S. (2014). Gold nanoparticles in breast cancer treatment: Promise and potential pitfalls. *Cancer Lett*, *347*(1), 46-53. https://doi.org/10.1016/j.canlet.2014.02.006

Leitlinienprogramm Onkologie. (2020). *Interdisziplinäre S3-Leitlinie für die Früherkennung, Diagnostik, Therapie und Nachsorge des Mammakarzinoms - Langversion*. Retrieved May, 2021 from https://www.leitlinienprogramm-onkologie.de/fileadmin/user_upload/Downloads/Leitlinien/Mammakarzinom_4_0/Version_4.3/LL_Mammakarzinom_Langversion_4.3.pdf

Li, W. B., Belchior, A., Beuve, M., Chen, Y. Z., Di Maria, S., Friedland, W., Gervais, B., Heide, B., Hocine, N., Ipatov, A., Klapproth, A. P., Li, C. Y., Li, J. L., Multhoff, G., Poignant, F., Qiu, R., Rabus, H., Rudek, B., Schuemann, J., . . . Zhang, Y. B. (2020). Intercomparison of dose enhancement ratio and secondary electron spectra for gold nanoparticles irradiated by X-rays calculated using multiple Monte Carlo simulation codes. *Phys Med*, *69*, 147-163. https://doi.org/10.1016/j.ejmp.2019.12.011

Li, Z., & Srivastava, P. (2004). Heat-shock proteins. *Curr Protoc Immunol*, *Appendix 1*, Appendix 1T. https://doi.org/10.1002/0471142735.ima01ts58

Libutti, S. K., Paciotti, G. F., Byrnes, A. A., Alexander, H. R., Jr., Gannon, W. E., Walker, M., Seidel, G. D., Yuldasheva, N., & Tamarkin, L. (2010). Phase I and pharmacokinetic studies of CYT-6091, a novel PEGylated colloidal gold-rhTNF nanomedicine. *Clin Cancer Res*, *16*(24), 6139-6149. https://doi.org/10.1158/1078-0432.CCR-10-0978

Lin, Y., McMahon, S. J., Paganetti, H., & Schuemann, J. (2015). Biological modeling of gold nanoparticle enhanced radiotherapy for proton therapy. *Phys Med Biol*, *60*(10), 4149-4168. https://doi.org/10.1088/0031-9155/60/10/4149

Lindquist, S., & Craig, E. A. (1988). The heat-shock proteins. *Annu Rev Genet*, *22*, 631-677. https://doi.org/10.1146/annurev.ge.22.120188.003215

Liu, C. J., Wang, C. H., Chen, S. T., Chen, H. H., Leng, W. H., Chien, C. C., Wang, C. L., Kempson, I. M., Hwu, Y., Lai, T. C., Hsiao, M., Yang, C. S., Chen, Y. J., & Margaritondo, G. (2010). Enhancement of cell radiation sensitivity by pegylated gold nanoparticles. *Phys Med Biol*, *55*(4), 931-945. https://doi.org/10.1088/0031-9155/55/4/002

Liu, J., Liang, Y., Liu, T., Li, D., & Yang, X. (2015). Anti-EGFR-conjugated hollow gold nanospheres enhance radiocytotoxic targeting of cervical cancer at megavoltage radiation energies. *Nanoscale Res Lett*, *10*, 218. https://doi.org/10.1186/s11671-015-0923-2

Longmire, M., Choyke, P. L., & Kobayashi, H. (2008). Clearance properties of nano-sized particles and molecules as imaging agents: Considerations and caveats. *Nanomedicine (Lond)*, *3*(5), 703-717. https://doi.org/10.2217/17435889.3.5.703

Lopez-Chaves, C., Soto-Alvaredo, J., Montes-Bayon, M., Bettmer, J., Llopis, J., & Sanchez-Gonzalez, C. (2018). Gold nanoparticles: Distribution, bioaccumulation, and toxicity. In vitro and in vivo studies. *Nanomedicine*, *14*(1), 1-12. https://doi.org/10.1016/j.nano.2017.08.011

Ma, N., Wu, F. G., Zhang, X., Jiang, Y. W., Jia, H. R., Wang, H. Y., Li, Y. H., Liu, P., Gu, N., & Chen, Z. (2017). Shape-dependent radiosensitization effect of gold nanostructures in cancer radiotherapy: Comparison of gold nanoparticles, nanospikes, and nanorods. *ACS Appl Mater Interfaces*, *9*(15), 13037-13048. https://doi.org/10.1021/acsami.7b01112

Mackey, M. A., & El-Sayed, M. A. (2014). Chemosensitization of cancer cells via gold nanoparticle-induced cell cycle regulation. *Photochem Photobiol*, *90*(2), 306-312. https://doi.org/10.1111/php.12226

Mambula, S. S., & Calderwood, S. K. (2006). Heat shock protein 70 is secreted from tumor cells by a nonclassical pathway involving lysosomal endosomes. *J Immunol*, *177*(11), 7849-7857. https://doi.org/10.4049/jimmunol.177.11.7849

Mathew, A., Mathur, S. K., Jolly, C., Fox, S. G., Kim, S., & Morimoto, R. I. (2001). Stress-specific activation and repression of heat shock factors 1 and 2. *Mol Cell Biol*, *21*(21), 7163-7171. https://doi.org/10.1128/MCB.21.21.7163-7171.2001

Mayer, M. P., & Bukau, B. (2005). Hsp70 chaperones: Cellular functions and molecular mechanism. *Cell Mol Life Sci*, *62*(6), 670-684. https://doi.org/10.1007/s00018-004-4464-6

McMahon, S. J., Hyland, W. B., Muir, M. F., Coulter, J. A., Jain, S., Butterworth, K. T., Schettino, G., Dickson, G. R., Hounsell, A. R., O'Sullivan, J. M., Prise, K. M., Hirst, D. G., & Currell, F. J. (2011). Nanodosimetric effects of gold nanoparticles in megavoltage radiation therapy. *Radiother Oncol*, *100*(3), 412-416. https://doi.org/10.1016/j.radonc.2011.08.026

Melancon, M. P., Lu, W., Yang, Z., Zhang, R., Cheng, Z., Elliot, A. M., Stafford, J., Olson, T., Zhang, J. Z., & Li, C. (2008). In vitro and in vivo targeting of hollow gold nanoshells directed at epidermal growth factor receptor for photothermal ablation therapy. *Mol Cancer Ther*, *7*(6), 1730-1739. https://doi.org/10.1158/1535-7163.MCT-08-0016

Menon, V., Thomas, R., Ghale, A. R., Reinhard, C., & Pruszak, J. (2014). Flow cytometry protocols for surface and intracellular antigen analyses of neural cell types. *J Vis Exp*(94). https://doi.org/10.3791/52241

Mesbahi, A. (2010). A review on gold nanoparticles radiosensitization effect in radiation therapy of cancer. *Rep Pract Oncol Radiother*, *15*(6), 176-180. https://doi.org/10.1016/j.rpor.2010.09.001

Mesbahi, A., Jamali, F., & Garehaghaji, N. (2013). Effect of photon beam energy, gold nanoparticle size and concentration on the dose enhancement in radiation therapy. *Bioimpacts*, *3*(1), 29-35. https://doi.org/10.5681/bi.2013.002

Mieszawska, A. J., Mulder, W. J., Fayad, Z. A., & Cormode, D. P. (2013). Multifunctional gold nanoparticles for diagnosis and therapy of disease. *Mol Pharm*, *10*(3), 831-847. https://doi.org/10.1021/mp3005885

Mikami, Y., Dhakshinamoorthy, A., Alvaro, M., & García, H. (2013). Catalytic activity of unsupported gold nanoparticles [10.1039/C2CY20068F]. *Catalysis Science & Technology*, *3*(1), 58-69. https://doi.org/10.1039/C2CY20068F

Mironava, T., Hadjiargyrou, M., Simon, M., Jurukovski, V., & Rafailovich, M. H. (2010). Gold nanoparticles cellular toxicity and recovery: Effect of size, concentration, and exposure time. *Nanotoxicology*, *4*(1), 120-137. https://doi.org/10.3109/17435390903471463

Misawa, M., & Takahashi, J. (2011). Generation of reactive oxygen species induced by gold nanoparticles under x-ray and UV Irradiations. *Nanomedicine*, *7*(5), 604-614. https://doi.org/10.1016/j.nano.2011.01.014

Monopoli, M. P., Aberg, C., Salvati, A., & Dawson, K. A. (2012). Biomolecular coronas provide the biological identity of nanosized materials. *Nat Nanotechnol*, *7*(12), 779-786. https://doi.org/10.1038/nnano.2012.207

Monopoli, M. P., Walczyk, D., Campbell, A., Elia, G., Lynch, I., Bombelli, F. B., & Dawson, K. A. (2011). Physical-chemical aspects of protein corona: Relevance to in vitro and in vivo biological impacts of nanoparticles. *J Am Chem Soc*, *133*(8), 2525-2534. https://doi.org/10.1021/ja107583h

Morimoto, R. I. (1998). Regulation of the heat shock transcriptional response: Cross talk between a family of heat shock factors, molecular chaperones, and negative regulators. *Genes Dev*, *12*(24), 3788-3796. https://doi.org/10.1101/gad.12.24.3788

Moseley, P. (2000). Stress proteins and the immune response. *Immunopharmacology*, *48*(3), 299-302. https://doi.org/10.1016/s0162-3109(00)00227-7

Muddineti, O. S., Ghosh, B., & Biswas, S. (2015). Current trends in using polymer coated gold nanoparticles for cancer therapy. *Int J Pharm*, *484*(1-2), 252-267. https://doi.org/10.1016/j.ijpharm.2015.02.038

Multhoff, G. (2007). Heat shock protein 70 (Hsp70): Membrane location, export, and immunological relevance. *Methods*, *43*(3), 229-237. https://doi.org/10.1016/j.ymeth.2007.06.006

Multhoff, G., Botzler, C., Jennen, L., Schmidt, J., Ellwart, J., & Issels, R. (1997). Heat shock protein 72 on tumor cells: A recognition structure for natural killer cells. *J Immunol*, *158*(9), 4341-4350. https://www.ncbi.nlm.nih.gov/pubmed/9126997

Multhoff, G., Botzler, C., Wiesnet, M., Eissner, G., & Issels, R. (1995). CD3- large granular lymphocytes recognize a heat-inducible immunogenic determinant associated with the 72-kD heat shock protein on human sarcoma cells. *Blood*, *86*(4), 1374-1382. https://www.ncbi.nlm.nih.gov/pubmed/7632945

Multhoff, G., Botzler, C., Wiesnet, M., Muller, E., Meier, T., Wilmanns, W., & Issels, R. D. (1995). A stress-inducible 72-kDa heat-shock protein (HSP72) is expressed on the surface of human tumor cells, but not on normal cells. *Int J Cancer*, *61*(2), 272-279. https://doi.org/10.1002/ijc.2910610222

Multhoff, G., & Hightower, L. E. (1996). Cell surface expression of heat shock proteins and the immune response. *Cell Stress Chaperones*, *1*(3), 167-176. https://doi.org/10.1379/1466-1268(1996)001<0167:cseohs>2.3.co;2

Multhoff, G., & Hightower, L. E. (2011). Distinguishing integral and receptor-bound heat shock protein 70 (Hsp70) on the cell surface by Hsp70-specific antibodies. *Cell Stress Chaperones*, *16*(3), 251-255. https://doi.org/10.1007/s12192-010-0247-1

Multhoff, G., Pfister, K., Botzler, C., Jordan, A., Scholz, R., Schmetzer, H., Burgstahler, R., & Hiddemann, W. (2000). Adoptive transfer of human natural killer cells in mice with severe combined immunodeficiency inhibits growth of Hsp70-expressing tumors. *Int J Cancer*, *88*(5), 791-797. https://doi.org/10.1002/1097-0215(20001201)88:5<791::aid-ijc17>3.0.co;2-i

Münter, M., & Weber, K. J. (2006). Strahlenbiologie In M. Reiser, F. P. Kuhn, & J. Debus (Eds.), *Radiologie* (4 ed., pp. 37-62). Georg Thieme Verlag.

Murakami, N., Kuhnel, A., Schmid, T. E., Ilicic, K., Stangl, S., Braun, I. S., Gehrmann, M., Molls, M., Itami, J., & Multhoff, G. (2015). Role of membrane Hsp70 in radiation sensitivity of tumor cells. *Radiat Oncol*, *10*, 149. https://doi.org/10.1186/s13014-015-0461-1

Murphy, M. E. (2013). The HSP70 family and cancer. *Carcinogenesis*, *34*(6), 1181-1188. https://doi.org/10.1093/carcin/bgt111

Nel, A., Xia, T., Madler, L., & Li, N. (2006). Toxic potential of materials at the nanolevel. *Science*, *311*(5761), 622-627. https://doi.org/10.1126/science.1114397

Netzker, R. (2012). Zellzyklus und molekulare Genetik. In J. Rassow, K. Hauser, R. Netzker, & R. Deutzmann (Eds.), *Biochemie* (3 ed., pp. 401-524). Georg Thieme Verlag.

Nunez, C., Estevez, S. V., & Del Pilar Chantada, M. (2018). Inorganic nanoparticles in diagnosis and treatment of breast cancer. *J Biol Inorg Chem*, *23*(3), 331-345. https://doi.org/10.1007/s00775-018-1542-z

Nylandsted, J., Gyrd-Hansen, M., Danielewicz, A., Fehrenbacher, N., Lademann, U., Hoyer-Hansen, M., Weber, E., Multhoff, G., Rohde, M., & Jaattela, M. (2004). Heat shock protein 70 promotes cell survival by inhibiting lysosomal membrane permeabilization. *J Exp Med*, *200*(4), 425-435. https://doi.org/10.1084/jem.20040531

Otsuka, H., Nagasaki, Y., & Kataoka, K. (2003). PEGylated nanoparticles for biological and pharmaceutical applications. *Adv Drug Deliv Rev*, *55*(3), 403-419. https://doi.org/10.1016/s0169-409x(02)00226-0

Owens, D. E., 3rd, & Peppas, N. A. (2006). Opsonization, biodistribution, and pharmacokinetics of polymeric nanoparticles. *Int J Pharm*, *307*(1), 93-102. https://doi.org/10.1016/j.ijpharm.2005.10.010

Ozcelik, S., & Pratx, G. (2020). Nuclear-targeted gold nanoparticles enhance cancer cell radiosensitization. *Nanotechnology*, *31*(41), 415102. https://doi.org/10.1088/1361-6528/aba02b

Pan, Y., Leifert, A., Ruau, D., Neuss, S., Bornemann, J., Schmid, G., Brandau, W., Simon, U., & Jahnen-Dechent, W. (2009). Gold nanoparticles of diameter 1.4 nm trigger necrosis by oxidative stress and mitochondrial damage. *Small*, *5*(18), 2067-2076. https://doi.org/10.1002/smll.200900466

Pawlik, T. M., & Keyomarsi, K. (2004). Role of cell cycle in mediating sensitivity to radiotherapy. *Int J Radiat Oncol Biol Phys*, *59*(4), 928-942. https://doi.org/10.1016/j.ijrobp.2004.03.005

Pernodet, N., Fang, X., Sun, Y., Bakhtina, A., Ramakrishnan, A., Sokolov, J., Ulman, A., & Rafailovich, M. (2006). Adverse effects of citrate/gold nanoparticles on human dermal fibroblasts. *Small*, *2*(6), 766-773. https://doi.org/10.1002/smll.200500492

Perrault, S. D., Walkey, C., Jennings, T., Fischer, H. C., & Chan, W. C. (2009). Mediating tumor targeting efficiency of nanoparticles through design. *Nano Lett*, *9*(5), 1909-1915. https://doi.org/10.1021/nl900031y

Pfister, K., Radons, J., Busch, R., Tidball, J. G., Pfeifer, M., Freitag, L., Feldmann, H. J., Milani, V., Issels, R., & Multhoff, G. (2007). Patient survival by Hsp70 membrane phenotype: Association with different routes of metastasis. *Cancer*, *110*(4), 926-935. https://doi.org/10.1002/cncr.22864

Picot, J., Guerin, C. L., Le Van Kim, C., & Boulanger, C. M. (2012). Flow cytometry: Retrospective, fundamentals, and recent instrumentation. *Cytotechnology*, *64*(2), 109-130. https://doi.org/10.1007/s10616-011-9415-0

Pockley, A. G., Henderson, B., & Multhoff, G. (2014). Extracellular cell stress proteins as biomarkers of human disease. *Biochem Soc Trans*, *42*(6), 1744-1751. https://doi.org/10.1042/BST20140205

Polf, J. C., Bronk, L. F., Driessen, W. H., Arap, W., Pasqualini, R., & Gillin, M. (2011). Enhanced relative biological effectiveness of proton radiotherapy in tumor cells with internalized gold nanoparticles. *Appl Phys Lett*, *98*(19), 193702. https://doi.org/10.1063/1.3589914

Porcel, E., Liehn, S., Remita, H., Usami, N., Kobayashi, K., Furusawa, Y., Le Sech, C., & Lacombe, S. (2010). Platinum nanoparticles: A promising material for future cancer therapy? *Nanotechnology*, *21*(8), 85103. https://doi.org/10.1088/0957-4484/21/8/085103

Radons, J. (2016). The human HSP70 family of chaperones: Where do we stand? *Cell Stress Chaperones*, *21*(3), 379-404. https://doi.org/10.1007/s12192-016-0676-6

Rahman, W. N., Bishara, N., Ackerly, T., He, C. F., Jackson, P., Wong, C., Davidson, R., & Geso, M. (2009). Enhancement of radiation effects by gold nanoparticles for superficial radiation therapy. *Nanomedicine*, *5*(2), 136-142. https://doi.org/10.1016/j.nano.2009.01.014

Rakha, E. A., Reis-Filho, J. S., Baehner, F., Dabbs, D. J., Decker, T., Eusebi, V., Fox, S. B., Ichihara, S., Jacquemier, J., Lakhani, S. R., Palacios, J., Richardson, A. L., Schnitt, S. J., Schmitt, F. C., Tan, P. H., Tse, G. M., Badve, S., & Ellis, I. O. (2010). Breast cancer prognostic classification in the molecular era: The role of histological grade. *Breast Cancer Res*, *12*(4), 207. https://doi.org/10.1186/bcr2607

Ravagnan, L., Gurbuxani, S., Susin, S. A., Maisse, C., Daugas, E., Zamzami, N., Mak, T., Jaattela, M., Penninger, J. M., Garrido, C., & Kroemer, G. (2001). Heat-shock protein 70 antagonizes apoptosis-inducing factor. *Nat Cell Biol*, *3*(9), 839-843. https://doi.org/10.1038/ncb0901-839

Ritossa, F. (1962). A new puffing pattern induced by temperature shock and DNP in drosophila. *Experientia*, *18*(12), 571-573. https://doi.org/10.1007/BF02172188

Ross, G. M. (1999). Induction of cell death by radiotherapy. *Endocr Relat Cancer*, *6*(1), 41-44. https://doi.org/10.1677/erc.0.0060041

Sabella, S., Carney, R. P., Brunetti, V., Malvindi, M. A., Al-Juffali, N., Vecchio, G., Janes, S. M., Bakr, O. M., Cingolani, R., Stellacci, F., & Pompa, P. P. (2014). A general mechanism for intracellular toxicity of metal-containing nanoparticles. *Nanoscale*, *6*(12), 7052-7061. https://doi.org/10.1039/c4nr01234h

Sadauskas, E., Wallin, H., Stoltenberg, M., Vogel, U., Doering, P., Larsen, A., & Danscher, G. (2007). Kupffer cells are central in the removal of nanoparticles from the organism. *Part Fibre Toxicol*, *4*, 10. https://doi.org/10.1186/1743-8977-4-10

Saptarshi, S. R., Duschl, A., & Lopata, A. L. (2013). Interaction of nanoparticles with proteins: Relation to bio-reactivity of the nanoparticle. *J Nanobiotechnology*, *11*, 26. https://doi.org/10.1186/1477-3155-11-26

Sarria, G. R., Berenguer Frances, M. A., & Linares Galiana, I. (2019). Enhancing radiotherapy effect in breast cancer with nanoparticles: A review. *Rep Pract Oncol Radiother*, *24*(1), 65-67. https://doi.org/10.1016/j.rpor.2018.10.003

Sauer, R. (2010a). Mammakarzinom. In R. Sauer (Ed.), *Strahlentherapie und Onkologie* (5 ed., pp. 347-356). Elsevier.

Sauer, R. (2010b). *Strahlentherapie und Onkologie* (5 ed.). Elsevier.

Schild, H., Arnold-Schild, D., Lammert, E., & Rammensee, H. G. (1999). Stress proteins and immunity mediated by cytotoxic T lymphocytes. *Curr Opin Immunol*, *11*(1), 109-113. https://doi.org/10.1016/s0952-7915(99)80019-3

Schilling, D., Gehrmann, M., Steinem, C., De Maio, A., Pockley, A. G., Abend, M., Molls, M., & Multhoff, G. (2009). Binding of heat shock protein 70 to extracellular phosphatidylserine promotes killing of normoxic and hypoxic tumor cells. *FASEB J*, *23*(8), 2467-2477. https://doi.org/10.1096/fj.08-125229

Schulz-Ertner, D., Sterzing, F., & Karger, C. P. (2006). Strahlentherapie. In M. Reiser, F. P. Kuhn, & J. Debus (Eds.), *Radiologie* (4 ed., pp. 107-150). Georg Thieme Verlag.

Semmler-Behnke, M., Kreyling, W. G., Lipka, J., Fertsch, S., Wenk, A., Takenaka, S., Schmid, G., & Brandau, W. (2008). Biodistribution of 1.4- and 18-nm gold particles in rats. *Small*, *4*(12), 2108-2111. https://doi.org/10.1002/smll.200800922

Shahhoseini, E., Ramachandran, P., Patterson, W. R., & Geso, M. (2018). Determination of dose enhancement caused by AuNPs with Xoft((R)) Axxent((R)) Electronic (eBx) and conventional brachytherapy: In vitro study. *Int J Nanomedicine*, *13*, 5733-5741. https://doi.org/10.2147/IJN.S174624

Sharma, S. S., & Dietz, K. J. (2009). The relationship between metal toxicity and cellular redox imbalance. *Trends Plant Sci*, *14*(1), 43-50. https://doi.org/10.1016/j.tplants.2008.10.007

Sherman, M., & Multhoff, G. (2007). Heat shock proteins in cancer. *Ann N Y Acad Sci*, *1113*, 192-201. https://doi.org/10.1196/annals.1391.030

Shevtsov, M. A., Nikolaev, B. P., Ryzhov, V. A., Yakovleva, L. Y., Marchenko, Y. Y., Parr, M. A., Rolich, V. I., Mikhrina, A. L., Dobrodumov, A. V., Pitkin, E., & Multhoff, G. (2015). Ionizing radiation improves glioma-specific targeting of superparamagnetic iron oxide nanoparticles conjugated with cmHsp70.1 monoclonal antibodies (SPION-cmHsp70.1). *Nanoscale*, *7*(48), 20652-20664. https://doi.org/10.1039/c5nr06521f

Shevtsov, M. A., Nikolaev, B. P., Yakovleva, L. Y., Marchenko, Y. Y., Dobrodumov, A. V., Mikhrina, A. L., Martynova, M. G., Bystrova, O. A., Yakovenko, I. V., & Ischenko, A. M. (2014). Superparamagnetic iron oxide nanoparticles conjugated with epidermal growth factor (SPION-EGF) for targeting brain tumors. *Int J Nanomedicine*, *9*, 273-287. https://doi.org/10.2147/IJN.S55118

Shu, C. W., & Huang, C. M. (2008). HSP70s: From tumor transformation to cancer therapy. *Clin Med Oncol*, *2*, 335-345. https://doi.org/10.4137/cmo.s475

Sibuyi, N. R. S., Moabelo, K. L., Fadaka, A. O., Meyer, S., Onani, M. O., Madiehe, A. M., & Meyer, M. (2021). Multifunctional gold nanoparticles for improved diagnostic and therapeutic applications: A review. *Nanoscale Res Lett*, *16*(1), 174. https://doi.org/10.1186/s11671-021-03632-w

Sigma-Aldrich. (2020a). Dimethyl sulfoxide. https://www.sigmaaldrich.com/catalog/product/sigma/d2650?lang=de&region=DE&gclid=Cj0KCQjwmpb0BRCBARIsAG7y4zbCRB286XIFed8Q7ssd6Ps4iAIir5aYN6RasipZMgyiPqbxWe7LZM8aAgD_EALw_wcB

Sigma-Aldrich. (2020b). *Trypsin-EDTA Solution*. https://www.sigmaaldrich.com/catalog/product/sigma/t4299?lang=de&region=DE

Sindhwani, S., Syed, A. M., Ngai, J., Kingston, B. R., Maiorino, L., Rothschild, J., MacMillan, P., Zhang, Y., Rajesh, N. U., Hoang, T., Wu, J. L. Y., Wilhelm, S., Zilman, A., Gadde, S., Sulaiman, A., Ouyang, B., Lin, Z., Wang, L., Egeblad, M., & Chan, W. C. W. (2020). The entry of nanoparticles into solid tumours. *Nat Mater*, *19*(5), 566-575. https://doi.org/10.1038/s41563-019-0566-2

Singh, P., Pandit, S., Mokkapati, V., Garg, A., Ravikumar, V., & Mijakovic, I. (2018). Gold nanoparticles in diagnostics and therapeutics for human cancer. *Int J Mol Sci*, *19*(7). https://doi.org/10.3390/ijms19071979

Singh-Jasuja, H., Toes, R. E., Spee, P., Munz, C., Hilf, N., Schoenberger, S. P., Ricciardi-Castagnoli, P., Neefjes, J., Rammensee, H. G., Arnold-Schild, D., & Schild, H. (2000). Cross-presentation of glycoprotein 96-associated antigens on major histocompatibility complex class I molecules requires receptor-mediated endocytosis. *J Exp Med*, *191*(11), 1965-1974. https://doi.org/10.1084/jem.191.11.1965

Sousa, R., Liao, H. S., Cuellar, J., Jin, S., Valpuesta, J. M., Jin, A. J., & Lafer, E. M. (2016). Clathrin-coat disassembly illuminates the mechanisms of Hsp70 force generation. *Nat Struct Mol Biol*, *23*(9), 821-829. https://doi.org/10.1038/nsmb.3272

Srivastava, P. K. (1994). Heat shock proteins in immune response to cancer: The fourth paradigm. *Experientia*, *50*(11-12), 1054-1060. https://doi.org/10.1007/bf01923461

Srivastava, P. K., Udono, H., Blachere, N. E., & Li, Z. (1994). Heat shock proteins transfer peptides during antigen processing and CTL priming. *Immunogenetics*, *39*(2), 93-98. https://doi.org/10.1007/bf00188611

Stangl, S., Gehrmann, M., Dressel, R., Alves, F., Dullin, C., Themelis, G., Ntziachristos, V., Staeblein, E., Walch, A., Winkelmann, I., & Multhoff, G. (2011). In vivo imaging of CT26 mouse tumours by using cmHsp70.1 monoclonal antibody. *J Cell Mol Med*, *15*(4), 874-887. https://doi.org/10.1111/j.1582-4934.2010.01067.x

Stangl, S., Gehrmann, M., Riegger, J., Kuhs, K., Riederer, I., Sievert, W., Hube, K., Mocikat, R., Dressel, R., Kremmer, E., Pockley, A. G., Friedrich, L., Vigh, L., Skerra, A., & Multhoff, G. (2011). Targeting membrane heat-shock protein 70 (Hsp70) on tumors by cmHsp70.1 antibody. *Proc Natl Acad Sci U S A*, *108*(2), 733-738. https://doi.org/10.1073/pnas.1016065108

Stangl, S., Varga, J., Freysoldt, B., Trajkovic-Arsic, M., Siveke, J. T., Greten, F. R., Ntziachristos, V., & Multhoff, G. (2014). Selective in vivo imaging of syngeneic, spontaneous, and xenograft tumors using a novel tumor cell-specific hsp70 peptide-based probe. *Cancer Res*, *74*(23), 6903-6912. https://doi.org/10.1158/0008-5472.CAN-14-0413

Surapaneni, S. K., Bashir, S., & Tikoo, K. (2018). Gold nanoparticles-induced cytotoxicity in triple negative breast cancer involves different epigenetic alterations depending upon the surface charge. *Sci Rep*, *8*(1), 12295. https://doi.org/10.1038/s41598-018-30541-3

Tao, C. (2018). Antimicrobial activity and toxicity of gold nanoparticles: Research progress, challenges, and prospects. *Lett Appl Microbiol*, *67*(6), 537-543. https://doi.org/10.1111/lam.13082

Tavaria, M., Gabriele, T., Kola, I., & Anderson, R. L. (1996). A hitchhiker's guide to the human Hsp70 family. *Cell Stress Chaperones*, *1*(1), 23-28. https://doi.org/10.1379/1466-1268(1996)001<0023:ahsgtt>2.3.co;2

Terlecky, S. R. (1994). Hsp70s and lysosomal proteolysis. *Experientia*, *50*(11-12), 1021-1025. https://doi.org/10.1007/bf01923456

Todryk, S. M., Gough, M. J., & Pockley, A. G. (2003). Facets of heat shock protein 70 show immunotherapeutic potential. *Immunology*, *110*(1), 1-9. https://doi.org/10.1046/j.1365-2567.2003.01725.x

Tudda, A., Donzelli, E., Nicolini, G., Semperboni, S., Bossi, M., Cavaletti, G., Castriconi, R., Mangili, P., Vecchio, A. D., Sarno, A., Mettivier, G., & Russo, P. (2022). Breast radiotherapy with kilovoltage photons and gold nanoparticles as radiosensitizer: An in vitro study. *Med Phys*, *49*(1), 568-578. https://doi.org/10.1002/mp.15348

van de Looij, S. M., Hebels, E. R., Viola, M., Hembury, M., Oliveira, S., & Vermonden, T. (2022). Gold nanoclusters: Imaging, therapy, and theranostic roles in biomedical applications. *Bioconjug Chem*, *33*(1), 4-23. https://doi.org/10.1021/acs.bioconjchem.1c00475

van Engeland, M., Nieland, L. J., Ramaekers, F. C., Schutte, B., & Reutelingsperger, C. P. (1998). Annexin V-affinity assay: A review on an apoptosis detection system based on

phosphatidylserine exposure. *Cytometry*, *31*(1), 1-9. https://doi.org/10.1002/(sici)1097-0320(19980101)31:1<1::aid-cyto1>3.0.co;2-r

Vecchio, G., Galeone, A., Brunetti, V., Maiorano, G., Rizzello, L., Sabella, S., Cingolani, R., & Pompa, P. P. (2012). Mutagenic effects of gold nanoparticles induce aberrant phenotypes in Drosophila melanogaster. *Nanomedicine*, *8*(1), 1-7. https://doi.org/10.1016/j.nano.2011.11.001

Vega, V. L., Rodriguez-Silva, M., Frey, T., Gehrmann, M., Diaz, J. C., Steinem, C., Multhoff, G., Arispe, N., & De Maio, A. (2008). Hsp70 translocates into the plasma membrane after stress and is released into the extracellular environment in a membrane-associated form that activates macrophages. *J Immunol*, *180*(6), 4299-4307. https://doi.org/10.4049/jimmunol.180.6.4299

Wang, B., Xing, Z., Wang, F., Yuan, X., & Zhang, Y. (2017). Fangchinoline inhibits migration and causes apoptosis of human breast cancer MDA-MB-231 cells. *Oncol Lett*, *14*(5), 5307-5312. https://doi.org/10.3892/ol.2017.6831

Wang, C., Jiang, Y., Li, X., & Hu, L. (2015). Thioglucose-bound gold nanoparticles increase the radiosensitivity of a triple-negative breast cancer cell line (MDA-MB-231). *Breast Cancer*, *22*(4), 413-420. https://doi.org/10.1007/s12282-013-0496-9

Wang, C., Li, X., Wang, Y., Liu, Z., Fu, L., & Hu, L. (2013). Enhancement of radiation effect and increase of apoptosis in lung cancer cells by thio-glucose-bound gold nanoparticles at megavoltage radiation energies. *Journal of Nanoparticle Research*, *15*(5), 1642. https://doi.org/10.1007/s11051-013-1642-1

Wang, H., Mu, X., He, H., & Zhang, X. D. (2018). Cancer Radiosensitizers. *Trends Pharmacol Sci*, *39*(1), 24-48. https://doi.org/10.1016/j.tips.2017.11.003

Wei, Y. Q., Zhao, X., Kariya, Y., Teshigawara, K., & Uchida, A. (1995). Inhibition of proliferation and induction of apoptosis by abrogation of heat-shock protein (HSP) 70 expression in tumor cells. *Cancer Immunol Immunother*, *40*(2), 73-78. https://doi.org/10.1007/bf01520287

Wolfe, T., Chatterjee, D., Lee, J., Grant, J. D., Bhattarai, S., Tailor, R., Goodrich, G., Nicolucci, P., & Krishnan, S. (2015). Targeted gold nanoparticles enhance sensitization of prostate tumors to megavoltage radiation therapy in vivo. *Nanomedicine*, *11*(5), 1277-1283. https://doi.org/10.1016/j.nano.2014.12.016

Wolfram, J., Zhu, M., Yang, Y., Shen, J., Gentile, E., Paolino, D., Fresta, M., Nie, G., Chen, C., Shen, H., Ferrari, M., & Zhao, Y. (2015). Safety of nanoparticles in medicine. *Curr Drug Targets*, *16*(14), 1671-1681. https://doi.org/10.2174/1389450115666140804124808

Wood, J. C., & Ghugre, N. (2008). Magnetic resonance imaging assessment of excess iron in thalassemia, sickle cell disease, and other iron overload diseases. *Hemoglobin*, *32*(1-2), 85-96. https://doi.org/10.1080/03630260701699912

Wu, C. (1995). Heat shock transcription factors: Structure and regulation. *Annu Rev Cell Dev Biol*, *11*, 441-469. https://doi.org/10.1146/annurev.cb.11.110195.002301

Wu, Z., Stangl, S., Hernandez-Schnelzer, A., Wang, F., Hasanzadeh Kafshgari, M., Bashiri Dezfouli, A., & Multhoff, G. (2023). Functionalized hybrid iron oxide-gold nanoparticles targeting membrane Hsp70 radiosensitize triple-negative breast cancer cells by ROS-mediated apoptosis. *Cancers (Basel)*, *15*(4). https://doi.org/10.3390/cancers15041167

Xia, T., Kovochich, M., Brant, J., Hotze, M., Sempf, J., Oberley, T., Sioutas, C., Yeh, J. I., Wiesner, M. R., & Nel, A. E. (2006). Comparison of the abilities of ambient and manufactured nanoparticles to induce cellular toxicity according to an oxidative stress paradigm. *Nano Lett*, *6*(8), 1794-1807. https://doi.org/10.1021/nl061025k

Yaglom, J. A., Gabai, V. L., & Sherman, M. Y. (2007). High levels of heat shock protein Hsp72 in cancer cells suppress default senescence pathways. *Cancer Res*, *67*(5), 2373-2381. https://doi.org/10.1158/0008-5472.CAN-06-3796

Yang, L. X., Douple, E. B., O'Hara, J. A., & Wang, H. J. (1995). Production of DNA double-strand breaks by interactions between carboplatin and radiation: A potential mechanism for radiopotentiation. *Radiat Res*, *143*(3), 309-315. https://www.ncbi.nlm.nih.gov/pubmed/7652169

Yao, X., Huang, C., Chen, X., Yi, Z., & Sanche, L. (2015). Chemical radiosensitivity of DNA induced by gold nanoparticles. *J Biomed Nanotechnol*, *11*(3), 478-485. https://doi.org/10.1166/jbn.2015.1922

Yogo, K., Misawa, M., Shimizu, H., Kitagawa, T., Hirayama, R., Ishiyama, H., Yasuda, H., Kametaka, S., & Takami, S. (2022). Radiosensitization effect of gold nanoparticles on plasmid DNA damage induced by therapeutic MV X-rays. *Nanomaterials (Basel)*, *12*(5). https://doi.org/10.3390/nano12050771

Yu, Y., Yang, T., & Sun, T. (2020). New insights into the synthesis, toxicity, and applications of gold nanoparticles in CT imaging and treatment of cancer. *Nanomedicine (Lond)*, *15*(11), 1127-1145. https://doi.org/10.2217/nnm-2019-0395

Yun, C. W., & Lee, S. H. (2018). The roles of autophagy in cancer. *Int J Mol Sci*, *19*(11). https://doi.org/10.3390/ijms19113466

Zhang, G., Yang, Z., Lu, W., Zhang, R., Huang, Q., Tian, M., Li, L., Liang, D., & Li, C. (2009). Influence of anchoring ligands and particle size on the colloidal stability and in vivo biodistribution of polyethylene glycol-coated gold nanoparticles in tumor-xenografted mice. *Biomaterials*, *30*(10), 1928-1936. https://doi.org/10.1016/j.biomaterials.2008.12.038

Zhang, R., Kiessling, F., Lammers, T., & Pallares, R. M. (2023). Clinical translation of gold nanoparticles. *Drug Deliv Transl Res*, *13*(2), 378-385. https://doi.org/10.1007/s13346-022-01232-4

Zhang, S., Li, J., Lykotrafitis, G., Bao, G., & Suresh, S. (2009). Size-dependent endocytosis of nanoparticles. *Adv Mater*, *21*, 419-424. https://doi.org/10.1002/adma.200801393

Zhang, X. D., Wu, H. Y., Wu, D., Wang, Y. Y., Chang, J. H., Zhai, Z. B., Meng, A. M., Liu, P. X., Zhang, L. A., & Fan, F. Y. (2010). Toxicologic effects of gold nanoparticles in vivo by different administration routes. *Int J Nanomedicine*, *5*, 771-781. https://doi.org/10.2147/IJN.S8428

Zhu, M., Nie, G., Meng, H., Xia, T., Nel, A., & Zhao, Y. (2013). Physicochemical properties determine nanomaterial cellular uptake, transport, and fate. *Acc Chem Res*, *46*(3), 622-631. https://doi.org/10.1021/ar300031y

Zygmanski, P., & Sajo, E. (2016). Nanoscale radiation transport and clinical beam modeling for gold nanoparticle dose enhanced radiotherapy (GNPT) using X-rays. *Br J Radiol*, *89*(1059), 20150200. https://doi.org/10.1259/bjr.20150200

Zylicz, M., King, F. W., & Wawrzynow, A. (2001). Hsp70 interactions with the p53 tumour suppressor protein. *EMBO J*, *20*(17), 4634-4638. https://doi.org/10.1093/emboj/20.17.4634

7 Acknowledgement

Without the support and help of some people, I would not have been able to complete this dissertation. I want to express my heartfelt gratitude towards them.

First and foremost, I would like to thank Prof. Gabriele Multhoff for her trust, expertise, valuable insights, and constructive feedback throughout the process. She made this incredible project possible, providing me with the opportunity to complete my dissertation on such an exciting topic, as well as supporting the processes with kind and thorough supervision of my work. Being given the opportunity to work on such a crucial topic and contribute towards improving breast cancer treatment is an incredible privilege that I am very grateful for.

I also owe a special thanks to Dr. Stefan Stangl, who supervised and helped me with experiments, planning, and always had advice. Special gratitude also goes to Zhiyuan Wu, who took over the project for further studies, went on to produce amazing work, and successfully continued the project. In addition, I would like to thank the remaining members of Prof. Multhoff's group for the open exchange and fruitful discussions on our respective projects, namely, Dr. Wolfgang Sievert, Dr. Maxim Shevtsov, Caroline Werner, and all others.

Finally, I want to thank my family and friends – for everything. For all the comfort on sunny and cloudy days over the years, for constructive input and encouragement, for pushing me when I needed pushing, for believing in me when I needed reassurance, and for always having my back. From the bottom of my heart, I would like to specifically thank my parents, who have shown me nothing but love and support, made sacrifices to enable everything I have achieved and are the main reason I have gotten to where I am today. I want to dedicate this thesis to you as a sign of appreciation and a promise to continue making you proud.